UNIVERSITY OF LEEDS

Understanding the formation of the "Great Atlantic *Sargassum* Belt"

Sophie Louise Durston

Submitted in accordance with the requirements for the

degree of Doctor of Philosophy

The University of Leeds

School of Earth and Environment

January 2026

Intellectual Property

I confirm that the work submitted is my own and that appropriate credit has been given where reference has been made to the work of others.

Acknowledgements

I would like to show my sincere appreciation to my supervisors Jason Holt, Daniel Grosvenor, Samantha Lavender, Christine Gommenginger, and Judith Wolf. Thank you for all the guidance, the patience with my numerous emails, and for all the comments on the many drafts I have sent. The skills and knowledge I have gained from you all not only helped me with my PhD but will help me as I navigate my future career. It was a pleasure to work with you all.

I would like to thank the SENSE CDT for the training experiences and network, especially during a challenging start in the lockdowns of 2020. I'd also like to thank the National Oceanography Centre in Liverpool for hosting me and providing the best atmosphere to collaborate and learn.

Thank you to my examiners William Homoky and Robert Marsh for their time and effort in reading and examining my thesis.

I'd like to say a huge thank my family and friends - especially Mam, Dad, and Megan - thank you for your unconditional love and support through my many years of being a student.

To my husband, Toby - thank you for always being there, for the coffee runs, and for the endless encouragement. I'm forever grateful.

This project was funded by the Natural Environment Research Council SENSE CDT studentship.

Abstract

The aim of this thesis is to develop a Lagrangian particle tracking model to explore the 2011 formation of the 'Great Atlantic *Sargassum* Belt' (GASB). A new population of free-floating Sargassum was discovered approximately 20 degrees south of its existing source, the North Atlantic Subtropical Gyre, also known as the Sargasso Sea. This new population blooms within the Equatorial Atlantic and flows into coastal waters within the Caribbean Sea, creating a multitude of environmental and socioeconomic issues.

Firstly, I produced a particle tracking model to simulate *Sargassum* transport across the North Atlantic Ocean ±7 years around the anomalous initial bloom of the GASB. Simulations demonstrated an increase in particle transport between the Sargasso Sea and the Equatorial Atlantic in 2010/2011 when the residual transport from waves (Stokes drift) was included in the advection field and that the transport path includes the not previously considered Azores Current.

Next, I added a *Sargassum* biological model to the particle tracking outputs to explore along-trajectory changes in biomass to those *Sargassum* particles that formed the GASB. Enhanced growth rates were observed within the path of particle trajectories, indicative of an upwelling event within that region. Results were able to further support that the GASB was formed due to an anomalous transport event rather than an extreme bloom of an existing population.

Lastly, I dived deeper into the GASB interannual variability by applying the *Sargassum* biological model to a simple box model of the Equatorial Atlantic. Outputs of the box model were able to determine that variability in GASB biomass was significantly linked to phosphate availability.

Contents

List of Figures

List of Tables

Acronyms and Abbreviations

AFAI Alternative Floating Algae Index.

AzC Azores Current.

BGC Biogeochemical.

CC Canary Current.

CCI Climate Change Initiative.

CMEMS Copernicus Marine Ecosystems Monitoring Service.

ECMWF European Centre for Medium-Range Weather Forecasts.

EKE Eddy Kinetic Energy.

ESA European Space Agency.

FAI Floating Algae Index.

GASB Great Atlantic *Sargassum* Belt.

GS Gulf Stream.

HYCOM Hybrid Coordinate Ocean Model.

MAR Mid-Atlantic Ridge.

MCI Maximum Chlorophyll Index.

MODIS Moderate Resolution Image Spectroradiometer.

MSI Multispectral Instrument.

NAO North Atlantic Oscillation.

NASA National Aeronautics and Space Administration.

NDVI Normalised Difference Vegetation Index.

NEC North Equatorial Current.

NECC North Equatorial Counter Current.

NEMO Nucleus for European Modelling of the Ocean.

NIR Near Infrared.

nSEC Northern South Equatorial Current.

OLCI Ocean and Land Colour Instrument.

SaWS Sargassum Watch System.

SSS Sea Surface Salinity.

SST Sea Surface Temperature.

SWIR Shortwave Infrared.

WOA World Ocean Atlas.

Chapter 1

Introduction

Since 2011, small Caribbean Island states have been impacted with inundations of a large seaweed, Sargassum, creating a multitude of economic and environmental issues. Previously, Sargassum was found mainly entrained within the Sargasso Sea with small patches in the Gulf of Mexico (Gower and King 2011). The new source is thought to be in the North Equatorial Recirculation Region, in the Equatorial Atlantic, southeast of the Caribbean Sea (Wang et al. 2019). Since 2011, a large bloom of Sargassum has formed annually in the summer months and is referred to as the Great Atlantic *Sargassum* Belt (GASB). At its peak, the GASB can extend from the Gulf of Guinea, West Africa, to the Caribbean Sea with a wet weight of 32 million tons but this varies annually (Wang et al. 2019). Factors that might influence the growth of the GASB include increased nutrients and changes in sea surface temperatures. Movement of *Sargassum* between the GASB and the Caribbean Sea, however, are more influenced by wind and waves as well as large-scale ocean currents.

1.1 What is *Sargassum*?

Sargassum is a genus of macroalgae (seaweed), with over 100 species and subspecies distributed throughout the temperate and tropical oceans of the world, generally attached to rocks along coasts (Liu et al. 2018). An individual strand can grow to approximately 1m long and is composed of air-filled sacs among leaflike fronds (Figure 1.1) (García-Sánchez et al. 2020). Only two of those species of *Sargassum*, *S. natans* and *S. fluitans*, are holopelagic (i.e. spend their entire lifecycle free-floating) with three subspecies comprising

most of the Atlantic population: *S. fluitans III*, *S. natans I*, *S. natans VIII* (Schell et al. 2015; Fidai et al. 2020). From here on, the term *Sargassum* will act as an umbrella term for all species and sub-species that comprises the Atlantic population. All the species of *Sargassum* within the Atlantic population behave similarly, with a similar size range and lifecycle (Lapointe 1986). *Sargassum* reproduces using a fragmentation method; decaying sections of the *Sargassum* strands break off, leaving the healthy section to grow and form a new strand with the entire lifecycle spanning approximately a year (Gower and King 2011).The broken off aging strands become less buoyant and start to fall through the water column as the air-filled sacs start to decay. Individual *Sargassum* strands can vary from as little as 1cm to over a meter in length, with strands typically aggregating together to form floating rafts (Zhong et al. 2012). Strands can aggregate to form large mats at the surface of the ocean and are solely found within the Atlantic Ocean (Figure 1.1) (Schneider and Searles 1991).

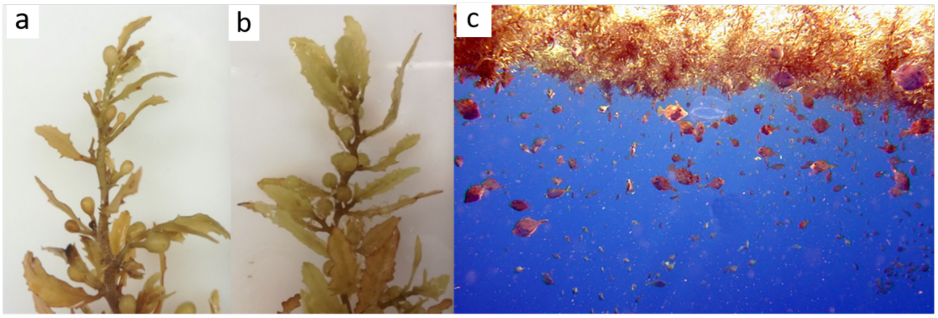

Figure 1.1: a) *Sargassum fluitans* and b) *S. natans* pictured as part of a study by García-Sánchez et al. 2020. c) Image of a *Sargassum* raft full of life from Lapointe et al. 2014

The first reports of *Sargassum* mats were in the 15th century by sailors travelling with Christopher Columbus; sailors described an extensive 'dessert of gold' engulfing the Sargasso Sea, in a seemingly isolated North Atlantic. *Sargassum* was documented within the Sargasso Sea and Gulf of Mexico in substantial quantities (Parr 1939). Ryther (1956) first posed the questions of what sustains the *Sargassum* population? Until advancements in satellite data, there was no explanation for this "dessert of gold". Gower and King (2011) were able to show that *Sargassum* aggregations were not only present within the Gulf of Mexico but this population was injected into the Sargasso Sea annually through the Loop Current which links the two bodies of water (Figure 1.2). Gower and King (2011) stated that the productive Gulf of Mexico acted as a "nursery" for *Sargassum* providing regular nutrient influxes from the Mississippi River, however, this influx would not be able to

sustain the vast amount of *Sargassum* present annually in the Sargasso Sea. Lapointe et al. (2014) provided an interesting theory that excretions by fishes may have provided the needed nutrients, nitrates and phosphates, within the Sargasso Sea. A mutualistic relationship between fish populations and *Sargassum* mats demonstrates both the importance of nutrients to Sargassum growth and the use of *Sargassum* to marine life (Lapointe et al. 2014). The floating mats of *Sargassum* create habitats within open oceans providing food and shelter to many rare species, including the sargassum shrimp (*Latreutes fucorum*) and the sargassum fish (*Histrio histrio*), as well as for migratory species and juveniles during their "lost years" (Alliance 2011; Witherington et al. 2012). Green turtle (Chelonia mydas) hatchlings for example, within the Sargasso Sea, were discovered to primarily feed on *Sargassum* while using the rafts as cover from seabirds and larger marine life (Carr et al. 1982). Huffard et al. (2014) noted that over the course of its lifespan, *Sargassum* rafts can accumulate a community of fungi, bacteria, and invertebrates.

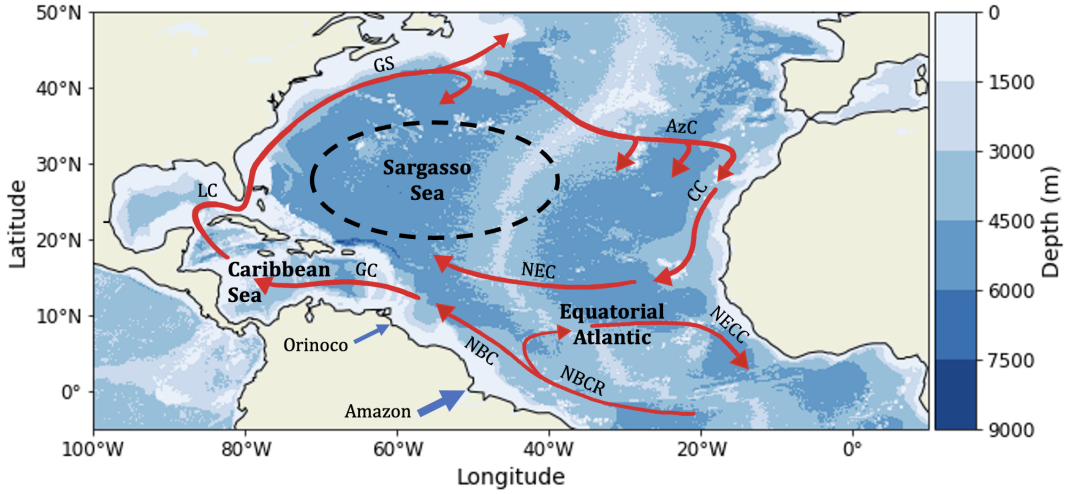

Figure 1.2: Schematic of the currents, forming and surrounding the North Atlantic Subtropical Gyre. The Sargasso Sea bound by the Gulf Stream (GS), Azores Current (AzC), Canary Current (CC) and the North Equatorial Current (NEC) which form the North Atlantic Subtropical Gyre. The new population of Sargassum is situated within the Equatorial Atlantic which is a recirculation region consisting of the North Brazil Current (NBC), the North Brazil Current Retroflection (NBCR) and the North Equatorial Counter Current (NECC). The Equatorial Atlantic and the Caribbean Sea are linked by the northwesterly flowing NBC and the Guiana Current (GC) which then flows back into the subtropical gyre through the Loop Current (LC). Outflow locations of the Orinoco and Amazon Rivers are indicated with blue arrows.

Since 2011, a new source of *Sargassum* has repeatedly been present in Equatorial Atlantic, southeast of the Caribbean Sea between 0°and 10°N (Figure 1.2) (Gower et al. 2013;

Franks et al. 2016; Johns et al. 2020; Wang et al. 2019). Gower et al. (2013) mapped the *Sargassum*, using reflectance values from satellite observations, to visualise the extent of the 2011 bloom and found the population spanned the Atlantic basin from the Caribbean Sea to the coast of West Africa. Gower et al. (2013) determined that a population this size was not previously seen within the Equatorial Atlantic and has been since named the GASB by Wang et al. (2019).

The GASB has continued to reoccur with nearly annual blooms. In 2012, the bloom first developed in spring and summer but decreased rapidly from August to December, suggesting a circannual rhythm seen in other brown seaweeds (Luning 1994). Gower and King (2020) demonstrate that the population of *Sargassum* has been increasing with each bloom; the initial bloom peaked at approximately 5 million tons (wet-weight) in July 2011 which increased to approximately 32 million tons in July 2018 (Figure 1.3) (Gower and King 2020).

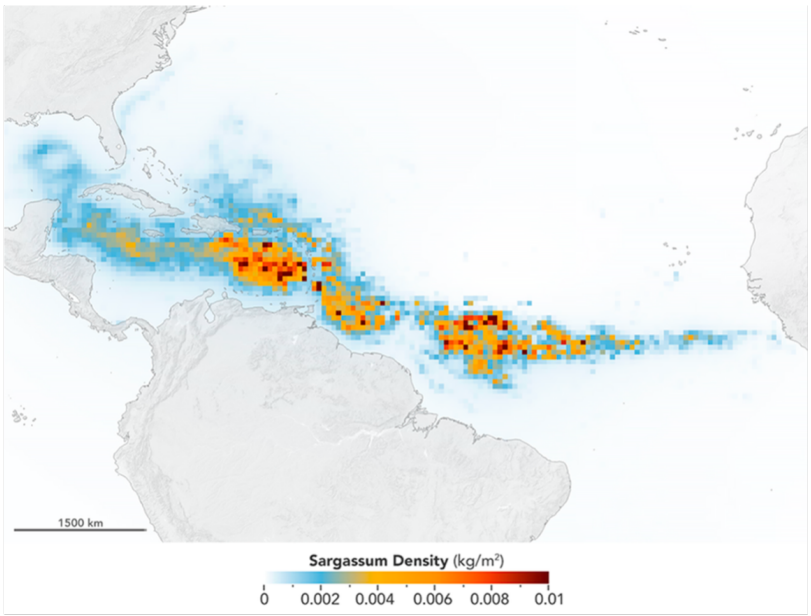

Figure 1.3: Mean *Sargassum* density (kg/m^2) for July 2018 produced from an Alternative Floating Algae Index applied to satellite observations. Image retrieved from Wang et al. 2019

High interannual variability is seen in the GASB size and distribution, but generally the bloom increases in size each year. 2013, however, was an anomaly with little to no *Sargassum* present in the Equatorial Atlantic but was followed by a large bloom again in 2014 (Wang et al. 2019). The winter population of the GASB, or the seed population, is thought to control the size of the subsequent bloom (Putman et al. 2018). It is unknown

how influential the seed population is on the next bloom, possibly due to the lack of knowledge on seed population size and distribution (Wang et al. 2019; Johns et al. 2020). The buoyancy is determined by the age and health of individual strands, therefore, it is highly probable that coupled with an increase in mortality over winter, the population also sinks below the surface. While it is currently understood that *Sargassum* density declines over winter, it is possible that it is actually just sat below the surface and undetectable by satellite reflectance.

1.2 Caribbean Impacts

Sargassum itself has not had any known direct impacts on the environment when floating in open water, however, rafts of *Sargassum* have been inundating the beaches of coastal countries within the Caribbean Sea. Maréchal et al. (2017) state there is a significant chance of *Sargassum* beaching when it is within 150km of the coast in the Caribbean, based off surface current model data. Beaching events cause the most significant economic and environmental problems.

As *Sargassum* acts as a floating habitat, when it enters coastal areas, it can alter the ecosystem while also acting as marine debris (Putman et al. 2020). *Sargassum* can absorb toxic elements like lead, mercury, and arsenic (Rodríguez-Martínez et al. 2020; Davis et al. 2021). These pollutants can leach into the coastal waters impacting vulnerable seagrass communities and coral reefs while altering water quality (Olguin-Maciel et al. 2022). Dense *Sargassum* rafts in the coastal environment could impact local fisheries and limit ocean-based activities for tourists (Caribbean Alliance for Sustainable Tourism, 2015). Within coastal waters, rafts of *Sargassum* can act as a physical barrier to nesting sea turtles which is especially an issue within the Caribbean with multiple threatened species returning to nest each year (Maurer et al. 2015).

In unprecedented beaching events, *Sargassum* can accumulate up to 2m high across vast stretches of coast. Once on land, *Sargassum* will start to decay. The decaying process causes Sargassum to release dangerous concentrations of hydrogen sulfide (Resiere et al. 2021). When exposed to humans, high concentrations of hydrogen sulfide could cause respiratory, cardiovascular, and neurological issues after long-term exposure (Mendez-Tejeda and Jiménez 2019).

In 2017, the tourism industry in the Caribbean Sea was estimated to be worth US$57.1B, with it projected to increase to US$83.3B by 2027 (Thompson et al. 2020). Impacts on tourism can cause significant economic losses. Those economies are not only impacted by the reduced income from their tourism and fisheries sectors but even clean-up efforts are costly and temporary. A cost analysis, issued by the city of Ft Lauderdale (Florida, USA), stated that they spend US$380,000 annually on Sargassum clean-up efforts (Blare et al. 2023). While Mexico's annual clean-up costs are US$1.5 million per beach kilometre, which increased from US$0.3 million since the first inundations in 2011 (Rodríguez-Martínez et al. 2020). Currently countries take reactive measures by manually removing already beached *Sargassum* from the shore and disposing of the algae at either landfill or designated compost sites.

With the knowledge that *Sargassum* only causes issues when it is within shallow waters or beached, preventative measures seem like the most obvious choice. These methods include the use of temporary floating barriers to block the *Sargassum* from reaching the shore so that it circulates back into the open ocean. However, this method relies on the predictability of inundation events to time the deployment of barriers with an incoming *Sargassum* raft. The inability to be able to predict when and where *Sargassum* will appear makes this method less effective.

1.3 Factors that Affect *Sargassum* Transport

Understanding the motion of floating matter is not just important for *Sargassum*¸ but for other flotsam within the ocean. These include marine plastic (Onink et al. 2019), airplane wreckages (Trinanes et al. 2016), larvae (Röhrs et al. 2012), and oil (Drivdal et al. 2014). Floating debris are subject to the effects of large-scale surface currents, direct transfer of momentum from waves, and from the winds (Figure 1.4).

1.3.1 Effects of Currents on Transport

In the open ocean, the transport of debris is affected by ocean currents at multiple scales. Large-scale currents are directed to the right (left) of the wind in the Northern (Southern) hemisphere due to Coriolis force. The Coriolis effect is a result of different latitudes of the Earth rotating at different speeds, and the movement of the object (i.e. water) is

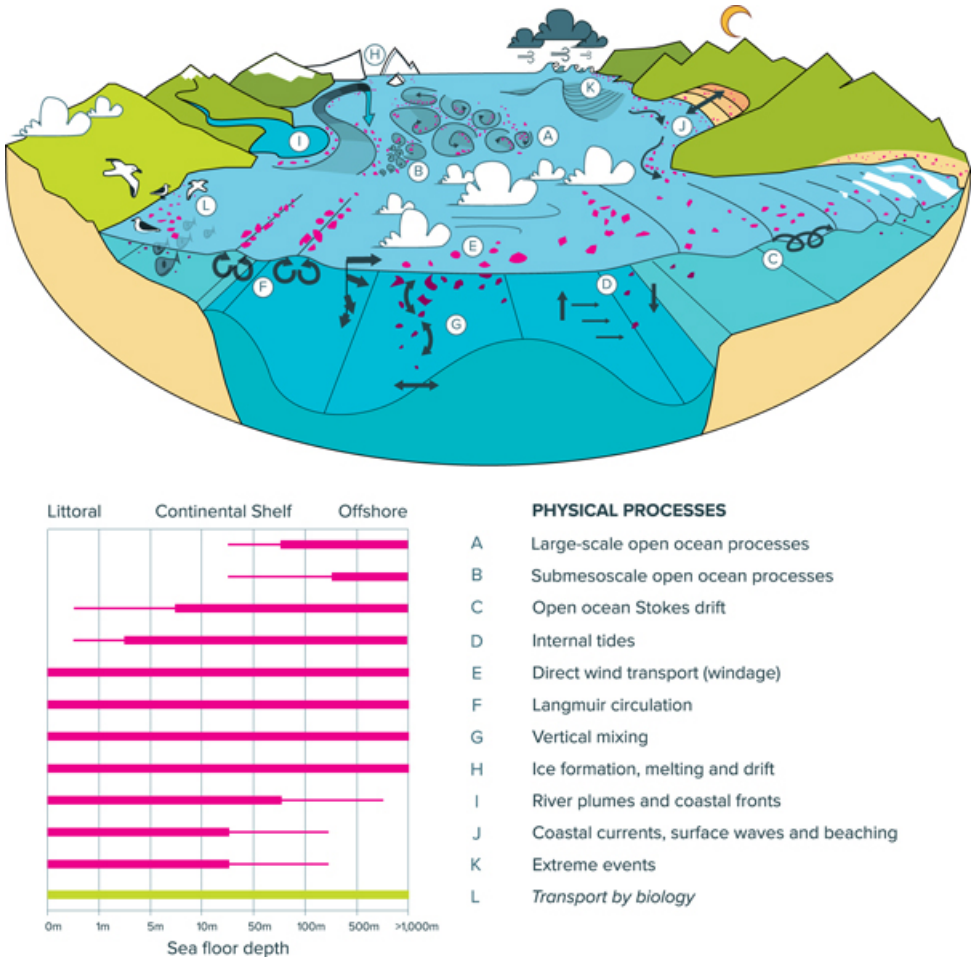

Figure 1.4: Schematic of the physical processes that affect various types of floating debris taken from Sebille et al. 2020. Transport of offshore debris is most affected by open ocean processes (currents), Stokes drift, internal tides, wind transport, and Langmuir circulation.

deflected as it moves between the areas of different rotation speeds. At higher latitudes, surface currents experience a strong Coriolis force due to their proximity to the poles. As the currents move east, the strong Coriolis force causes them to deflect towards the Equator earlier compared to when they are deflected towards the poles (Figure 1.5). This continuous deflection creates the circular flow of gyres within ocean basins. The early deflection gives eastern currents more space to flow through compared to the narrower western boundary currents, yet the same amount of water must flow through both, leading to the intensification of western boundary currents (Hogg and Johns 1995). Intrinsic baroclinic and barotropic instabilities of western boundary currents, together with interactions with topography, lead to meanders and consequently elevated levels of finescale eddies (Ribbe and Brieva 2016). Conversely, surface velocities within the center of the gyres typically fall below 2 cms^{-1} (Law et al. 2010). It is well known that floating plastics

accumulate within these convergence zones (Law et al. 2010; Eriksen et al. 2014; Goldstein et al. 2013). Most famously, the plastics within the Pacific Ocean accumulate within the North Pacific subtropical gyre, depicted in Figure, to form the 'Great Pacific Garbage Patch' (Goldstein et al. 2013). Law et al. (2010) demonstrated plastic concentrations across the North Atlantic subtropical gyre were higher towards the centre of the gyre than towards the edges.

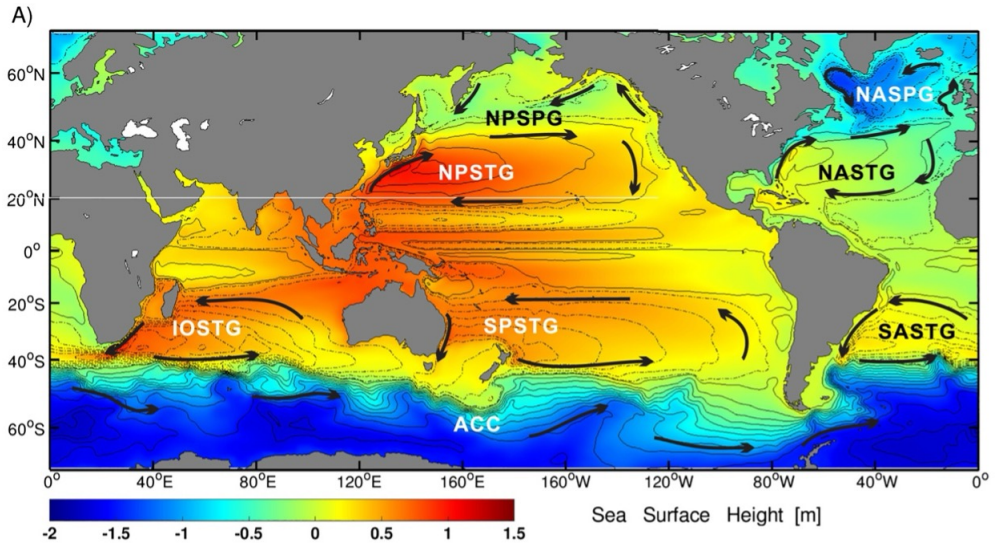

Figure 1.5: Map of the major ocean gyres. Backround colour depicts sea surface height, black arrows depict the significant currents of the gyres. The gyres noted by the abbreviations are listed as follows: North Atlantic Subtropical Gyre (NASTG), South Atlantic Subtropical Gyre (SASTG), North Pacific Subtropical Gyre (NPSTG), South Pacific Subtropical Gyre (SPSTG), Indian Ocean Subtropical Gyre (IOSTG), North Pacific Subpolar Gyres (NPSPG), North Atlantic Subplolar Gyres (NASPG), and Antarctic Circumpolar Current (ACC). Figure retrieved from Yang et al. 2021

1.3.2 Effects of Stokes Drift

Floating objects are also vulnerable to the residual transport from waves, Stokes drift. In the open ocean, the propagation of surface gravity waves creates a net drift velocity to floating particles at the surface in the direction of wave propagation (Figure 1.6) (Stokes 1847). Surface gravity waves, that generates Stokes drift, are generally created by winds. Therefore, it was assumed that Stokes drift could be parametrised by a fraction of the wind speed (Weber, 1983). However, wind affects are immediate while waves are slow to build and can evolve into swell waves. Once they have become swell waves, they can travel long distances with low dissipation and may act upon a floating particle at a different time and location than where it was generated. Wave propagation and strength can be predicted

using wave models, such as WaveWatch-III (Tolman 2009) and therefore predict Stokes drift.

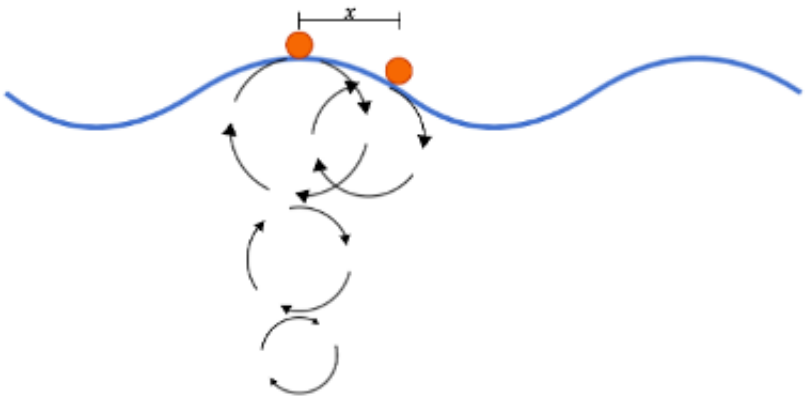

Figure 1.6: Visual representation of the horizontal displacement, x, of a floating object (seen here as an orange circle) caused by the surface waves in the ocean. The schematic is a side-on (vertical) view of the ocean to demonstrate the vertical processes of the ocean and the subsequent horizontal displacement that is produced.

Typical ocean hydrodynamic models describe the flow using a Eularian description, where fields such as velocity and temperature, vary in time and space. A Lagrangian perspective instead follows the movement of a water parcel and therefore a floating object. The total Lagrangian flow, u_L, of objects floating on the surface of the ocean is typically defined as:

$$u_L = u_E + u_S \tag{1.1}$$

where u_E is the surface currents from a Eularian model and u_S is the calculated Stokes drift. Röhrs et al. (2012) released surface drifters, and measured in situ observations of currents, waves and wind to estimate Stokes drift, and therefore the Langrangian flow within the Norwegian Sea. These observations were used to produce drift models to recreate the drifter pathways. Several floating drifters were released with their location recorded over time. Trajectories from the Lagrangian drift models most closely recreated the average path of the surface drifters (Figure 1.7), compared to the Eularian drift models.

Some studies that explored *Sargassum* transport had mixed views on the importance of Stokes drift. Zhang et al. (2024), for example, did not include Stokes drift when exploring *Sargassum* transport within the Gulf of Mexico because they assumed its effects within the open ocean would be negligible. Brooks et al. (2019) and Putman et al. (2018) also omitted Stokes drift from their studies and instead focussed on the role of wind in *Sar-*

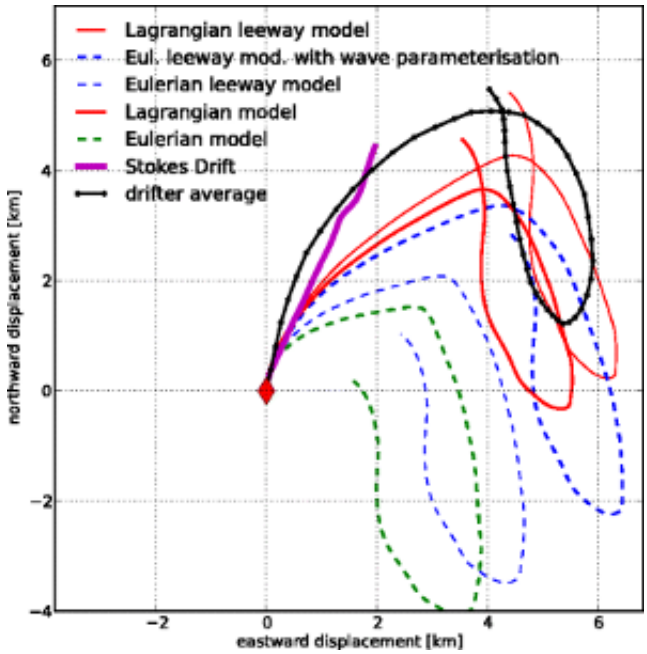

Figure 1.7: Particle trajectories demonstrating the effects of multiple model simulations and the comparison with the calculated Stokes drift. Red diamond indicates the starting point for all trajectories. Image retrieved from Röhrs et al. 2012

gassum transport. Jouanno et al. (2021), however, found Stokes drift to have a significant impact on the large-scale distribution of *Sargassum* in their model simulations across the Equatorial Atlantic.

1.3.3 Effects of Windage

Windage is the effect of wind on floating particles that protrude out of the water. Windage results from the combination of wind induced pressure drag and viscous drag (Sebille et al. 2020). Pressure drag is from the direct pressure exerted onto the floating object and is dependent on the buoyancy, shape, and density of the object. Numerically, windage is calculated as a percentage of the surface winds which for floating objects can range from 0% to 6% (Sainte-Rose et al. 2016).

Sargassum gathers as a raft at the surface of the ocean in varying densities and raft sizes, therefore, the area that experiences pressure drag can vary. Many studies have tried to estimate the average windage experienced by *Sargassum* by using modelling, in situ measurements, or a combination (Putman et al. 2018; Brooks et al. 2019; Wang et al. 2019; Berline et al. 2020; Putman et al. 2020; Marsh et al. 2021).

Putman et al. (2018) tracked *Sargassum* rafts within the Caribbean Sea and ran modelling

simulations to recreate the path taken by the real *Sargassum*. Their results indicated that windage significantly improved the model's ability to follow the path taken by the tracked *Sargassum* (Figure 1.8). Typically, the windage values 1-3% are used for *Sargassum* transport (Johns et al. 2020; Putman et al. 2020; Jouanno et al. 2021; Marsh et al. 2021). However, Berline et al. (2020) and Olascoaga et al. (2023) agree that the windage could be as little as 0.5% for small clusters of *Sargassum*.

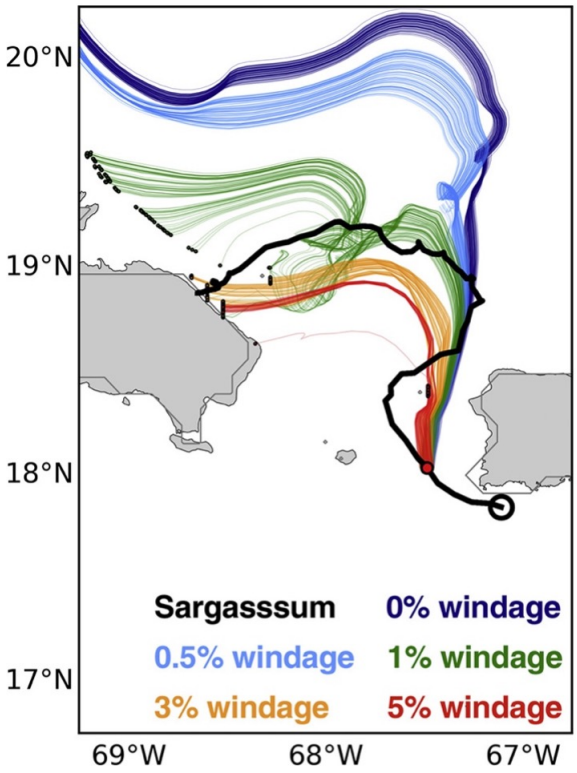

Figure 1.8: Graphical abstract of particle tracking results with varying windage values in comparison to a GPS tracked *Sargassum* raft. Figure retrieved from Putman et al. 2020

1.3.4 Formation of the GASB

Southward flow of *Sargassum* within the North Atlantic would have been needed to form the GASB, however, when the GASB first formed it was unclear how it was transported south to the Equatorial Atlantic. Johns et al. (2020) proposed that an extreme negative phase in 2009/2010 of the North Atlantic Oscillation (NAO) could have caused this shift from the Sargasso Sea to the Equatorial Atlantic. The NAO is a large-scale atmospheric phenomenon of fluctuations of sea level pressure between low pressure centered over Iceland (sub-polar low) and high pressure over the Azores islands (subtropical high). The NAO is present in one of two phases, positive and negative (Figure 1.9). A negative NAO phase occurs when both the sub-polar low and the subtropical high are weaker than average.

Variability in the North Atlantic wind and surface ocean waves have been linked to the variability in the NAO (Gleeson et al. 2017; Rogers 1997). The increased velocity in winds in the extreme negative phase, along with the southward shift is suggested to transport *Sargassum* rafts eastwards out of the Sargasso Sea into the Canary Current (CC) and therefore southwards to the Equatorial Atlantic (Wang et al. 2019; Johns et al. 2020).

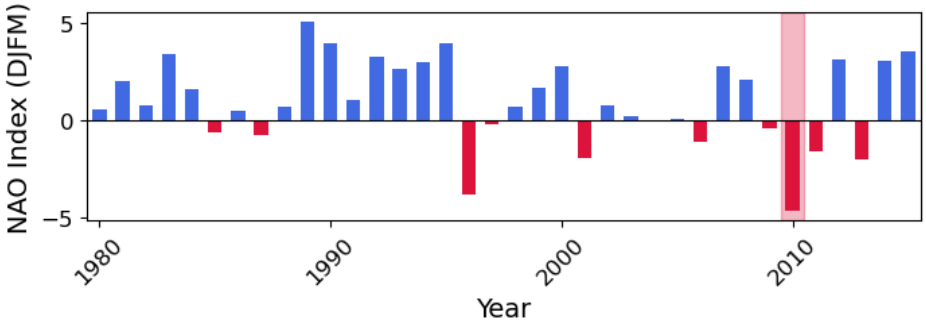

Figure 1.9: North Atlantic Oscillation (NAO) winter (northern hemisphere) anomalies from 1980 to 2020. Blue indicates a positive phase of the NAO, while red indicates a negative phase. The 2010 negative anomaly is highlighted as an anomalous year.

1.4 Factors that Affect *Sargassum* Lifecycle

Algal blooms, including *Sargassum* blooms, are likely to be the result of a combination of environmental factors, including nutrients, temperature, mixing conditions, and hydrography. In the current literature, there have been discussions as to what controls *Sargassum* growth rates. Through *in vitro* studies, Lapointe (1986) demonstrated that *Sargassum* growth was mainly limited by phosphorus availability within the surrounding water, while recent studies by Lapointe et al. (2014) and Michotey et al. (2020) suggested the possibility that *Sargassum* could form a "self-sustaining ecosystem", where urea and ammonium are excreted by grazing fish and aggregated nitrifying epiphytes supply nutrients to surrounding water. It's also possible that like other brown algae, *Sargassum* may be able to store nutrients within its tissues (Hanisak 1993; Lapointe et al. 2021). Growth is also sensitive to temperature and light changes. 26°C and 62.3 W/m^2 are the optimal Sea Surface Temperature (SST) and light intensity for growth based on studies completed both in labs and in the field (Carpenter and Cox 1974; Lapointe 1986; Lapointe et al. 2014). However, *Sargassum* has a broad temperature range for growth from 18°C to 30°C, with growth ceasing below 12°C (Hanisak and Samuel 1987). It is key to note the lack of recent studies on *Sargassum*'s physiological behaviours and that those that do exist, focus primarily on

the *Sargassum* morphological types that are prominent within the Sargasso Sea.

Wang et al. (2019) stated that there is a correlation between high *Sargassum* coverage and low SST anomalies. It is unlikely that low SSTs would directly cause an increase in growth, however, SSTs may have a role in controlling other processes. Crespo et al. (2019) ran model simulations of atmospheric responses to SST across the Equatorial Atlantic and described an increase in precipitation over the Brazil and the west of Africa occurring due to low SST anomalies, leading to higher river discharge.

1.4.1 Within the Sargasso Sea

The Sargasso Sea is placed within the boundary currents of the North Atlantic Subtropical gyre. Subtropical gyres are typically depleted with nutrients at the surface due to their permanent stratification and weak seasonal upwards mixing of nutrients. Sunlit euphotic surface waters, at the centre of the gyre, are a large distance from land-derived nutrients and therefore once used by photosynthetic plankton aren't typically replenished by rivers like coastal waters. Therefore, vertical transport from nutrient rich waters is the main source of nutrients to surface waters (Gupta et al. 2022). It was shown that vertically supplied phosphates were the dominant nutrient source in both the North Atlantic and Pacific subtropical gyres, accounting for 60% of the total phosphorus supply measured in each gyre (Xiang et al. 2023). This vertical supply of nutrients to subtropical gyres is still minimal when comparing nutrient concentrations within other ocean regions, however, *Sargassum* has been present within the Sargasso Sea for centuries. As mentioned in 1.1, *Sargassum* forms its own habitat as the only source of food and refuge within the Sargasso Sea. This relationship between fauna and *Sargassum* has been suggested to be symbiotic, where secreted ammonium and phosphorus from the migratory and foraging fish could provide supplementary nutrients (Lapointe et al. 2014).

While supplied nutrients from fish and vertical transport within the subtropical gyre may support growth within the Sargasso Sea, (Gower and King 2011) suggested that *Sargassum* originates within the Gulf of Mexico before floating along the currents into the Sargasso Sea (Figure 1.10). Satellite observations from between 2002 to 2008 show relatively significant *Sargassum* abundance within the western Gulf of Mexico within March and May. In July, *Sargassum* was spread throughout the Gulf of Mexico and east of Cape

Hatteras indicating that *Sargassum* travelled from the Gulf of Mexico into the western Sargasso Sea (Figure 1.10). Terrestrial sources of nitrate (NO_3) and phosphate (PO_4) are injected into coastal waters through river discharge which regulates the biogeochemical cycles (Hopkinson and Vallino 2005). The Mississippi River plume has been documented to be associated with high chlorophyll level, indicating a high level of nutrients within the river discharge (Wysocki et al. 2006). The observed *Sargassum* within the Gulf of Mexico, together with the enhanced nutrient input from the Mississippi River lead to Gower and King's suggestion of the Gulf acting as a nursery.

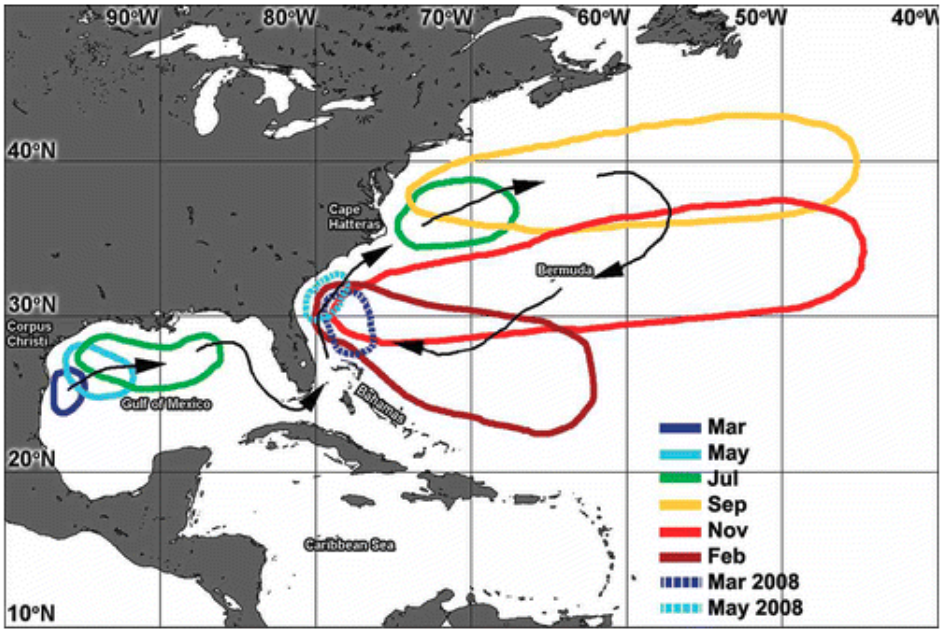

Figure 1.10: Schematic describing the average seasonal *Sargassum* distribution within the North Atlantic, observed with satellite observations from 2002 to 2008. *Sargassum* was observed within the western Gulf of Mexico in spring months and then circulating within the subtropical gyre in the remaining months. Figure retrieved from (Gower and King 2011).

1.4.2 Within the Equatorial Atlantic

The Amazon is the largest river system in the world, emptying into the Equatorial Atlantic, within the North Brazilian Current (Muller-Karger et al. 1988), see Figure 1.2 for a diagram and description of North Atlantic currents. The discharge can be observed in remote sensing images as an area with low surface salinity within this region of the Atlantic (Vizy and Cook 2010). Freshwater plumes, such as this from the Amazon, are stratified and inhibit vertical mixing. Due to these characteristics, the Amazon plume can persist

and extend over 1000 kilometres into the Equatorial Atlantic (Muller-Karger et al. 1995). The plume is visible within satellite images as discoloured water suggesting riverine nutrients and organic material are transported out into the ocean. However, the plume extent and direction vary depending on discharge volume and strength of the NBC retroflection (Vizy and Cook 2010). Recently, the drainage basin for the Amazon River has experienced deforestation on an exponential scale with forest loss increasing by 25%, increasing the discharge (Wang et al. 2019). While fertiliser consumption in the surrounding area has increased by 67%, increasing the nutrient levels (Wang et al. 2019). Nutrients within the Amazon River runoff were shown to have increased within *in situ* data collected in 2010 and 2018. Interestingly, the world's third largest river, the Orinoco, also impacts the path of *Sargassum* as it reaches the Caribbean (Figure 1.2. The Orinoco flows directly into the Caribbean Sea and drifts northwestwards controlling the annual cycle of chlorophyll and primary production from nutrient input (Muller-Karger et al. 1988). An increased influx of nitrate and phosphates into both the Equatorial Atlantic and Caribbean Sea coincides with the appearance of the *Sargassum*, however, there is no evidence in literature to demonstrate that nutrients from river discharge have a direct link to the growth of the blooms.

In the east of the Equatorial Atlantic, the primary source of nutrients is thought to be upwelling. Coastal upwelling brings colder, nutrient-rich deep water to the surface due to winds blowing parallel to a continent. Together Ekman transport moves the water 90 degrees to the wind with the colder water replacing it from below (Ingham 1971). As the colder nutrient-rich water moves vertically up in the water column, nutrients are injected into the photic zone of the ocean, an area rich with phytoplankton, therefore, upwelling events create large areas with high primary productivity (Brandt et al. 2023).

Two distinct seasons of upwelling are seen around the Gulf of Guinea, characterized as major and minor upwelling. Major upwelling season starts in June and a large drop in SST is visible in July (Hardman-Mountford and McGlade 2003). Upwelling within the Gulf of Guinea interestingly does not follow a classical wind driven process like other eastern boundary upwelling systems such as Peru (Gruber et al. 2011). Four proposed causes of this upwelling are divergence induced by seasonal changes in a local current, vertical motion associated with cyclonic eddies generated downstream, Ekman pumping caused by

wind stress curl, and upwelling propagation by Kelvin waves remotely generated at the equator (Ingham 1971; Djakouré et al. 2014). The significance in this difference is that the upwelling is prone to both seasonal and interannual variability like the *Sargassum* bloom in the Equatorial Atlantic. Slightly further north, the Mauritania-Senegalese upwelling region provides enhanced nutrients within the winter and spring months (Vázquez et al. 2023). Upwelling within this region can be enhanced under the influence of the Azores High, as part of the NAO. An intensified Azores High over the upwelling region generates a cyclonic circulation anomaly, which in turn intensifies the upwelling favourable winds (Vázquez et al. 2023). As well as continental upwelling, the Equatorial Atlantic also experiences a region of open-ocean upwelling known as the Equatorial Upwelling region. This upwelling region is formed by a mixture of Ekman pumping and wave upwelling (Wang and Hu 2017).

Nutrient inputs into the Equatorial Atlantic, as described above, are not exclusively used by Sargassum. Phytoplankton within the surface waters also use the nitrates and phosphates to grow, also blooming in the spring and summer months. Therefore, it is easy to assume that competition must arise between Sargassum and phytoplankton blooms. Jouanno et al. (2021) determined that Sargassum and phytoplankton are observed in separate areas of the Equatorial Atlantic and Caribbean Sea (Figure 1.11). Sargassum aggregated within 0 - 10°N between the North Equatorial Counter Current (NECC) and the Northern South Equatorial Current (nSEC), within the recirculation region of the Equatorial Atlantic. The chlorophyll observations, however, peak southeast of the nSEC at the marked Equatorial upwelling region (Figure 1.11). The difference in the distributions could be due to competition or the difference in limiting nutrients. Sargassum mats, if dense enough, can block light to the mixed layer below altering phytoplankton community structure and productivity (Franks et al. 2016; Gower et al. 2013) but there are no studies specifically exploring the *Sargassum* and phytoplankton competition.

While multiple studies suggest the nutrient sources in the Equatorial Atlantic promote the large blooms of *Sargassum* since 2011 (Gower et al. 2013; Lapointe et al. 2014; Wang et al. 2019; Prospero et al. 2020; Marsh et al. 2021), there is little evidence to show the nutrient input is enough to sustain the annual GASB blooms and send unprecedented amounts of Sargassum to the Caribbean Sea. A prominent *Sargassum* study, Johns et al. (2020),

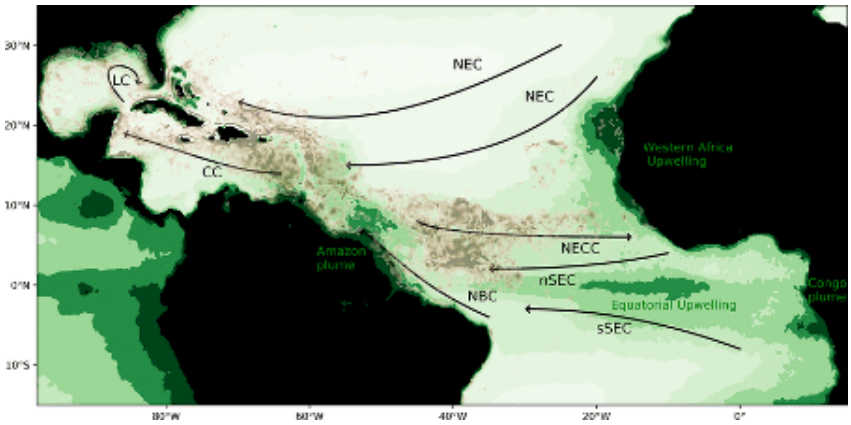

Figure 1.11: *Sargassum* fractional coverage for July-August 2017 shown in the brown colour scale (0.001% to 0.002%) and surface chlorophyll in the green colour scale (mgm^3). Ocean currents for the region are added, as in Figure 1.2, except the addition of the northern and southern branches of the North Equatorial Current (nSEC and sSEC). Figure by Jouanno et al. 2021 with data from Brooks et al. 2019

suggested that nutrients from upwelling in the Equatorial Atlantic might not have a role in supporting *Sargassum* growth due to the distance between nutrient source location and *Sargassum* bloom distributions and instead growth is due to an upward flux of nutrients from mixed layer dynamics within the Equatorial Atlantic.

1.5 Aims and Objectives

This thesis aims to investigate the transport, growth, and survival of *Sargassum* from the Sargasso Sea to the Equatorial Atlantic, focusing on the formation and sustainability of the GASB. Despite extensive research on the GASB, there has yet to be a clear demonstration of *Sargassum*'s ability to flow out of the Sargasso Sea or if the conditions along the transport route provide favourable conditions for growth providing a key gap that this thesis aims to address. The following list of objectives were derived to accomplish this:

1. Develop a particle tracking model of *Sargassum* transport in the North Atlantic using Ocean Parcels
2. Assess whether changes in typical conditions within the North Atlantic, during 2009/2010, enabled the release of *Sargassum* from the North Atlantic subtropical gyre
3. Develop a *Sargassum* growth model that is applied to particle tracking model outputs
4. Investigate if the transport route from the Sargasso Sea to the Equatorial Atlantic

supports *Sargassum* survival and growth

5. Develop a simple box model of the Equatorial Atlantic to simulate *Sargassum* inflow and outflow and growth

6. Evaluate the sustainability of the *Sargassum* population in the Equatorial Atlantic and the environmental conditions necessary for its persistence

1.6 Thesis Structure

This chapter has outlined the issues the Great Atlantic *Sargassum* Belt has caused to provide a basis as to why it is important to further the knowledge and understanding of *Sargassum*. Chapter 2 provides an outline of the models used within this study and introduces methods that are commonly used throughout the thesis. Research and findings are presented across three research chapters. Chapter 3 investigates the formation of the GASB, using particle tracking methodologies to simulate transport. Chapter 4 builds on the particle tracking model developed in chapter 3, by developing a growth model that applies *Sargassum* physiological behaviours to the particle tracking outputs to explore the change in growth and decay. The final research chapter, Chapter 5, now investigates the *Sargassum* population within the Equatorial Atlantic. Research in this chapter explore if *Sargassum* can survive without an outside source, using a simple box model of the Equatorial Atlantic. The thesis concludes with a summary and discussion within Chapter 6.

Chapter 2

Methods

2.1 Ocean Models

2.1.1 Numerical Models

Numerical ocean models focus on the physical properties and processes of the ocean. These include the global Hybrid Coordinate Ocean Model (HYCOM) and the global Nucleus for European Modelling of the Ocean (NEMO) model. There are four specific ingredients necessary for a successful ocean model: the primitive hydrostatic equations, boundary conditions, initial conditions, and forcing fields (Fox-Kemper et al. 2019). The ocean can be described to a good approximation by equations of motion of fluids, also known as the Navier-Stokes equations (Bistafa 2018). Some small-scale proceses (such as turbulence, submesoscale eddies, or internal waves) may occur at smaller scales than the model grid can represent, leaving them to be unresolved within the equations of motion. Models deal with this by parameterisations that aim to capture the net impact of these processes (Berloff et al. 2021). These equations of motion formulate the time evolution of mass, momentum, heat and salt. Boundary conditions consist of the basin geometry, bottom topography, and the atmosphere on top as all three influence the flow. Initial conditions depend on the study but typically include initial temperature and salinity fields, that may come from a previously spun up model, and potentially the initial velocity fields. Forcing fields include multiple variables that may alter the flow over time including radiation, river runoff, winds, and tides.

When considering an ocean model, there are four practicalities to consider: vertical grid, horizontal grid, resolution, and parameterisations. The choice of vertical grid is important as the oceans are forced at the surface, strongly stratified, density dependent, and flow against complex topography. There are three approaches to vertical grids based on either depth, terrain, or density intervals which allow for the choice or a hybrid combination of these. The vertical resolution also controls the model's ability to represent boundary currents and topographic detail. Meaning a model with a higher vertical resolution would be more suitable to coastal applications where topography interactions are important, but would be too computationally expensive to apply the same resolution to a global scale model. Global ocean models usually describe their horizontal resolution with their ability to permit or resolve mesoscale eddies. For example, a resolution $\geq 1^{\circ}$ is described as course with no eddies and a resolution of $\geq 0.02^{\circ}$ is described as eddy-resolving which generates eddies at a realistic strength and rate (Chelton et al. 1998).

The Copernicus Marine Ecosystems Monitoring Service (CMEMS) provides the GLORYS12V1 Global Ocean Physics Reanalysis product outputs. CMEMS reanalysis products use an ocean circulation model with assimilated satellite sea level anomaly, sea surface temperature, and sea ice concentration as well as in situ temperature and salinity profiles. Observations are assimilated by means of a reduced-order Kalman filter to produce model outputs that produce a truer representation of previous ocean conditions. The GLORYS12V1 model component (Jean-Michel et al. 2021) is the NEMO platform driven at the surface by both the ERA-Interim and ERA5 reanalysis from the European Centre for Medium-Range Weather Forecasts (ECMWF). This study used daily outputs at a $1/12^{\circ}$ (8km) spatial resolution for a sub-region between 0°to 60°N and 80°W to 5°W; this spatial resolution includes both large scale surface currents and eddies but does not resolve sub-mesoscale processes that occur at a 1km resolution (McWilliams 2016).

2.1.2 Wave Models

Wave models aim to predict the evolution of the spectral energy of wind waves. Waves are a key modulator in the transfer of energy between the air and sea and play an important role within the transfer and dissipation of that energy throughout the ocean. Waves produced by surface winds evolve over time, propagating wave energy far from the region of generation. Wave models use atmospheric wind forcing, non-linear wave interactions,

and dissipation to produce outputs such as wave height, swell wave height, and Stokes drift. It is important to note that wave models are less accurate within coastal regions than the open ocean, due to a large range of factors. These factors include, but are not limited to, a more complex topography and the occurrence of remotely generated waves.

The CMEMS ocean physical-wave analysis and forecast product (Law-Chune et al. 2021) estimated 3D Stokes drift, u_s, using the surface wave-induced drift u_s^0, the wave height H_s, and the mean wave period T_01 using the equation by Breivik et al. (2016):

$$u_s = u_s^0[e^{2k_e z} - \beta\sqrt{-2k_e\pi z}erfc(\sqrt{2k_e z})] \tag{2.1}$$

where $\beta = 1$; $k_e = (8|u_s^0|T_01)/(\gamma\pi H_s^2)$ with $\gamma = 5.97$ and z is the depth. For 2D velocities, the Stokes drift at the first ocean level from the 3D product can be used.

2.1.3 Biogeochemical Models

While hydrodynamic ocean models aim to simulate the physical ocean properties, Biogeochemical (BGC) models describe their BGC properties and transformations over time using differential equations and are dynamically coupled to hydrodynamic models. PISCES-v2 (Pelagic Interactions Scheme for Carbon and Ecosystem Studies volume 2) is a commonly used BGC model that simulates the cycles of carbon and the main nutrients (phosphates, nitrates, iron and silicon) as well as simulating phytoplankton and microzooplankton ecosystems (Aumont et al. 2015). The CMEMS Global Ocean Biogeochemistry hindcast uses the PISCES BGC model and provides BGC fields at a 1/4° spatial resolution, between 1993 and 2024. This product contains daily outputs for chlorophyll, nitrate, phosphate, silicate, dissolved oxygen, and primary production. The initial conditions used to set up the model were the World Ocean Atlas (WOA) 2013 (for nitrate, phosphate, silicate, and dissolved oxygen), the CMEMS GLODAPv2 model (for dissolved inorganic carbon and alkalinity), and climatological model outputs (for iron and dissolved organic carbon).

2.2 Meteorological Data

ERA5 is a ECMWF reanalysis that provides global weather and climate for the last 8 decades (Hersbach et al. 2020). This product assimilates data from global weather stations to update forecasts every 12 hours to provide a best estimate of global weather patterns. Within the context of studying *Sargassum* transport and growth, the following three ERA5 variables are used: global eastward and northward wind components at 10m above the surface, and clear-sky direct solar radiation (irradiance) at the surface. The direct solar radiation, which can also be known as the shortwave radiation, is the amount of radiation that reaches the surface after passing through the atmosphere.

2.3 Lagrangian Particle Tracking

Particle-tracking is a useful method of modelling transport using synthetic particle trajectories within a velocity field. Particle tracking follows the particle over time, rather than observe changes in ocean variables within a fixed spatial grid as used by Eularian models. There are multiple coding packages available to use for particle tracking simulations, the main difference being the coding language used. These packages include, but are not limited to, Parcels (Delandmeter and Sebille 2019), Ichthyop (Lett et al. 2008), ARIANE (Marsh et al. 2021), LTRANS (Schlag et al. 2012), and OpenDrift (Dagestad et al. 2018). This study uses Parcels for particle tracking simulations, for a further comparison on ocean particle tracking software see Xiang et al. (2023).

Parcelsv2 (Probably a Really Computationally Efficient Lagrangian Simulator - version 2)(Delandmeter and Sebille 2019) can be used to model *Sargassum* transport as synthetic particles within a Eularian framework, such as a numerical ocean model. A synthetic particle's position (X) at a timestep of (Δt) can be calculated by:

$$X(t + \Delta t) = X(t) + \int_{t}^{t+\Delta t} v(X(t), t)dt \tag{2.2}$$

where $v(X(t), t)$ is the velocity from the model outputs at the particle's location $X(t)$ at time t. The velocity at the particle's location is obtained through linear interpolation of the velocity field, which depending on the simulation, can consist of a combination of surface currents, Stokes drift and wind. Further descriptions of the Parcels model, and its

code, can be found in Sebille et al. (2018).

Particle tracking, or more specifically Parcels, can be used to explore physical properties of the ocean such as ocean currents (Saporta-Katz et al. 2024; Freitas et al. 2024; Jutras et al. 2023), river plumes (Aijaz et al. 2024) and eddy formation (Jones-Kellett and Follows 2024). BGC changes can also be explored, for example Birchill et al. (2024) modelled hydrothermal iron and magnesium transport within the deep ocean. Particle tracking was used to simulate the flow of water from hydrothermal vents over 20 years to pinpoint regions that may receive elevated levels of nutrients from the vents. As well as simulating water, Parcels can also simulate planktonic organisms within a 3D ocean. The movement of plankton can be simulated to explore the connectivity and possible settling of coral reef larvae (Vogt-Vincent et al. 2024), phytoplankton distributions (Ferronato et al. 2023), and the connectivity of deep-sea ecosystems (Wang et al. 2024). Interestingly, trajectories of organisms that swim can also be simulated by adding in a parameter to account for swimming within the advection. This was done within Malul et al. (2024) to assess the swimming patterns of jellyfish.

Within the context of modelling the transport of floating objects, 2D particle tracking simulations have been successful in modelling floating plastics (Nakajima et al. 2024; Vogt-Vincent et al. 2024; Cunningham et al. 2022), oil spills (Nobre et al. 2022), and *Sargassum* (Franks et al. 2016; Putman et al. 2018; Putman et al. 2020; Marsh et al. 2021; Lara-Hernández et al. 2024). Particle tracking was seen to recreate real *Sargassum* mat trajectories in Putman et al. (2018) by comparing simulated trajectories with the path of a GPS tracked *Sargassum* mat. Different windage values provided varying results, but overall, trajectories were consistent with observed paths. Currently, particle tracking has been used to explore the connectivity between the Caribbean Sea and the Equatorial Atlantic to aid understanding in *Sargassum* beaching events. Particles were backtracked to the Equatorial Atlantic from known beaching sites along the North Brazilian Current (Franks et al. 2016; Putman et al. 2018). Both Franks et al. (2016) and Putman et al. (2018) produced similar results, that beached *Sargassum* within the Caribbean had travelled from the Equatorial Atlantic, but used different particle tracking software. Putman et al. (2018) used the ICTHYOP (Lett et al. 2008) software for their simulations, while Franks et al. (2016) independently calculated the lagrangian particle trajectories without

the use of a premade software. Therefore, while different particle tracking softwares differ in their designed use and coding language, the choice in software is thought to have minimal effect on the outcome of the study. For this study, I chose to use Parcels for particle tracking simulations based on the ability to produce custom kernels so there was freedom in producing *Sargassum*-like particles. Also, Parcels has an active online discussion forums for when issues are encountered, producing a community with similar skill sets.

2.4 *Sargassum* Observations

Satellite observations can be used to measure properties at the surface of the ocean. Active sensors can send out signals and use the return to measure sea surface height. Passive sensors measure signals emitted at the surface of the ocean, which could be electromagnetic radiation to give sea surface temperature or remote-sensing reflectance (R_{rs}) to give ocean colour. Typical seawater contains a certain concentration of phytoplankton and debris and acts as a baseline reflectance. R_{rs} values that differ from that baseline "normal" ocean reflectance are used to estimate particles within the ocean. Photosynthetic pigments in phytoplankton and algae absorb certain wavelengths of light while reflecting others, creating a spectral signature (Figure 2.1). Biermann et al. (2020) demonstrated in Figure 2.1 that optical imagery is able to determine floating objects using their spectral signature against seawater. *Sargassum*, uniquely, has enhanced red-edge reflectance (in the near-infrared spectral bands) with a unique reflectance curvature of 630nm due to its chlorophyll composition (Wang et al. 2018). Another distinguishing feature, to determine *Sargassum* blooms from other algal blooms is the low reflectance in the green wavelengths compared to the bacterium Trichodesmium (Wang et al. 2018).

Reflectance is measured by a multitude of different sensors on varying satellites. A Moderate Resolution Image Spectroradiometer is a common sensor type used for *Sargassum*; named MODIS on the National Aeronautics and Space Administration (NASA) Aqua and Terra satellites and MERIS on the ESA Envisat satellite. However, the Envisat satellite has since been replaced by the ESA Copernicus Sentinel-3 satellites which instead carry the Ocean and Land Colour Instrument (OLCI) sensor.

To identify *Sargassum* using the reflectance, a common method is to apply indices. Common indices used include the Normalised Difference Vegetation Index (NDVI), Floating

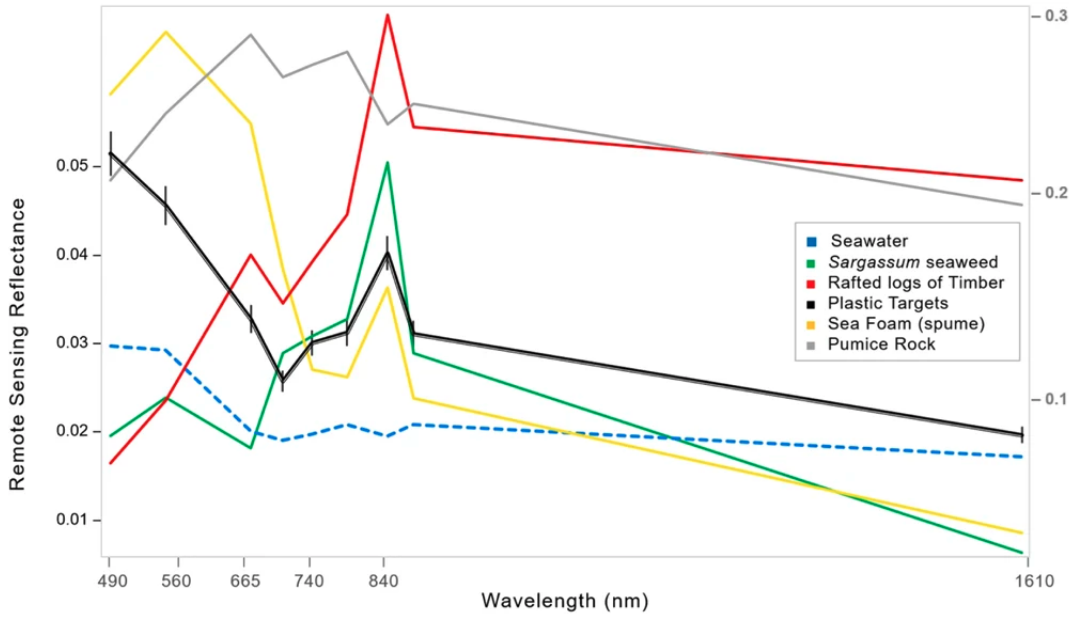

Figure 2.1: Spectral signatures from the mean spectra of plastic control samples deployed in a study (black line with error bars), suspected Sargassum (green), and seawater (dashed blue line). The wavelengths show the span of Sentinel-2 MSI bands, from visible light at 490nm to short-wave infrared at 1610nm. Figure from Biermann et al. (2020)

Algae Index (FAI) (Hu et al. 2015), and the Alternative Floating Algae Index (AFAI) (Wang et al. 2018). Indices compute a value using a specified equation that utilises the reflectance measurements to classify each pixel. NDVI is calculated using the Near Infrared (NIR) and red (Red) reflectance and is expressed as:

$$NDVI = \frac{(NIR - Red)}{(NIR + Red)} \tag{2.3}$$

The NDVI is primarily used to explore the health and density of vegetation. For *Sargassum* the NDVI provides a high contrast between observed *Sargassum* and the background within images. While León-Pérez et al. (2023) found the NDVI useful in observing fresh and un-decaying *Sargassum* rafts, the NDVI isn't commonly used for long-term *Sargassum* datasets. Instead studies have preferred to use either the FAI or AFAI. The FAI includes Shortwave Infrared (SWIR), and is expressed as:

$$FAI = R_{RC}(NIR) - R'_{RC}(NIR) \tag{2.4}$$

$$R'_{RC}(NIR) = R_{RC}(Red) + [R_{RC}(SWIR) - R_{RC}(Red)]\frac{\lambda(NIR) - \lambda(Red)}{\lambda(SWIR) - \lambda(Red)} \tag{2.5}$$

where R_{RC} is the Rayleigh corrected top of atmosphere reflectance and $\lambda(NIR)$, $\lambda(SWIR)$, and $\lambda(Red)$ are the wavelengths of the NIR, SWIR, and red bands respectively. When using Moderate Resolution Image Spectroradiometer (MODIS) imagery, the AFAI is the most common applied index for *Sargassum*. The AFAI is essentially measuring enhanced red-edge reflectance (an enhanced reflectance in the NIR wavelengths). While similar to the FAI, the AFAI is expressed as:

$$AFAI = R_{RC}(NIR_1) - R'_{RC}(NIR_1) \tag{2.6}$$

$$R'_{RC}(NIR_1) = R_{RC}(Red) + [R_{RC}(NIR_2) - R_{RC}(Red)]\frac{\lambda(NIR_1) - \lambda(Red)}{\lambda(NIR-2) - \lambda(Red)} \tag{2.7}$$

where NIR_1 is the MODIS band at 748nm and NIR_2 is the band at 869nm. The application of an index relies on the availability of bands depending on the satellite used as bands vary dependent on sensors, see Table 2.1 for the band wavelengths for varying satellite datasets.

Table 2.1: Specifications for the satellites commonly used to observe *Sargassum*: Aqua, Terra, Envisat, and Sentinels. Specifications include the sensor, spatial resolution (m) of the products, and wavelengths (nm) for the red, NIR, and SWIR bands where applicable.

Satellite	**Sensor**	**Spatial Resolution (m)**	**Red (nm)**	**NIR (nm)**	**SWIR (nm)**
Aqua	MODIS	250, 1000	620-670	841–876	1628-1652
Terra	MODIS	250, 1000	620-670	841–876	1628-1652
Envisat	MERIS	300	620 - 680	760-900	N/A
Sentinel-2A	MSI	10, 20	650-680	780-880	1565-1655
Sentinel-2B	MSI	10, 20	650-680	780-880	1565-1655
Sentinel-3	OLCI	300	600-700	700-900	N/A

The use of the 1km resolution of the long 19-year MODIS reflectance dataset allowed for the full extent of the GASB to be visualised by Wang et al. (2019). The formation of the GASB in 2011, and the consequent years of blooms was displayed using the percentage cover of *Sargassum* per pixel and analysed using applied indices, such as the FAI, to the images. FAI values detect the enhanced NIR reflectance on the ocean surface, to spot rafts of *Sargassum* floating in thin bands (Figure 2.2). Enhanced FAI values combined with the shape of *Sargassum* values indicate the presence of *Sargassum* rafts but cannot distinctively quantify the amount of *Sargassum* present. MODIS provides a global dataset compared to Sentinel-2's sparse coverage of the open ocean, therefore providing a more comprehensive view of the extent of *Sargassum* across the North Atlantic Ocean. Sentinel-2 would be

better suited to studying coastal populations of *Sargassum* and subsequent inundation events. However, Ody et al. (2019) hypothesised that when solely using MODIS data to observe *Sargassum*, smaller rafts go unaccounted for due to its spatial resolution which may have large impacts on the movement and growth of the bloom. To assess these smaller rafts, Ody et al. (2019) suggested the use of a combination of the OLCI on-board Sentinel-3 and the Multispectral Instrument (MSI) on-board Sentinel-2 to measure *Sargassum* at a higher resolution. The OLCI sensor can produce images at a 300m resolution while the MSI images are at a 10m resolution. To detect *Sargassum*, a Maximum Chlorophyll Index (MCI) was computed from the radiance differences from the OLCI data meaning it is relatively insensitive to the effects of cloud and aerosols (Gower and King 2011). An issue with these higher resolution images is that the temporal resolutions, of 4 and 5 days for the OLCI and MSI respectively, are significantly lower than the one-day revisit time that MODIS has. However, a solution of combining the datasets within a study would eliminate the issue of temporal resolution, as the MODIS data could be used for a time-series of the *Sargassum* with the OLCI/MSI looking into detail of MODIS determined *Sargassum* areas.

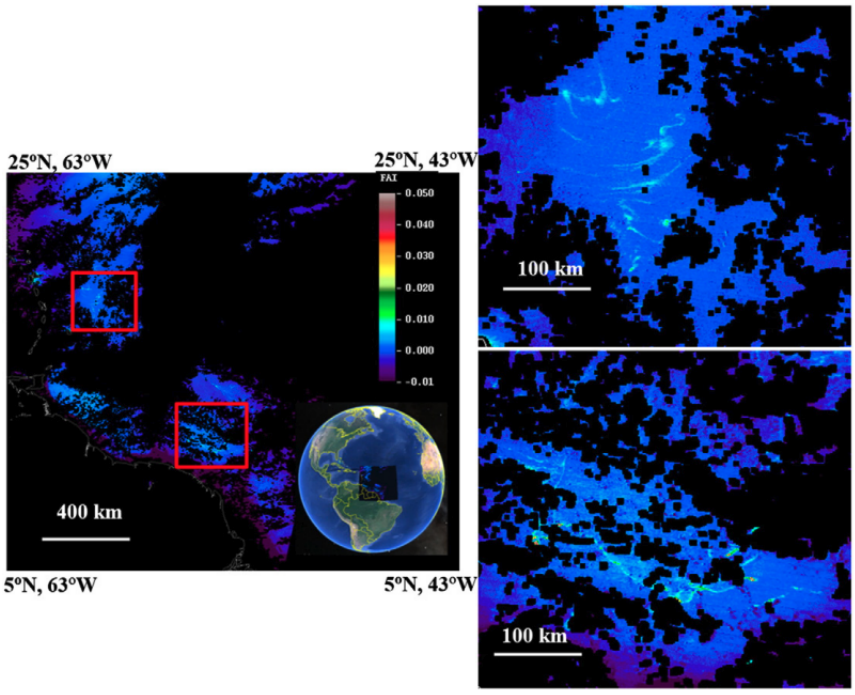

Figure 2.2: MODIS/Terra FAI image on 1 July 2012 (14:15 GMT) over the central West Atlantic showing surface slicks with enhanced NIR reflectance. Black colour indicates land or clouds or a sun glint mask. Figure from Hu et al. (2015).

Using these earth observation techniques can aid in the prediction of *Sargassum* inunda-

tion events. Maréchal et al. (2017) conducted a study on an early prediction system called the Sargassum Watch System (SaWS). SaWS uses a combination of earth observation images, an AFAI index and surface ocean currents. To provide near real-time updates on *Sargassum*, the system uses the Virtual Antenna System which creates quick processed MODIS datasets 4-6 hours after an overpass with a real-time numerical model for the surface currents. The study highlighted some issues with the SaWS, the biggest factor was false signals created by both cloud shadow and coastal eutrophication. Detecting *Sargassum* within the open ocean faces fewer errors compared to detecting it in coastal waters within the Caribbean Sea. The false signals can alter the index readings by enhanced reflectance received, however, one solution to minimise the error is by observing the shape of the reflectance in the images. *Sargassum* has a distinctive signal shape, described by Maréchal et al. (2017) as slicks, that form long curved lines that are visible over a few days, this separates the *Sargassum* from phytoplankton blooms which are ephemeral and vary each day.

2.5 Modelling *Sargassum* Physiological Behaviours

Sargassum physiology has been modelled in several recent studies demonstrating distributions in particle tracking simulations of *Sargassum* are improved with the addition of growth and decay as dense patches of particles may not always relate to dense patches of biomass (Brooks et al. 2019; Wang et al. 2019; Jouanno et al. 2021; Marsh et al. 2021). Brooks et al. (2019) was the first to integrate *Sargassum* physiology along particle trajectories using a simple growth and decay equation:

$$\frac{\partial Sarg}{\partial t} = Sarg \times f(I) \times f(T) \times f(N) \times \mu max_S - m \times Sarg \tag{2.8}$$

Where the change in *Sargassum* depends on individual functions of measured irradiance (I), temperature (T), nitrates (N) and a predetermined mortality rate. While Jouanno et al. (2021) used a more complex description of *Sargassum* physiology as the difference between the uptake and loss rates of organic carbon (C), nitrogen (N), and phosphorus

(P) applied in a Eularian framework:

$$\frac{\partial C}{\partial t} = U_C - \theta_C \tag{2.9}$$

$$\frac{\partial N}{\partial t} = U_N - \theta_N \tag{2.10}$$

$$\frac{\partial P}{\partial t} = U_P - \theta_P \tag{2.11}$$

Where U_C, U_N and U_P are the uptake rates of C, N, and P, respectively, while θ_C, θ_N, and θ_P determine the loss rates. The net change in U_C and θ_C determine the growth and mortality in *Sargassum* organic carbon, C. U_C is determined by:

$$U_C = C \times \mu_{max} \times f[T] \times f[I] \times f[Q_N] \times f[Q_P] \tag{2.12}$$

where individual functions of sea surface temperature (T), irradiance (I), N quota (Q_N) and P quota (Q_P) are multiplied by the maximum uptake rate for *Sargassum* (μ_{max}) and the value for *Sargassum*. It has been shown that it is possible to model *Sargassum* using a simplified growth model onto particle tracking trajectories, as in Marsh et al. (2021)'s SARTRAC model and within Brooks et al. (2019). Jouanno et al. (2021) increased the complexity of their physiological model, by adding in phosphates and independent nutrient uptake rates, but also increased the computational effort by producing a stand alone Eularian NEMO framework.

The C content of *Sargassum* can be determined from observed biomass using a mean carbon-to-dry-weight ratio of 27% (Wang et al. 2019; Jouanno et al. 2021). The maximum uptake rate of *Sargassum* is determined in Jouanno et al. (2021) as 0.084 d^{-1} based on the results a previous study of *Sargassum* nutrient limitation (Lapointe et al. 2014). This value falls within the range of growth rates, 0.029 to 0.11 d^{-1}, that have been used within *Sargassum* studies (Lapointe 1986; Lapointe et al. 2014; Hanisak and Samuel 1987).

Temperature dependence for macroalgae typically follows an optimum growth curve (Martins and Marques 2002), where growth is maximum at the optimum temperature but the rate falls as the temperature deviates from this optimum value. Brooks et al. (2019) used a simplified version of a temperature dependence function, with the assumption that growth

ceases below 18°C (T_{ref}):

$$f[T] = \begin{cases} 1, Temp \geq T_{ref} \\ 0, Temp < T_{ref} \end{cases} \tag{2.13}$$

While Jouanno et al. (2021) and (Marsh et al. 2021) used a more complex function to better create the temperature dependence curve, based on the earlier stated results from Martins and Marques (2002):

$$f[T] = e^{-\frac{1}{2}\left(\frac{T-T_{opt}}{T_x-T}\right)^2} \tag{2.14}$$

where T_x is determined as T_{min} if $T \leq T_{opt}$; or T_{max} if $T \geq T_{opt}$. T_{opt} is the optimum temperature for maximum *Sargassum* growth, T_{min} is the minimum temperature for *Sargassum* growth, and T_{max} is the maximum temperature for *Sargassum* growth. However, within the Fortran code of the model produced by Jouanno et al. (2021), there is a deviation from their written equation. This study used the equation found within the Fortran code, with only a minor change to the value multiplied within the exponent:

$$f(T) = e^{-2\left(\frac{T-T_{opt}}{T_x-T}\right)^2} \tag{2.15}$$

Brooks et al. (2019) describes *Sargassum*'s dependence on light as:

$$f[I] = \left(1 - e^{\frac{-I}{I_k}}\right) \times f(age) \tag{2.16}$$

where there is an exponential decay in a light response at increasing ages. Jouanno et al. (2021) opted to not include age as a component in their model, but instead described the light dependency as:

$$f[I] = \frac{1}{2} + e^{\left(-0.1 \times \frac{I}{I_{opt}}\right)} \tag{2.17}$$

where, similar to temperature, it describes the relationship between the measured radiation, I, and the optimum radiation for *Sargassum* growth (I_{opt}) (I_k in (Brooks et al. 2019)). This function was created by Jouanno et al. (2021) in order to recreate results by Hanisak and Samuel (1987). However, the effect of light intensity on macroalgae was described in Martins and Marques (2002) as:

$$f(I) = \frac{I}{I_{opt}} \times e^{\frac{I}{I_{opt}}} \tag{2.18}$$

This irradiance function by Martins and Marques (2002) closely follows the relationship described within both Brooks et al. (2019) and Jouanno et al. (2021) but is based on a greater amount of research (Häder et al. 1999; Martins and Marques 2002). This equation was chosen to represent the effects of light intensity.

Sargassum growth is nutrient limited, specifically nitrate and phosphate limited. Where the availability of inorganic nitrates and phosphates directly impact the growth rate (Lapointe et al. 2014; Lapointe et al. 2021; McGillicuddy et al. 2023). As nitrate is considered a limiting nutrient, Brooks et al. (2019) modelled the nutrient uptake as a Monod function:

$$f(N) = \frac{N}{k_{Sarg} + N} \tag{2.19}$$

where N is the measured inorganic nitrate and k_{Sarg} is the uptake half-saturation ($mmolNm^{-3}$). Jouanno et al. (2021) not only included phosphates in their *Sargassum* model, but also increased the complexity by including the internal C:N:P stoichiometry and consider the uptake separately. With the limited research on *Sargassum* nutrient quotas, Jouanno et al. (2021) applied the hyperbolic relationship shown in brown seaweed to their *Sargassum* model (Hanisak and Samuel 1987). Therefore, the dependence on the internal nitrogen and phosphorus quotas ($Q_N = N/C$; $Q_P = P/C$) was computed as a hyperbolic curve controlled by the minimum and maximum quotas:

$$\begin{aligned} f\left(Q_N\right) &= \left(\frac{1 - \frac{Q_{N\,\min}}{Q_N}}{1 - \frac{Q_{N\,\min}}{Q_{N\,\max}}}\right) \\ f\left(Q_P\right) &= \left(\frac{1 - \frac{Q_{P\,\min}}{Q_P}}{1 - \frac{Q_{P\,\min}}{Q_{P\,\max}}}\right) \end{aligned} \tag{2.20}$$

where the values are dependent on predetermined minimum (Q_{Nmin}; Q_{Pmin}) and maximum quota values (Q_{Nmax}; Q_{Pmax}).

Jouanno et al. (2021) described the uptake of nitrogen and phosphorus as a relationship between the maximum nitrate (V_{Nmax}) and phosphate (V_{Pmax}) rates, Monod functions N and P uptakes, and a function of quota to represent the down regulation of the transport system for N and P when approaching the maximum quotas, taken from Lehman et al.

(1975):

$$U_N = V_{N\max} \times C \times \left(\frac{N}{K_N + N}\right)\left(\frac{Q_{N\max} - Q_N}{Q_{N\max} - Q_{N\min}}\right)$$
$$U_P = V_{P\max} \times C \times \left(\frac{P}{K_P + P}\right)\left(\frac{Q_{P\max} - Q_P}{Q_{P\max} - Q_{P\min}}\right) \tag{2.21}$$

Loss rates describe the mortality of the *Sargassum*. In the model by Brooks et al. (2019), Equation 2.8, mortality is simply described as a constant mortality rate. Jouanno et al. (2021), however, relate natural ageing and decomposition of *Sargassum* as a growing function of temperature based on previous studies (Bendoricchio et al. 1994; Ren et al. 2014). Therefore, a maximum mortality rate (m), mortality coefficient (λ_m) and temperature (T) are used to describe the loss in carbon:

$$\theta_C = C \times \left(\frac{m}{e^{-\lambda_m \times (T-30)}}\right) \tag{2.22}$$

while the loss of the nutrients is a function of the loss of biomass and internal nutrient quotas:

$$\theta_N = \theta_C \times Q_N \tag{2.23}$$

$$\theta_P = \theta_C \times Q_P \tag{2.24}$$

Brooks et al. (2019), Wang et al. (2019), Marsh et al. (2021), and Jouanno et al. (2021) are currently the only studies to utilize *Sargassum* growth models within their investigations. Brooks et al. (2019), Wang et al. (2019), and Marsh et al. (2021) calculated along-trajectory growth using particle tracking outputs. Wang et al. (2019) used a simplified model with a growth rate based off satellite observations rather than directly considering *Sargassum* physiology. Marsh et al. (2021) produced the SARTRAC Ensemble Forecast System where a simplified physiological model was applied to particle trajectories and was able to produce a clear seasonal cycle. Similarly, Brooks et al. (2019) calculated growth and mortality but with added individual functions of irradiance and nitrates. For this study, I have chosen to follow the more complex model provided by Jouanno et al. (2021) but with modifications based on the previous literature and my own sensitivity tests.

2.5.1 Summary of the *Sargassum* Model

While the above section explored the formulation and reasoning behind the *Sargassum* model for this study, for clarity and a clear reference this section will summarise the equations and terms used.

Sargassum was defined as the change in uptake (U) and loss (θ) rates of C, N and P:

$$\frac{\partial C}{\partial t} = U_C - \theta_C \tag{2.25}$$

$$\frac{\partial N}{\partial t} = U_N - \theta_N \tag{2.26}$$

$$\frac{\partial P}{\partial t} = U_P - \theta_P \tag{2.27}$$

Uptake of *Sargassum* biomass, U_C, was defined as:

$$U_C = C \times \mu_{max} \times f[T] \times f[I] \times f[Q_N] \times f[Q_P] \tag{2.28}$$

where individual functions of temperature (T), irradiance (I), N quota (Q_N) and P quota (Q_P) are multiplied by the maximum uptake rate for *Sargassum* (μ_{max}) and the value for *Sargassum*.

The temperature function, $f[T]$ was described as:

$$f(T) = e^{-2\left(\frac{T-T_{opt}}{T_x-T}\right)^2} \tag{2.29}$$

where T is the sampled temperature, T_{opt} is the optimum temperature and T_x is determined as T_{min} if $T \leq T_{opt}$; or T_{max} if $T \geq T_{opt}$.

The irradiance function, $f[I]$, was described as:

$$f[I] = \frac{1}{2} + e^{\left(-1 \times \frac{I}{I_{opt}}\right)} \tag{2.30}$$

where the sampled I is related to the optimum Irradiance, I_{opt}.

The dependence on the internal nitrogen and phosphorus quotas ($Q_N = N/C$; $Q_P = P/C$)

was computed as a hyperbolic curve controlled by the minimum and maximum quotas:

$$\begin{aligned} f\left(Q_N\right) &= \left(\frac{1-\frac{Q_{N\,\min}}{Q_N}}{1-\frac{Q_{N\,\min}}{Q_{N\,\max}}}\right) \\ f\left(Q_P\right) &= \left(\frac{1-\frac{Q_{P\,\min}}{Q_P}}{1-\frac{Q_{P\,\min}}{Q_{P\,\max}}}\right) \end{aligned} \tag{2.31}$$

A maximum mortality rate (m), mortality coefficient (λ_m) and temperature (T) were used to describe the loss in carbon:

$$\theta_C = C \times \left(\frac{m}{e^{-\lambda_m \times (T-30)}}\right) \tag{2.32}$$

N (U_N) and P (U_P) uptake rates were described as a relationship using maximum N (V_{Nmax}) and P (V_{Pmax}) rates:

$$\begin{aligned} U_N &= V_{N\,\max} \times C \times \left(\frac{N}{K_N+N}\right)\left(\frac{Q_{N\,\max}-Q_N}{Q_{N\,\max}-Q_{N\,\min}}\right) \\ U_P &= V_{P\,\max} \times C \times \left(\frac{P}{K_P+P}\right)\left(\frac{Q_{P\,\max}-Q_P}{Q_{P\,\max}-Q_{P\,\min}}\right) \end{aligned} \tag{2.33}$$

While the N (θ_N) and P (θ_P) loss rates were described as:

$$\theta_N = \theta_C \times Q_N \tag{2.34}$$

$$\theta_P = \theta_C \times Q_P \tag{2.35}$$

Chapter 3

Variability in transport from the Sargasso Sea to the Equatorial Atlantic: Lagrangian View

3.1 Introduction

Pelagic *Sargassum* seaweed has populated the North Atlantic for centuries, with early recordings from transatlantic sailors. Two species, and their sub-species, are free floating and therefore predominantly found within the Sargasso Sea, bounded by the currents of the North Atlantic subtropical gyre, with limited observations outside of the Sargasso Sea (Huffard et al. 2014). See Section 1.1 for a detailed description on *Sargassum* species and its lifecycle within the North Atlantic. After 2011, sudden accumulations of *Sargassum* became an annual event for the countries within and surrounding the Caribbean Sea (Fidai et al. 2020). Using remote-sensing observations, a large population of *Sargassum* was first detected in 2011 within the Equatorial Atlantic, much further south than the original population within the Sargasso Sea, forming what Wang et al. (2019) named the GASB. At its peak, the GASB can span from the Gulf of Mexico to the west coast of Africa and weigh 20 million metric tons (Wang et al. 2019) (Figure 3.1). While showing seasonal variability, similar to other large macroalgae, the GASB also displays high interannual variability in which the mean coverage can differ by over at least $2000 km^2$ per year (Figure 3.1).

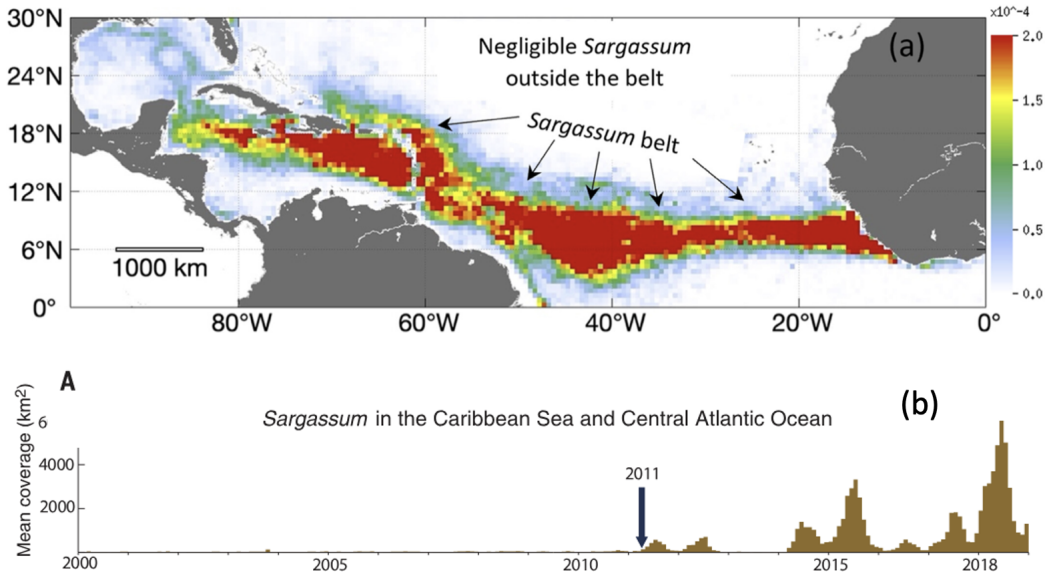

Figure 3.1: Sargassum distribution and interannual variability. (a) Satellite observations of the Great Atlantic Sargassum Belt (GASB) that stretches from west Africa to the Gulf of Mexico, using data between 2011 and 2020 during the months of June to November. The colour legend indicates fractional cover or areal density (e.g., $1.0 \times 10^{-4} = 0.01\%$). Figure retrieved from Putman and Hu (2022) (b) Monthly Sargassum coverage for the Caribbean Sea and Central Atlantic Ocean (area in plot above), retrieved from Wang et al. (2019).

Due to its free-floating nature, the movement of *Sargassum* is vulnerable to the forces of wind and waves, as well as to the large-scale surface currents. Before 2011, *Sargassum* was trapped by the currents of the subtropical gyre within the surface waters. Typically, this floating debris entrained within the gyres cannot escape (Martinez et al. 2009), therefore, the question arises as to how *Sargassum* was able to escape the Sargasso Sea to form the GASB within the Equatorial Atlantic. This is what we address in our study.

For movement to be solely due to the large-scale processes, floating particles need to be fully submerged within the surface waters within that Ekman layer. *Sargassum*, however, can protrude out of the water and can be influenced by direct wind force (windage), where an added wind-displacement velocity can alter the transport of floating debris (Astudillo et al. 2009). Another source of transport to consider is Stokes drift, which is the residual transport from waves. In the open ocean, the propagation of surface gravity waves creates a net drift velocity to floating particles at the surface in the direction of wave propagation (Stokes 1847). It is important to note that there are also sub-mesoscale processes that can impact the transport of floating debris that are not resolved within high resolution models and therefore typically not considered. Sub-mesoscale processes are on scales smaller than

a few tens of kilometres and are known to be important in surface drifter accumulations (Pearson et al. 2020) and even the transport and dispersion of oil spills (McWilliams 2016). Including dispersion when exploring surface debris transport represents the transport from sub-mesoscale processes, creating a more realistic representation of movement.

Due to the immediate impacts experienced in the Caribbean, studies have primarily focused on studying the GASB within the Equatorial Atlantic, either by satellite observations (Gower et al. 2013; Wang et al. 2019), ocean models (Putman et al. 2018; Jouanno et al. 2021), or a mix (Wang and Hu 2017; Marsh et al. 2021; Marsh et al. 2022); however, there have been some earlier studies on *Sargassum* within the Sargasso Sea (Niermann 1986; Gower and King 2011; Lapointe et al. 2014). As the Sargasso Sea has limited nutrient input, Gower and King (2011) explored the idea of an external source of *Sargassum* as one hypothesis as to why *Sargassum* has thrived there for so long. Satellite imagery revealed *Sargassum* within the Gulf of Mexico that flowed into the Sargasso Sea. The Gulf of Mexico has nutrient inputs from the Mississippi River with SSTs that fall within *Sargassum*'s optimal range and the currents within the Gulf of Mexico are consistent with the transport of *Sargassum* into the open ocean of the Sargasso Sea where it would recirculate. If this population of *Sargassum* in the Sargasso Sea was centuries old and trapped within the boundary currents of the subtropical gyre, how could it seed the GASB?

Prior to 2011, *Sargassum* was restricted to the Sargasso Sea by the circulation produced by the North Atlantic subtropical gyre. See Figure 1.2 (Section 1.1) for a schematic of the major currents within the North Atlantic. The gyre's boundary currents consists of the Gulf Stream (GS), Azores Current (AzC), and the North Equatorial Current (NEC), creating an area of convergence within the centre. This area of convergence is known as the Sargasso Sea. The strong boundary currents of the gyre typically constrained the pre-2011 *Sargassum* population, keeping it within the Sargasso Sea. Johns et al. (2020) hypothesised that *Sargassum* was somehow transported out of the gyre and into the main flow of the Canary Current (CC) to form the GASB. The AzC has not been named in relation to *Sargassum* transport, however, its most eastern branch feeds into the CC. The AzC has three branches, with the most easterly branch being generally the weakest with the first two branches directing the currents in towards the gyre, producing the circular motion of the gyre. The AzC is fuelled by the GS, therefore the strength is directly related

to GS variability.

Johns et al. (2020) suggested that *Sargassum* was transported to the Equatorial Atlantic along the CC prior to the first bloom in 2011. To explore the transport, Johns et al. (2020) used a combination of surface drifter data, particle backtracking simulations, and satellite observations, to explore the connectivity between the Sargasso Sea and the Equatorial Atlantic. Johns et al. (2020) released particles within the Caribbean Sea, between April and June in 2011, to explore potential paths *Sargassum* may have taken. Their results indicate two pathways dependent on transport duration, the longest route of 2 years flowed through the Equatorial Atlantic and north towards the Sargasso Sea while the shorter 1-year route towards the western Sargasso Sea through the Greater Antilles which bypassed the majority of the Caribbean Sea (Figure 3.2).

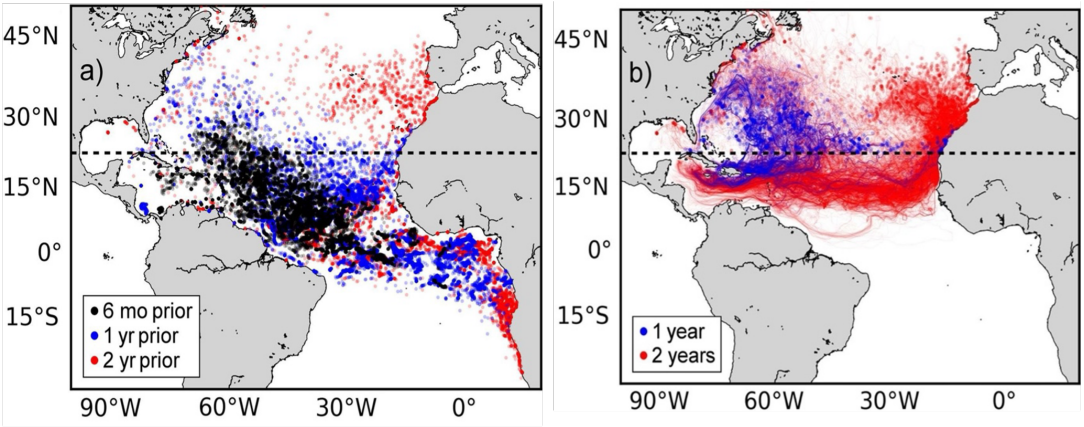

Figure 3.2: Results from Johns et al. (2020)'s study showing a) end of simulation locations for 30000 particles and b) trajectories of those particles that travelled above 23°N after (blue) 1 year and (red) 2 years. Figure extracted from Johns et al. (2020)

For *Sargassum* to be transported from the Sargasso Sea to the Equatorial Atlantic, as proposed by Johns et al. (2020), it needed to escape the boundary currents of the gyre. Using the timing of the GASB formation, an extreme NAO event was named as the cause (Wang et al. 2019; Johns et al. 2020). The NAO is an index related to the difference in atmospheric pressure between Iceland and the Azores and influences the position of the jet stream and the weather over Europe and the North Atlantic. The NAO can be in a positive or negative phase, which influences the strength and direction of the wind over the North Atlantic Ocean (Hurrell 1995). There are two major wind patterns over the North Atlantic: The Westerlies and the Northern Trade Winds. The westerlies originate between 30 and 45°N and blow towards the northeast. Further south, the stronger Northern Trade Winds

originate between approximately 10 and 20°N and blow towards the west and slightly southwest. A negative phase of the NAO is defined by the presence of high pressure over Greenland and a low pressure over the Azores, resulting in weakened Northern Trade Winds but strengthened Westerlies (Deser et al. 2017). The most extreme negative phase of the NAO in the last 150 years (Jung et al. 2011) occurred in the winter of 2009/2010, highlighted in Figure 1.9.

Particle tracking simulations, such as those used in Johns et al. (2020), use the outputs from ocean circulation models and can be used to simulate the movement of various quantities, such as water (Marez et al. 2024; Fried et al. 2024), plankton (Byers and Pringle 2024), and plastic Onink et al. 2019. Particle tracking simulations have proven to be very useful for determining the transport pathways of *Sargassum*. For example, Putman et al. (2018) used synthetic particle tracking to determine a transport pathway, along the North Brazil Current, connecting the Equatorial Atlantic and the Caribbean Sea. Putman et al. (2018) was also able to determine that *Sargassum* west of 50°W had a high probability of entering the Caribbean Sea.

As *Sargassum* is typically transported by a combination of surface currents, waves (Stokes drift), and wind (windage), studies using particle tracking methods can use a combination of these to explore transport under different conditions. Windage values for *Sargassum* can vary between 1-3% (Johns et al. 2020; Putman et al. 2020; Marsh et al. 2021; Jouanno et al. 2021; Marsh et al. 2022). (Putman et al. 2018) used a windage of 1%; simulations that included windage led to increased transport of *Sargassum* into the Caribbean from the Equatorial Atlantic, compared to the simulations that did not include windage. However, the results were not validated with in situ or remote observations, so it was not clear what value of windage fully represents the real-life windage experienced by *Sargassum*. Berline et al. (2020) used hindcast simulations and observations of *Sargassum* in 2017, within the Equatorial Atlantic, to determine the effect of the windage value on particle transport in relation to observations. Simulations with a 1% windage produced results that most closely aligned with observations, but it was noted that changes in windage values produced little differences in results. Jouanno et al. (2023) stated that the addition of Stokes drift created a significant difference in the large-scale distribution of *Sargassum* and have included it in the creation of their *Sargassum* model. However, some key *Sargassum* studies decided to

omit Stokes drift from their studies, focusing instead on the effects of wind (Brooks et al. 2019; Wang et al. 2018; Johns et al. 2020; Zhang et al. 2024).

Due to their usefulness in characterizing *Sargassum* transport, we also used particle tracking simulations in this study. Similarly to Johns et al. (2020), this study aimed to explore the necessary conditions needed to transport *Sargassum* from the Sargasso Sea to the Equatorial Atlantic and eventually the Caribbean Sea. However, unlike the backtracking models within Johns et al. (2020), these simulations used can include a random walk to include the variability (dispersion) caused by small-scale processes that otherwise isn't included in the ocean models. Also, this study aimed to explore the effect of Stokes drift, in combination with surface currents and wind, on the advection of *Sargassum* within the North Atlantic Ocean.

Although there is a hypothesised transport route from the Sargasso Sea to the Equatorial Atlantic, it remains uncertain whether changes in surface winds over the North Atlantic during 2009/2010 were sufficient to release *Sargassum* from the North Atlantic subtropical gyre. Additionally, it is unclear if this event was an isolated occurrence or part of a recurring pattern. To address this research gap, we employ particle tracking simulations to assess the potential for *Sargassum* to escape the Sargasso Sea and contribute to the formation of the GASB in 2011, and to characterize the conditions necessary for such an event.

3.2 Methods

3.2.1 Particle Tracking and Model Outputs

To explore the movement of *Sargassum* between the North Atlantic subtropical gyre and the equatorial Atlantic, version 2.0 of the Parcels (Probably a Really Computationally Efficient Lagrangian Simulator) (Delandmeter and Sebille 2019) was used to model *Sargassum* transport as synthetic particles that are advected by ocean model outputs. A particle's position is calculated using Equation 2.2, described in section 2.3. The velocity at the particle's location is obtained through linear interpolation of the velocity field, which depending on the simulation, can consist of a combination of surface currents, Stokes drift and wind, further described in Section 1.3. Only the horizontal transport is considered

in this study to calculate *Sargassum*'s transport across the surface of the ocean, therefore only 2D surface currents are used for the simulations. A fourth order Runge-Kutta integration was used to compute the particle tracking with a time-step of 2 days. Further descriptions of particle tracking, and its applications, can be found in (Sebille et al. 2018).

Ocean surface currents were obtained from the CMEMS Global Ocean Physics Reanalysis (GLORYS12V1) product outputs. CMEMS reanalysis products use an ocean circulation model with assimilated satellite sea level anomaly, sea surface temperature, and sea ice concentration as well as in situ temperature and salinity profiles. Observations are assimilated into the model by means of a reduced-order Kalman filter to produce model outputs that produce a truer representation of previous ocean conditions. Our study used daily GLORYS12V1 outputs at a 1/12° (8km) spatial resolution for a sub-region between 0 to 60°N and 80°W to 5°W; this spatial resolution includes both large scale surface currents and eddies but does not resolve sub-mesoscale processes that occur at and below a 1km resolution (McWilliams 2016). It is noted that the data outputs are pre-interpolated onto an A-grid from the NEMO model's native C-grid, somewhat degrading the resolution towards the coasts. For particle tracking simulations, this can lead to excessive particle beaching but for as this study is primarily focussed on open ocean transport, it is not as detrimental to the results.

Wave induced transport is parameterised by Stokes drift, which is calculated using wave height and period (Breivik et al. 2016). The CMEMS Global Ocean Waves Analysis and Forecast product was used at 1/12°spatial resolution and a temporal resolution of 3 hours (Ardhuin et al. 2009). The direct transfer of momentum from surface winds, the windage, is dependent on the floating object size, shape, and buoyancy (Chubarenko et al. 2016; Onink et al. 2019). It is achieved by adding a percentage of the surface wind velocity to the advection field. 1% windage was selected for this study due to it being the most favourable outcome of windage sensitivity tests within other studies that recreated *Sargassum* transport (Putman et al. 2018; Berline et al. 2020; Marsh et al. 2022). For consistency, we used the ERA5 reanalysis surface winds, which provided hourly outputs of the easterly and westerly components (Hersbach et al. 2020).

The effects of random walk were implemented to represent dispersion and to capture the sub-mesoscale processes, that may not be resolved within the ocean circulation model.

Within Parcels, this is achieved with a Brownian Motion kernel which applies a random walk to the advection of the particles with a specified horizontal diffusivity coefficient, which for this study was $100m^2s^{-1}$. The diffusivity coefficient was chosen due to its effectiveness within other similar studies (Franks et al. 2016; Beron-Vera et al. 2016; Putman et al. 2018; Johns et al. 2020; Berline et al. 2020). The diffusivity coefficient can vary across the North Atlantic from 10 to $1000m^2s^{-1}$ (Zhai and Greatbatch 2006) and so using a constant value will both overestimate and underestimate diffusion in different areas across the North Atlantic. Sensitivity tests were run to explore the impact of the dispersion on initial outputs of this study (Figure 3.3). Particles in both simulations were advected with currents, Stokes drift, and 1% windage but the first simulation had added diffusion with a diffusivity coefficient of $100m^2s^{-1}$ (Figure 3.3a), and the second simulation omitted the diffusion parameters (Figure 3.3b). Simulations ran for just 10 days to visualise the effects of dispersion on particle trajectories. Particles are seen to flow to the west from their release position, indicated with a black dot. Dispersion causes particle trajectories to spread more (Figure 3.3a) when compared to the simulation with no dispersion (Figure 3.3b) but does not impact the direction or distance travelled by the particles. Results determined minimal differences in outputs with and without dispersion, meaning the choice of coefficient likely causes minimal disruption to the results of our study.

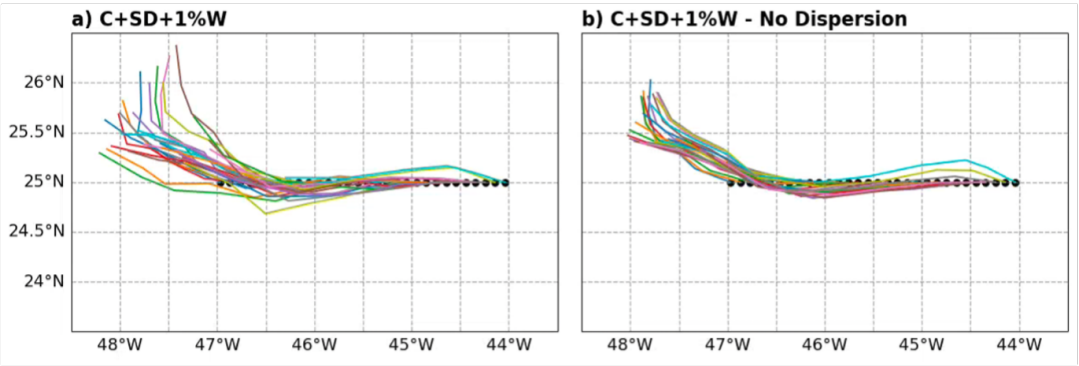

Figure 3.3: Dispersion sensitivity test. Particles in both simulations were advected with currents, Stokes drift, and 1% windage but a) included diffusion with a diffusivity coefficient of $100m^2s^{-1}$ and b) did not include diffusion. Release locations of particles are shown with black dots.

3.2.2 Experiment Design

Particles were released in a 100 by 100 grid, at the surface of the ocean, within the Sargasso Sea region and were re-released every 5 days from January 2007 to December 2015. To investigate the effect of the different hydrographic variables on particle transport, three simulations with varying conditions were used. All particle simulations included dispersion, but the three simulations used varying advection fields that included:

1. Surface currents only (C)
2. Surface currents + Stokes drift ($C + SD$)
3. Surface currents + Stokes drift + 1% windage ($C + SD + W$)

The three conditions were chosen based on similar studies using particle tracking to either model *Sargassum* or other floating particles (Putman et al. 2018; Johns et al. 2020). Particle locations were recorded every other day of the simulations for analysis. The domain of the study was set as 100°W to 10°E in longitude and 5°S to 60°N in latitude. Any particles that reached the edges of the domain were removed at that point. Similarly, any particles that became stranded, that is where the surface current values were equal to zero, were also removed . Trajectories were recorded up until the time of removal. The location of release was chosen to seed particles within the Sargasso Sea to observe their movement within the gyre. Release times of 5 days coincide with the general output times of most ocean numerical models and reduce bias when seeding particles in each simulation by producing a high volume of particles.

3.3 Results

This chapter aims to explore the possibility of particle transport between the North Atlantic Subtropical Gyre and the Equatorial Atlantic, and the conditions necessary for that transport.

3.3.1 Transport of Particles

Particle densities were calculated, averaged annually on a 1°x 1°grid across the North Atlantic (between 70 to 10°W and 10°S to 50°N) to show annual distributions of the different simulations on a logarithmic scale (Figure 3.4). The density plots for the $C + SD + W$

simulation show particles spread across the North Atlantic and into the Equatorial Atlantic (below 10°N) in 2009. Particles start with a high concentration within the Sargasso Sea (Figure 3.4a and Figure 3.4b). As particles become spread across the North Atlantic, the density below 10°N increases. Particles remain within the Equatorial Atlantic through to 2013, then the density starts to decrease. The decrease in particle density within this region could be due to increased beaching but also highlights a lack of particles entering the area after 2013. Particle densities increasing south of 10°N between 2009 and 2012 demonstrate the possibility of transport between the Equatorial Atlantic and the Sargasso Sea, whereas the decrease in particle density below 10°N after 2013 suggests this transport was an anomalous event.

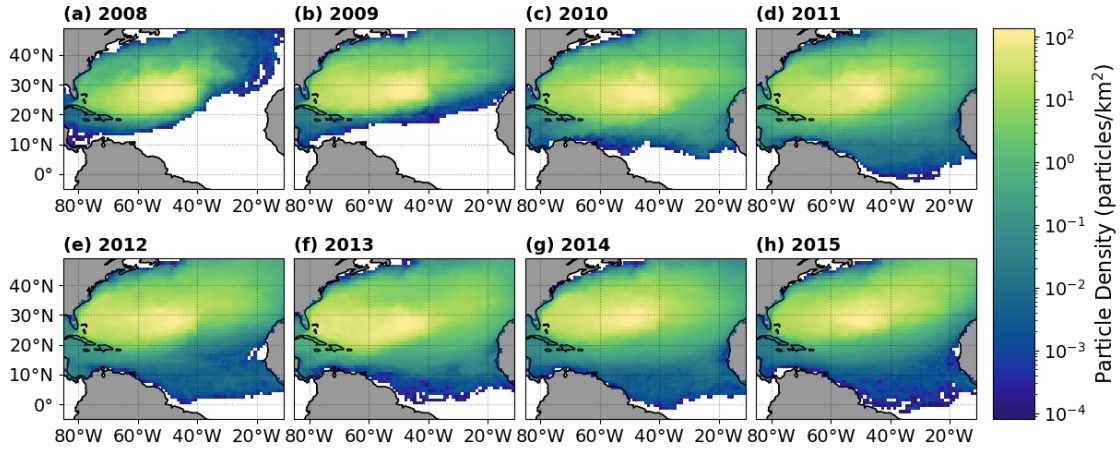

Figure 3.4: Particle densities across the North and Equatorial Atlantic for simulation $C + SD + W$ where particles are advected with currents, Stokes drift and 1% windage.

The annual densities provide an insight into the general distribution of particles during each year and demonstrate particle transport into the Equatorial Atlantic (Figure 3.4). To understand the driving forces behind the particle transport, we need to consider the timeline of events. Figure 3.5 shows the number of particles within the Equatorial Atlantic at each time step (2 days) for each release year of the $C + SD + W$ simulation. Up until 2009, there are no particles within the Equatorial Atlantic (below 10°N). In 2009, we the number of particles within the Equatorial Atlantic start to increase, with most of these particles having been released in both 2007 and 2008. The number of particles within this region peaks in 2010, with over 250 particles from the 2007 releases and more than 150 from 2008 (Figure 3.5). The maximum number of particles, from all releases, within the Equatorial Atlantic peaked at 0.018%. The percent of particles within the Equatorial

Atlantic then steadily dropped from 2011 onwards. Interestingly, particles only enter the Equatorial Atlantic in 2009 regardless of release date, suggesting that the same conditions sustained transport out of the Sargasso Sea for the particles released in both 2007 and 2008.

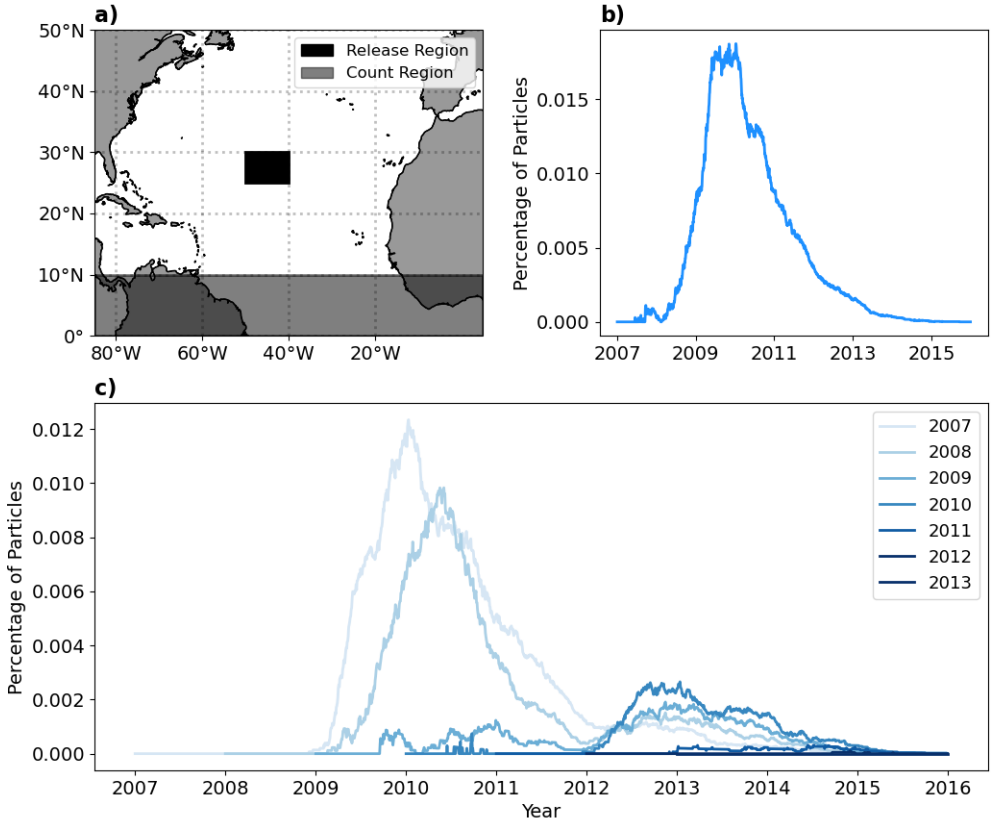

Figure 3.5: a) Map showing the particle release region (black box) and the Equatorial Atlantic region as defined in this study (grey box). b) The total number of particles within the Equatorial Atlantic region over time for the $C + SD + W$ simulation c) Number of particles within the Equatorial Atlantic over time for the $C+SD+W$ simulation separated by release year, e.g. the lightest line shows only those particles that were released in 2007.

Particle trajectories were able to show the transport route taken between the Sargasso Sea and the Equatorial Atlantic. The transport route is illustrated in Figure 3.6, within trajectories for selected particles that travelled below the 10°N line of latitude. We can see that particles moved east out of the Sargasso Sea towards West Africa (east of 20°W) and along the coast south into the Equatorial Atlantic (Figure 3.6). The particles travelled south along the CC, as hypothesised by Johns et al. (2020). Prior to entering the CC, the particles flow along the AzC, at 34°N where they leave the Sargasso Sea. The AzC is one of the currents that forms the North Atlantic subtropical gyre, as an outflow of the Gulf Stream, and forms three branches (Frazão et al. 2022). Two of the branches recirculate

the flow in towards the centre of the gyre, the third however feeds into the CC (Volkov and Fu 2011). The third branch, that feeds into the CC, is typically the weakest. However, our results indicate that it was a key method of transport of *Sargassum* out of the Sargasso Sea.

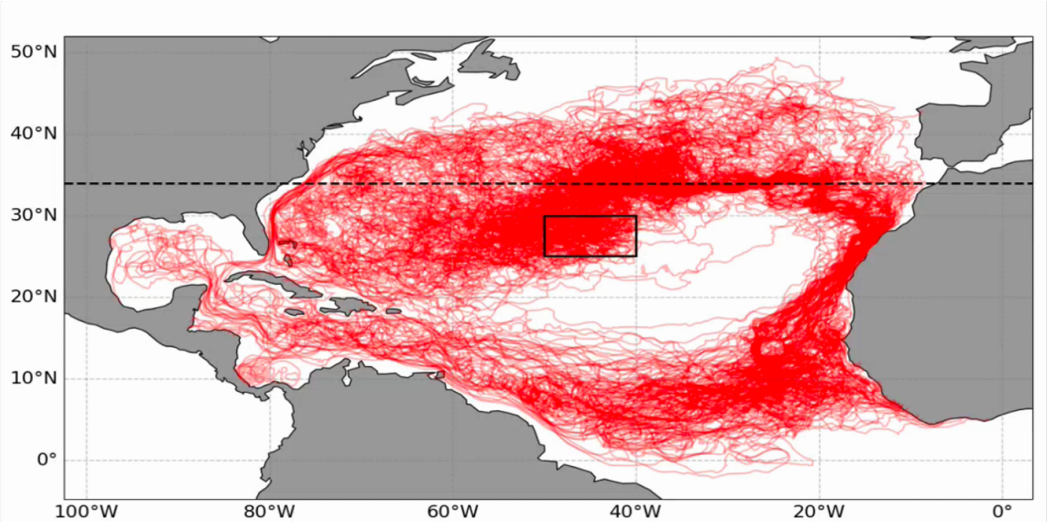

Figure 3.6: Particle trajectories, from the $C+S+W$ simulation, for particles that travelled below the 10°N line of latitude during the simulation. The dashed black line indicates the average latitude of the Azores Current (AzC) outlined in Figure 1.2. Solid black box indicates the particle release region.

So far, the results presented show particles advected with currents, Stokes drift and 1% windage to demonstrate simply that particle tracking simulations are able to determine *Sargassum* transport between the Sargasso Sea and the Equatorial Atlantic. As stated in Section 1.3.3, there are several windage values that have been used to simulate *Sargassum* but for the windage scenarios 1% windage was chosen based off its frequent use in leading studies (Franks et al. 2016; Putman et al. 2018; Johns et al. 2020; Berline et al. 2020). Sensitivity tests were conducted, similar to the sensitivity tests shown in Figure 3.3, to explore the effects of different windage values on particle trajectories. Particles were advected with 0%, 1%, 2%, and 3% windage for 10 days and to further explore the impact those windage values were tested with just currents and then repeated with wind ($C+W$; Figure 3.7 left column) and then again with the addition of Stokes drift ($C+SD+W$; Figure 3.7 right column). While the different windage of 1%, 2% and 3% do provide changes in particle trajectories, the difference in trajectory direction and distance is minor. The change is greater, however, between the 0% and 1% simulations for both $C+W$ and $C+SD+W$ simulations to confirm that the addition of wind to particle advection does

affect particle trajectory, but the choice of percentage is not as important.

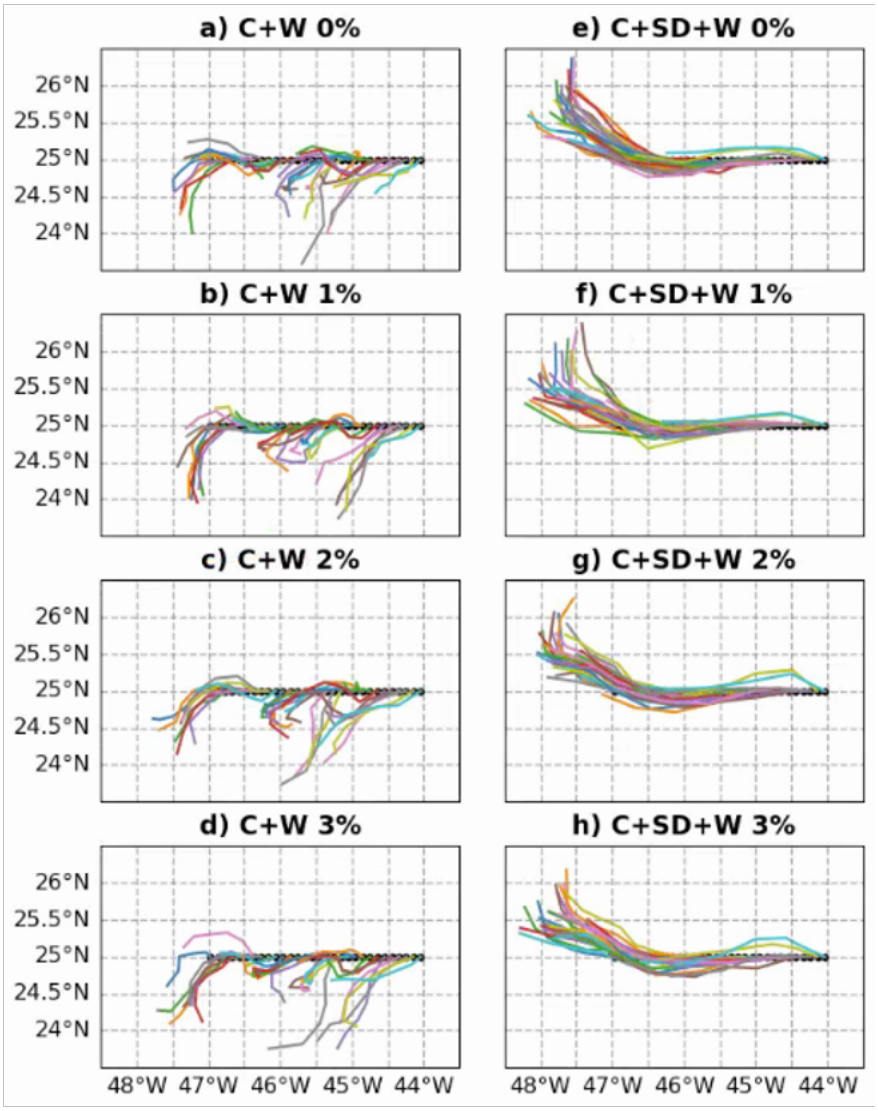

Figure 3.7: Simulations to test the effect of various windage values. Windage values of 0, 1, 2, and 3% were used for advection with currents (left column) and with added Stokes drift (right column).

3.3.2 Drivers of Transport

So far results have indicated a key driver of transport out of the Sargasso Sea was the AzC, due to the where particle trajectories were seen leaving the Sargasso Sea (Figure 3.6). The AzC is an area of increased eastward transport at about 34°N, the strength of which varies annually, with peaks of more than $0.15 ms^{-1}$ in 2010 and 2013 (Figure 3.8). Monthly NAO phases are illustrated in Figure 3.9b, positive in blue and negative in red, showing a prolonged negative NAO phase between mid 2009 to the end of 2011 which aligns with the peak surface current speed in Figure 3.8. The eastern component of the surface currents,

plotted in Figure 3.8, also shows a prolonged peak over the negative NAO phase across the winter months of 2009/2010. Across the whole NAO index, currents of the AzC increase in speed to the east during the negative phase.

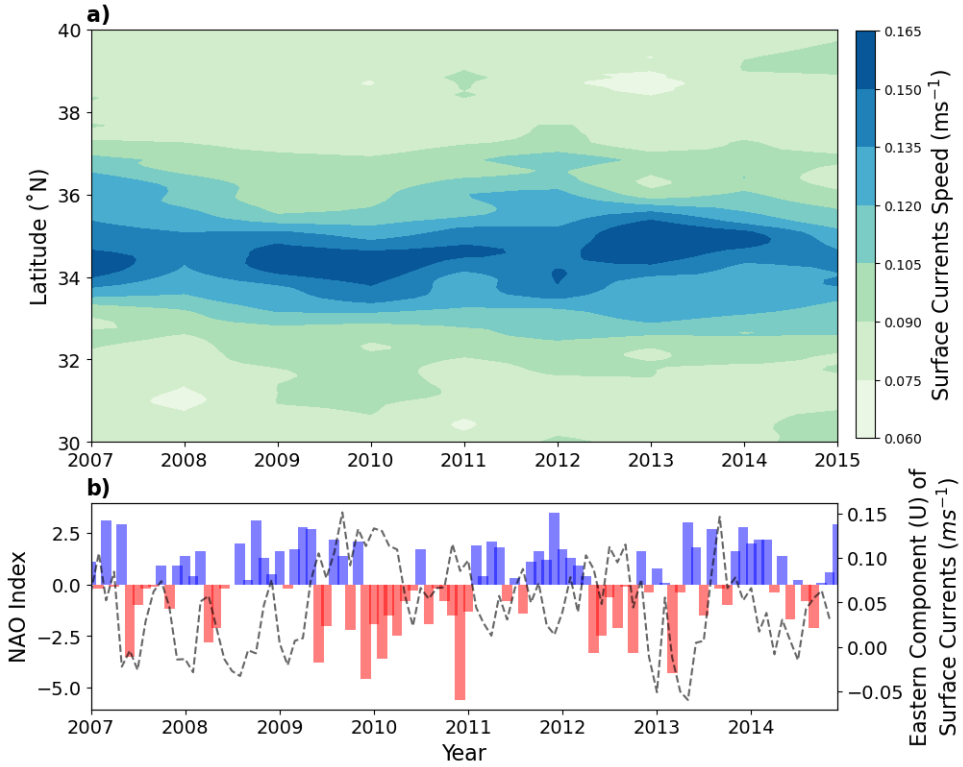

Figure 3.8: a) Hövmoller plot showing averaged surface currents between 30°N and 40°N over time. b) Monthly NAO index demonstrating the phase over time. Blue indicates a negative phase, red indicates a positive phase. A prolonged negative phase is seen from 2009 to 2011. Dashed line shows easterly component of surface currents for the Azores Current area in a) to show the relationship between NAO phase and magnitude of easterly flowing currents

The three simulations within this study used varying advection fields that included: Surface currents only (C), Surface currents + Stokes drift ($C + SD$), and Surface currents + Stokes drift + 1% windage ($C + SD + W$). Results show inconsistencies between these three simulations. While the results show that particles escape the Sargasso Sea using an enhanced AzC (Figure 3.6; Figure 3.8), advection with surface currents only, within simulation C, does not provide the same export to the Equatorial Atlantic that we see in simulations with added Stokes drift and windage to the advection field (Figure 3.9). Comparing the spatial distribution of particles over time gives an idea of the difference in spread to the Equatorial Atlantic between the three simulations. Annual particle densities were calculated, like Figure 3.4, for each simulation are shown in Figure 3.9. Although the simulations were run from 2007 to the end of 2015, 2007 was not shown because it

was considered a "spin-up" year for the particle tracking model. Biennial densities were plotted to compare changes during key years, particularly before and after 2011. Particle densities remain highest within the centre of the gyre for simulation C while simulation $C + SD + W$ demonstrates particles spreading more across the Atlantic (Figure 3.9). Densities in Figure 3.10 also demonstrate the difference in particles within the Equatorial Atlantic; the densities below 10°N for the C simulation was a lot sparser compared to the $C+SD+W$ simulation. The results demonstrate that more particles are being constrained within the Sargasso Sea in the simulation with just surface currents, suggesting that the Stokes drift and windage drive the transport out of the Sargasso Sea.

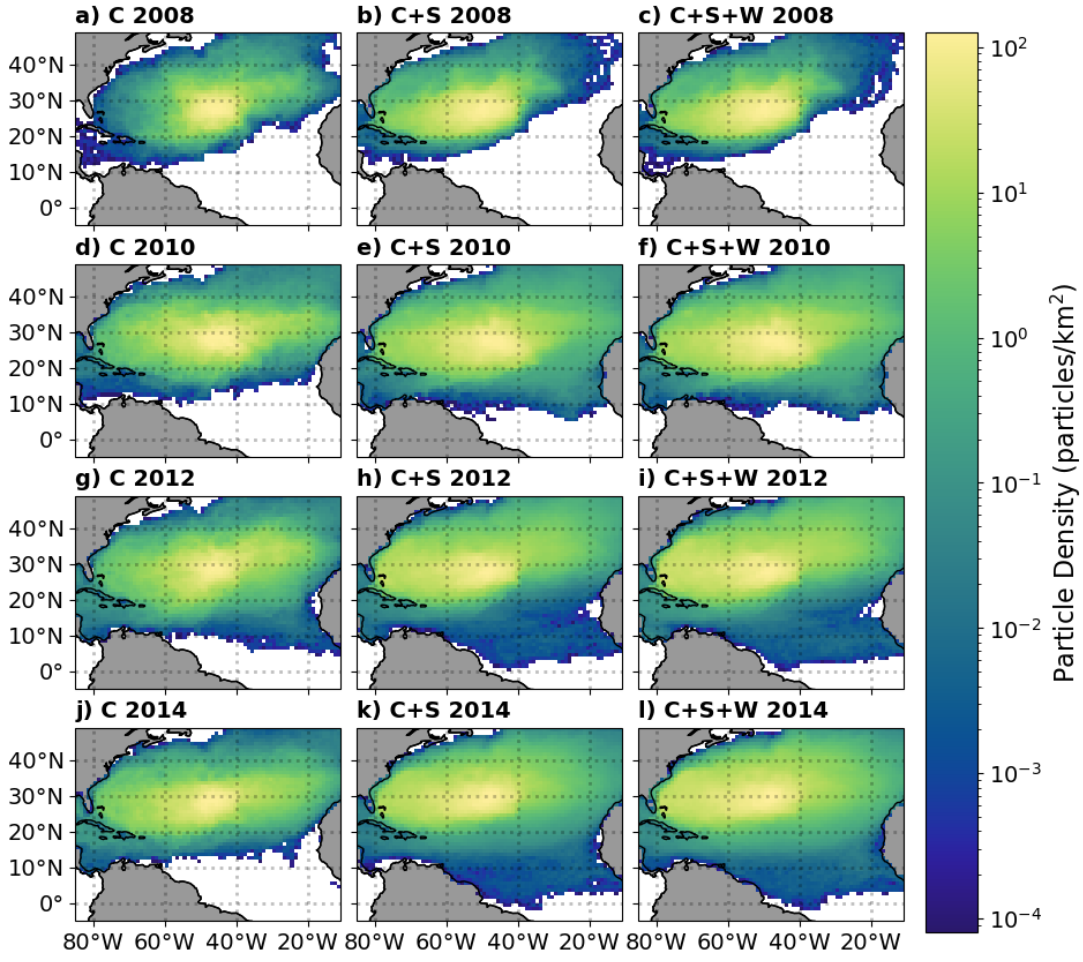

Figure 3.9: Particle density comparison between just surface currents, and with all three conditions: Currents (C), Stokes drift (SD) and 1% windage (W).

As results from the particle tracking simulations showed that advection with Stokes drift (simulation $C + SD$) and windage ($C + SD + W$) increased the transport of particles out of the Sargasso Sea and into the Equatorial Atlantic between 2009 and 2013, this

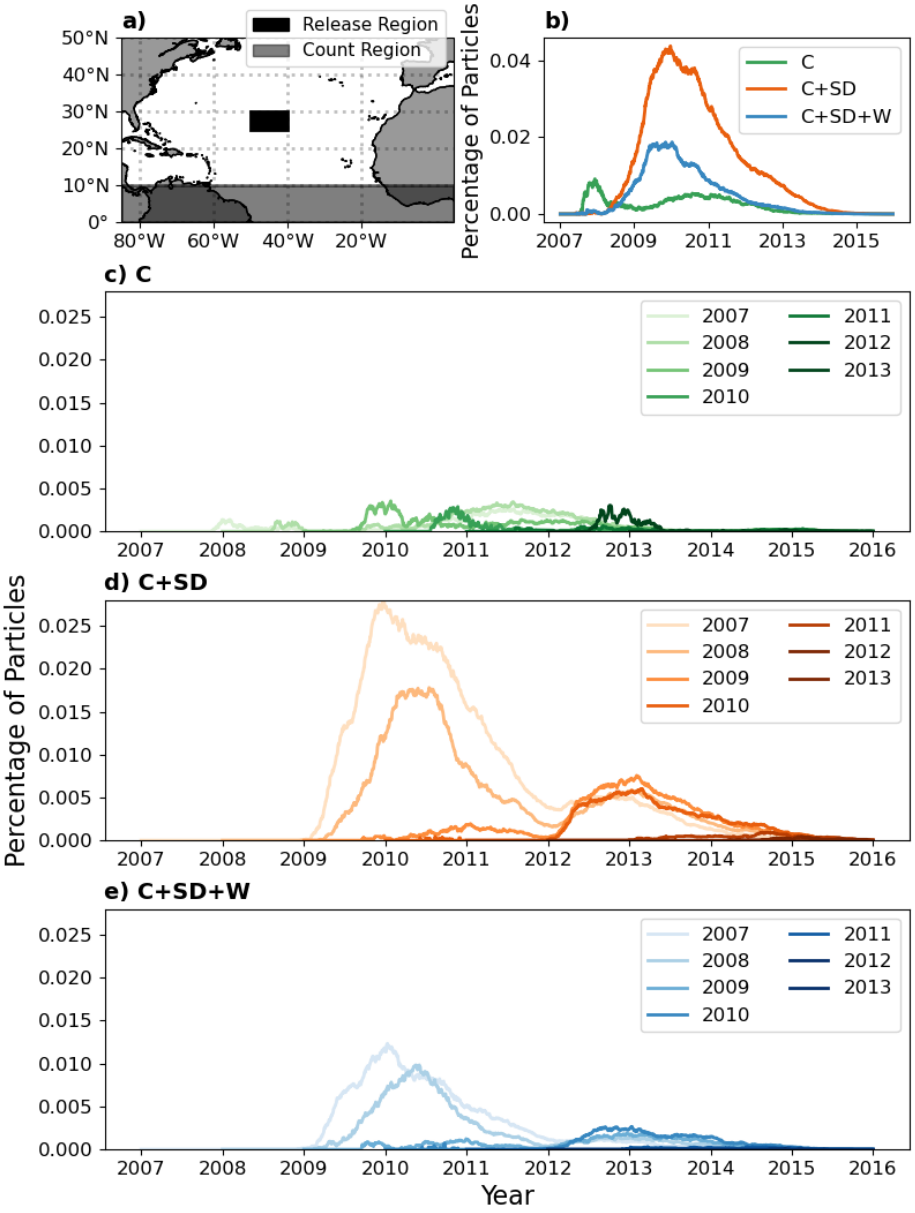

Figure 3.10: a) Map showing the particle release region (black box) and the Equatorial Atlantic region as defined in this study (grey box). b) The total number of particles within the Equatorial Atlantic region over time for each simulation. The number of particles within the Equatorial Atlantic are shown over time for the c) C d) $C + SD$ and e) $C + SD + W$ simulations. For c, d, and e, timelines are separated by release year, e.g. the lightest line shows only those particles that were released in 2007.

study looked for patterns within the currents, Stokes drift and wind. Figure 3.11 shows the averages for the entire simulation period from 2007 to 2015, for just 2010, and then the difference between the two. South of 25°N, the wind speed and Stokes drift values are lower in 2010 than the 2007-2015, but north of 25°N, the values are higher in 2010 then in the average values. In the areas that enhance transport to the east, values are increased, but where transport is enhanced back towards the centre of the gyre values

have decreased. As previously noted, a negative phase of the NAO tends to increase the strength of the Westerlies while weakening the Northern Trade Winds which is seen to have happened in 2010 (Figure 3.11i). The strengthened Westerlies is also shown within the Stokes drift data, with enhanced values over this region within 2010. While there is a slight southward shift within the Gulf Stream position, seen the most in Figure 3.11g, the basin wide change in surface currents is less extreme than the Stokes drift and wind.

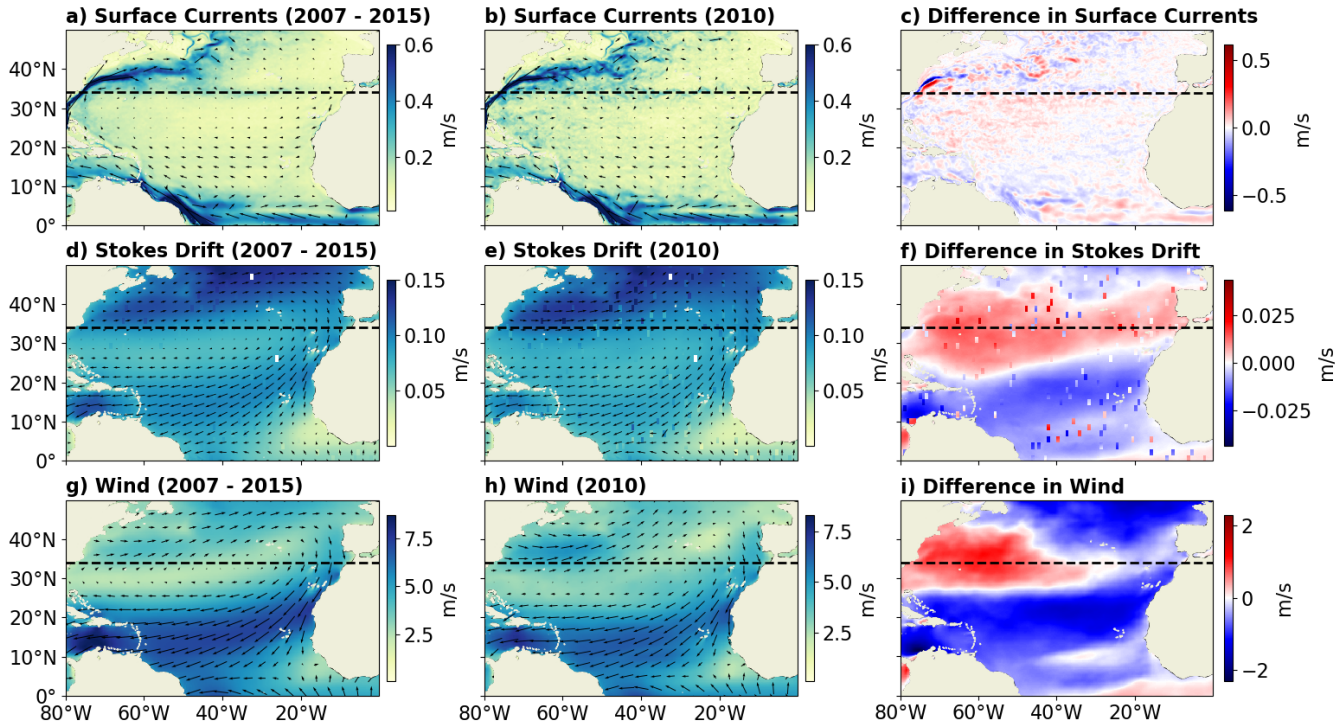

Figure 3.11: Plots of surface currents, stokes drift, and wind. The figure demonstrates the 2007-2015 average (a, d, g), the 2010 average (b, e, h) and the difference between the two (c, f, i). The difference is calculated as 2010 - the longer term average (2007 to 2015). The dashed line indicates the approximate latitude of the Azores Current.

The AzC was highlighted in Figure 3.11 (dashed line). Current velocities and wind speeds increased within this region in 2010, coinciding with both the timing of the transport of *Sargassum* (Fig 3.5) and latitude of which the trajectory paths exit the Sargasso Sea (Fig 3.6). The AzC flows eastward over the Mid-Atlantic Ridge (MAR) and is the most eastern outflow of the GS (Frazão et al. 2022). Due to its location and source, it is an unstable jet that is commonly observed forming multiple large eddies (Figure 3.12) (Silva-Fernandes and Peliz 2020). Prolonged strengthening of the AzC in 2010, visualised in Figure 3.8, was likely able to transport the Sargassum out of the Sargasso Sea and into the CC. It is also highly likely that the energy of the AzC from the eddies was not fully resolved within the ocean current model used within this Chapter's study. Therefore, underestimating transport and velocities within the AzC region.

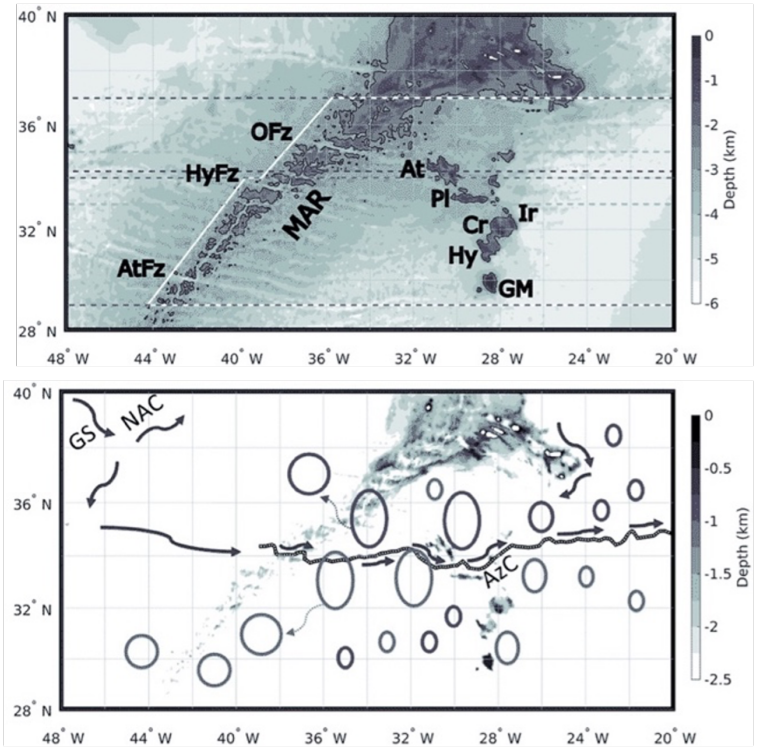

Figure 3.12: Bathymetry of the Azores Current (AzC) region (left) to show position of AzC in relation to the Mid-Atlantic Ridge (MAR). Schematic of the main currents and eddies within this region (right). Circles depict eddies that break off from the main branch of the AzC. Figure adapted from Silva-Fernandes and Peliz (2020)

3.4 Conclusions

Particle tracking simulations were able to demonstrate that transport of floating particles out of the Sargasso Sea was possible during 2009 to 2012, meaning that *Sargassum* was

able to be transported into the Equatorial Atlantic to form the GASB in 2011. Particle trajectories show that while particles travel along the CC, the AzC was key to them leaving the Sargasso Sea (Figure 3.6). A prolonged strengthening of the AzC in 2010 (Figure 3.8) was likely able to transport the *Sargassum* into the CC before it eventually reaching the Equatorial Atlantic.

Simulations demonstrated that Stokes drift was vital for transport between the Sargasso Sea and Equatorial Atlantic, while adding windage reduced the transport. Particles advected with surface currents and Stokes drift increased the spread of particles across the North Atlantic rather than them being concentrated within the centre of the gyre. Particles travelled from the Sargasso Sea to the Equtorial Atlantic during an extreme negative phase of the NAO over the winter of 2009/2010. In our results, stronger winds across the northwestern region of the North Atlantic, and in turn stronger Stokes drift, allowed the transport of particles out of the Sargasso Sea and towards the most eastern currents. The area surrounding both the AzC and CC, had reduced wind speeds within 2010 removing the barrier and allowing the particles to enter.

Chapter 4

Modelling Along Trajectory Growth and Decay

4.1 Introduction

Until 2011, holopelagic *Sargassum* was mostly confined to the Sargasso Sea (Gower and King 2011). *Sargassum* has since populated the Equatorial Atlantic with varying annual blooms that at their peak spanned the width of the Atlantic with a wet weight of >20 million metric tonnes (Wang et al. 2019). Although in open water it creates a useful symbiotic habitat, once *Sargassum* enters coastal waters it creates many environmental and socioeconomic impacts in the Caribbean Sea (Wang et al. 2019). Already vulnerable habitats, such as coral reefs, nesting sea turtles and birds have experienced worse conditions due to the huge volumes of *Sargassum*. Inundations also directly impact tourism and fisheries, which, for most countries within the Carribbean, make up most of their economies. Mexican authorities reported that between 10,105 - 40,903 m^3 per kilometre of *Sargassum* was harvested during their tourist seasons, costing between US$0.3 - 1.1 million per kilometre to recover and dispose of (Rodríguez-Martínez et al. 2020).

Growth of *Sargassum* is controlled by nitrogen and phosphorus availability, as well as temperature and light (Lapointe 1986; Lapointe et al. 2014). The Sargasso Sea is known as a nutrient limited, oligotrophic gyre which may inhibit *Sargassum* growth. This is why it is thought that the population of *Sargassum* was constrained when it was in the Sargasso Sea but abundant in the equatorial Atlantic where there are multiple sources

of nutrients from both upwelling regions and rivers (Kawase and Sarmiento 1985). Not much is known, however, on *Sargassum* growth during transport between the Sargasso Sea and the newly established population region within the Equatorial Atlantic. For example, does growth increase in regions of increased nutrient availability? As *Sargassum* rafts float within the surface waters of the ocean, its horizontal movement is driven by surface currents, the residual transport from waves (Stokes drift), and wind (Putman et al. 2018; Ody et al. 2019; Johns et al. 2020). Results from Chapter 3 determined that *Sargassum* was transported from the Sargasso Sea to the Equatorial Atlantic via the Azores and Canary Currents between 2009 and 2011, forming the GASB population. However, the particle tracking simulations provide insight into the physical transport of *Sargassum* but do not provide insights into any along-trajectory growth and decay that *Sargassum* may experience. Therefore, this study examined the changes in biomass associated with Chapter 3's particle trajectories to cement the idea that the formation of the GASB was caused by this physical movement of seaweed between the Sargasso Sea and Equatorial Atlantic.

A Eularian model framework was created by Jouanno et al. (2021) to reproduce *Sargassum* transport and physiology based on the existing NEMO model with added BGC state variables. The model was run for 2017 and tested against satellite measurements of *Sargassum* to evaluate its performance (Figure 4.1). The physiological parameters of the *Sargassum* NEMO model were able to reproduce the seasonal cycle of *Sargassum*, while the physical ocean model variables were able to recreate large-scale distributions. It is key to note that the highly patchy nature of *Sargassum*, where shapes, sizes, and locations of *Sargassum* rafts can change at daily timescales, make it a challenge to model at a fine resolution no matter the approach. Before the Jouanno et al. (2021) model, Brooks et al. (2019) used more simplified physiological parameters in combination with Lagrangian particle tracking and was able to reproduce *Sargassum* growth with a 65-75% accuracy when compared to satellite observations. Combining numerical and BGC models with Lagrangian particle tracking can produce *Sargassum* studies with minimal computational effort, compared to running the Eularian *Sargassum* ocean model, with the added ability of exploring factors that control both its transport and growth.

While it has been established that *Sargassum* can be transported from the Sargasso Sea

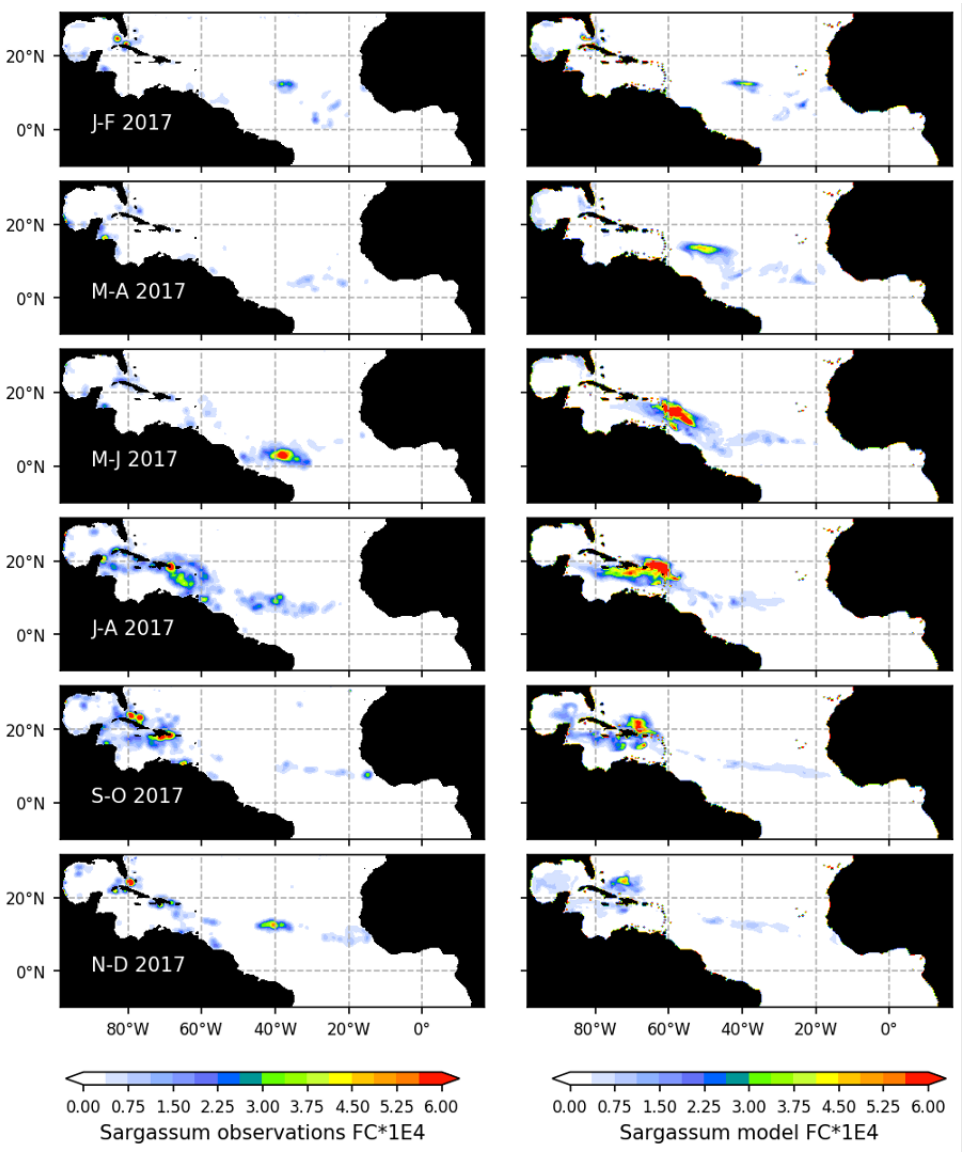

Figure 4.1: Seasonal distribution of Sargassum fractional coverage for the year 2017 from satellite observations (left) and from model outputs (right). Figure extracted from Jouanno et al. (2021)

to the Equatorial Atlantic, several questions still remain. Can it survive this journey? Does the transport route offer the conditions necessary for *Sargassum*'s survival and even its growth? To address this key research gap, this chapter aims to investigate the along-trajectory growth of *Sargassum* as it travels from the Sargasso Sea to the Equatorial Atlantic, forming the Great Atlantic *Sargassum* Belt. By combining known physiological behaviours with particle tracking outputs created within the previous chapter, we aim to identify areas of enhanced growth and assess the potential for *Sargassum*'s survival on its journey to the Equatorial Atlantic.

4.2 Methods

Sargassum biomass was modelled using a combination of particle tracking outputs and equations that describe physiological behaviours. Growth and mortality rates were calculated along trajectories to get an overall change in biomass. Particle tracking simulations sample ocean variables, such as temperature and light, as well as nutrient concentrations at each particle's location to get a view of the conditions the *Sargassum* would experience within the North Atlantic Ocean.

4.2.1 Particle Tracking and Growth Analysis

Sargassum movement can be simulated using synthetic particle tracking; refer to Section 2.3 for a full description of the particle tracking methodology. Velocity was obtained through linear interpolation of the velocity field which consists of the sum of the surface currents, Stokes drift (residual transport from waves) and windage. A fourth order Runge-Kutta integration was used to execute the particle tracking at a time-step of 2 days. Further descriptions of particle tracking, and its applications, can be found in Sebille et al. (2018). Parcels is a fully customisable python package that was used for the particle tracking simulations. Field sampling is a feature of parcels that allows the physical conditions of each particle (such as temperature or nutrients) to be sampled at each time step, for either exploration into physical drivers or for this case, growth analysis. At each particle's location, temperature, irradiance, nitrate and phosphate values were obtained to compute changes in biomass. Biomass was calculated as per the equations described in Section 2.5.

4.2.2 Model Based Driving Data

The CMEMS Global Ocean Physics Reanalysis (GLORYS12V1) ocean model provided the surface currents used for advection and the sampled temperature data. The reanalysis products use a numerical ocean circulation model with assimilated satellite sea level anomaly, sea surface temperature, and sea ice concentration, as well as *in situ* temperature and salinity profiles. Observations are assimilated by means of a reduced-order Kalman filter to produce a model that produces a truer representation of ocean conditions than a numerical model only. GLORYS12V1 outputs are daily with a 1/12°spatial resolution for a sub-region between 0 to 60°N and 80°W to 5°W. A 1/12°(8km) model includes both large

scale surface currents and eddies but does not resolve all submesoscale processes that occur at 1km resolution (McWilliams 2016). The CMEMS Global Ocean Waves Analysis and Forecast was used to provide Stokes drift at a 1/12°spatial resolution but with a temporal resolution of 3 hours. It was subset to the same sub-region as the GLORYS12V1 outputs. For consistency, ERA5 reanalysis wind data, which was used for advection, was also used to include the direct transfer of momentum to floating material (windage). ERA5 was also one of the forcing datasets for both CMEMS numerical models (Hersbach et al. 2020).

The CMEMS Global Ocean BGC Hindcast model was used to provide nitrate and phosphate concentrations that are sampled at a 1/4°spatial resolution, with daily outputs. The hydrodynamic model component is the CMEMS GLORYS2V4-FREE ocean physics model, and the atmosphere component is the ERA-Interim product. The BGC aspect of the model requires initial conditions combined with global parameters to reproduce biogeochemical properties of the ocean. This CMEMS BGC model used data from the WOA 2013 dataset for the initial nitrate, phosphate, silicate and oxygen values and the CMEMS GLODAPv2 dataset for initial dissolved inorganic carbon values. Nutrient data from the WOA are derived from a wide range of in-situ observations and is often used to initialise and validate numerical ocean models, such as this CMEMS model, as well as to validate satellite observations. This BGC model also includes external sources of nutrients, such as from atmospheric dust and rivers, within its nutrient calculations. Outputs from the GLORYS BGC model would be expected to differ from real concentrations due to it having a limited representation of the marine ecosystem within the model equations. For example, there may be enhanced nutrient uptake rates in certain regions from sudden algal blooms. It also means that the nutrient values used within the model do not represent any competition between *Sargassum* and other autotrophs, as was the case within Jouanno et al. (2021). Even though the CMEMS BGC model used the WOA dataset for the intial conditions, the differences will have a knock on impact along the length of the model run. Here we used the WOA data to explore the reliability of the BGC model data used within this study. Figure 4.2 shows the 2013 seasonal averages of nitrate concentrations in the WOA data, the GLORYS BGC model used in this study, and the difference between the two. Red areas indicate where the modelled nitrates are overestimated, while blue indicates where nitrates are underestimated. Figure 4.3 instead visualises phosphates.

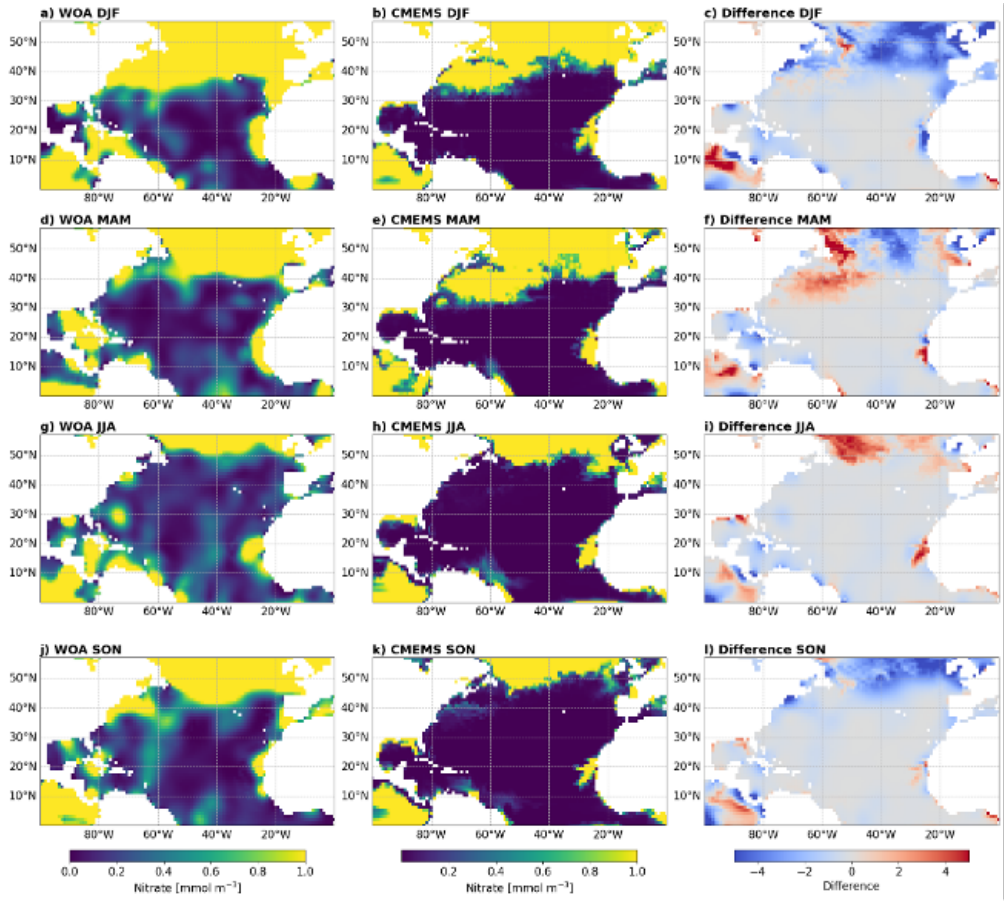

Figure 4.2: Seasonal averages in 2013 for (left) the World Ocean Atlas (WOA) nitrates, (middle) GLORYS BGC modelled nitrates, and (right) shows the differences between the two datasets. Red shows where the model overestimates nitrate availability and blue shows where the model underestimates.

There is a key difference to note within the nitrate data, in Figure 4.2f, where there is an overestimation within the northwest of the subtropical gyre during the spring months. Otherwise generally, the inconsistencies for both nutrient datasets are minimal, and it can be assumed that the GLORYS BGC model can represent the nutrient dynamics within the North Atlantic Subtropical Gyre well enough for this chapter's growth simulations.

4.2.3 Experiment Design

Study Experiment

Particles were released in a 100 × 100 grid within the Sargasso Sea (between 60 to 55°W, and 30 to 35°N) and were re-released every 5 days. Particles are advected horizontally with a summed velocity field that consists of surface currents, Stokes drift, and 1% windage to represent *Sargassum* transport as realistically as possible based on previous studies (Ody

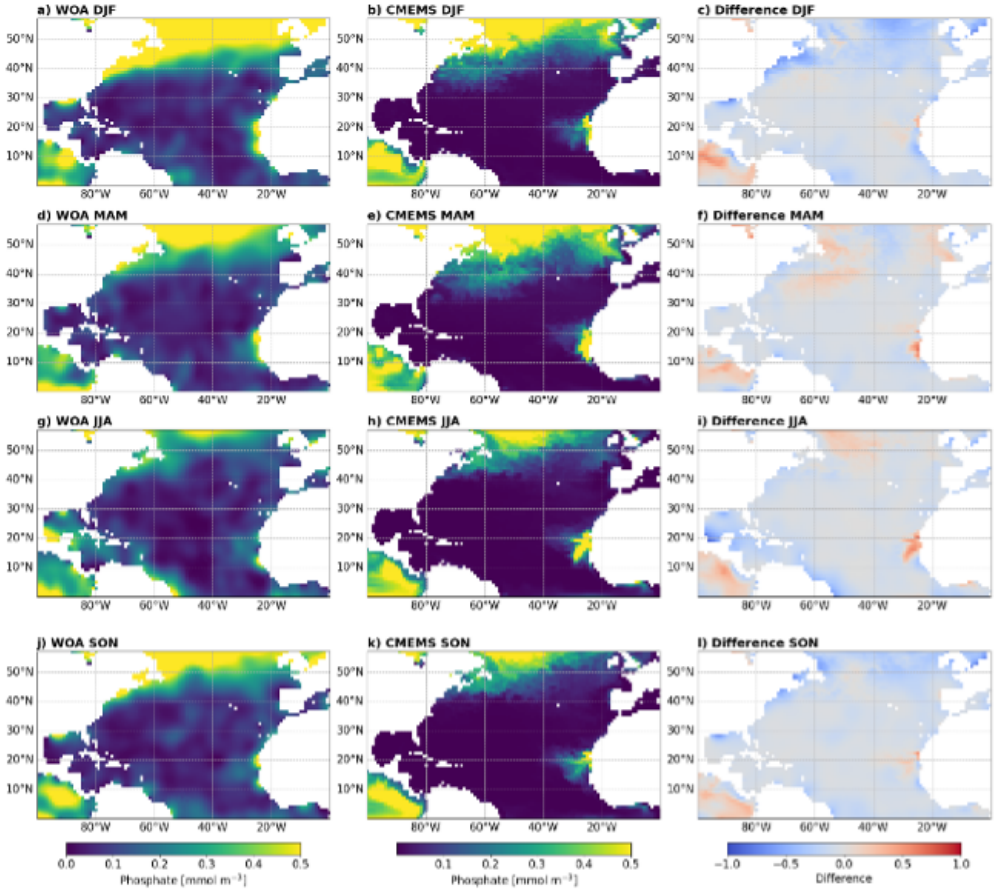

Figure 4.3: Seasonal averages in 2013 for (left) the World Ocean Atlas (WOA) phosphates, (middle) GLORYS BGC modelled phosphates, and (right) shows the differences between the two datasets. Red shows where the model overestimates phosphate availability and blue shows where the model underestimates.

et al. 2019; Johns et al. 2020; Lara-Hernández et al. 2024). Dispersion, with a dispersion coefficient of $100ms^{-2}$, was added to include advection from sub-mesoscale eddies that are not resolved within the numerical ocean current model. Temperature, solar radiation, inorganic nitrogen, inorganic phosphorus, inorganic carbon values were sampled at each particle location and at each timestep for post-processing analysis.

To investigate change in biomass along Lagrangian trajectories, particles need to be given an initial biomass which is then converted into carbon concentration. Figure 4.4 shows *Sargassum* wet-weight biomass density across the North Atlantic Ocean using satellite imagery from 2006-2011 (Wang et al. 2019). An initial carbon value for the particles was calculated using a single wet-weight biomass (kg/m^2) value averaged over the North Atlantic from 2007-2011, which was first converted into dry weight using a typical dry-to-wet-weight ratio of roughly 15% (Milledge and Harvey 2016) and then into carbon based on a carbon-to-dry-weight ratio of 27% (Wang et al. 2019).

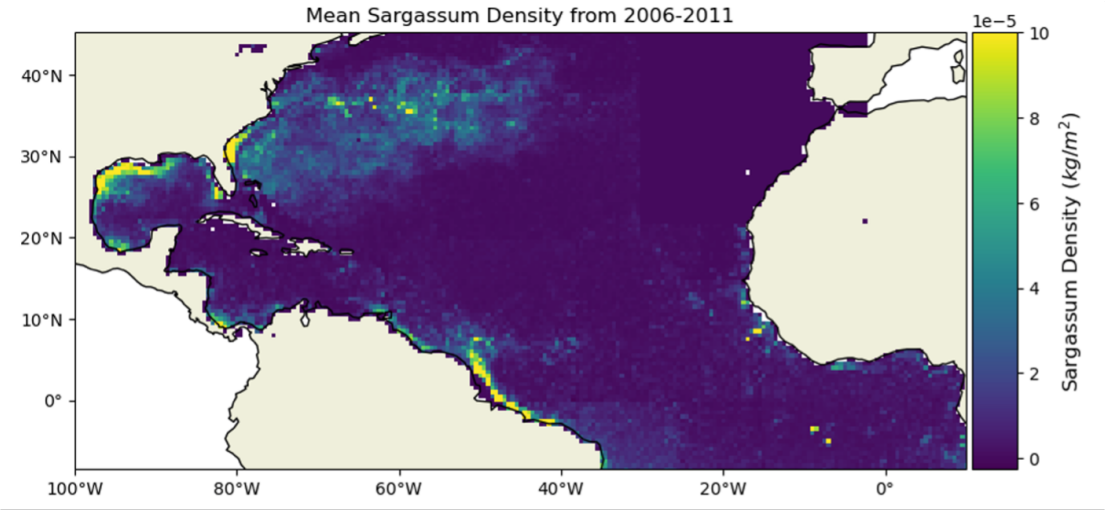

Figure 4.4: Mean Sargassum biomass density (kg/m2) from 2006-2011 across the Atlantic Ocean. Data for the figure was retrieved from Wang et al. (2019)

Initial values for nitrates (N) and phosphates (P), for each particle, are derived by calculating the ratio of nutrient to carbon, using the initial carbon value calculated previously and an average between the minimum (Q_{Nmin}, Q_{Pmin}) and maximum (Q_{Nmax}, Q_{Pmax}) nutrient ratios Jouanno et al. 2021. See Table 4.1 for the parameter constant values used within this study, derived both from results by Jouanno et al. (2021) and my own Monte Carlo method to produce a more realistic model of *Sargassum*.

The ranges of maximum growth rate, μ_{max}, were determined by Lapointe et al. (2014), where the growth rates of *Sargassum* in neritic waters were measured between 0.03 and 0.09 d^{-1}. Optimal, minimum, and maximum temperature values for growth were determined based off the results of Hanisak and Samuel (1987). The N and P quotas were estimated from measurements by Lapointe (1986) where the average C/N ratios vary between 20 and 30 in neritic waters and between 40 and 70 in oceanic waters, while the C/P ratios vary between 200 and 500 in neritic waters and 700 and 1000 in oceanic waters.

Table 4.1: Parameters used in this study's *Sargassum* model. The value column was selected by the Monte Carlo approach within the ranges provided by Jouanno et al. (2021)

Parameter	**Description**	**Value**	**From Jouanno et al. (2021)**	**Range**	**Unit**
μ_{max}	Max growth rate	0.072	0.084	[0.05–0.09]	d^{-1}
T_{opt}	Optimal temperature	27.7	26.0	[22–28]	°C
T_{min}	Minimum temperature for growth	13.75	10.5	[10–14]	°C
T_{max}	Maximum temperature for growth	40.03	43.8	[40–50]	°C
I_{opt}	Optimal light intensity	78.34	62.3	[60–80]	$\mathrm{W\,m^{-2}}$
Q_{Nmin}	Minimum nitrogen quota	0.0283	0.016	[0.016–0.029]	$\mathrm{mgP\,(mgC)^{-1}}$
Q_{Nmax}	Maximum nitrogen quota	0.0389	0.058	[0.033–0.058]	$\mathrm{mgP\,(mgC)^{-1}}$
Q_{Pmin}	Minimum phosphorus quota	0.0027	0.0025	[0.0025–0.0035]	$\mathrm{mgP\,(mgC)^{-1}}$
Q_{Pmax}	Maximum phosphorus quota	0.00551	0.0125	[0.005–0.0125]	$\mathrm{mgP\,(mgC)^{-1}}$
V_{Nmax}	Nitrogen max uptake rate	1.18×10^{-3}	1.3×10^{-3}	$[5 \times 10^{-4} - 1.3 \times 10^{-3}]$	$\mathrm{mgP\,(mgC)^{-1}\,d^{-1}}$
V_{Pmax}	Phosphorus max uptake rate	3.2×10^{-4}	7×10^{-4}	$[9 \times 10^{-5} - 7 \times 10^{-4}]$	$\mathrm{mgP\,(mgC)^{-1}\,d^{-1}}$
K_N	Half-saturation constant for N	0.0756	0.0035	[0.001–0.1]	$\mathrm{mmol\,m^{-3}}$
K_P	Half-saturation constant for P	0.00273	0.01	[0.001–0.1]	$\mathrm{mmol\,m^{-3}}$
m	Max mortality rate	0.042	0.04	[0.04–0.1]	d^{-1}
λ_m	Mortality coefficient	0.65	0.68	[0.2–0.7]	–

Monte Carlo Experiment

To determine parameter values to use within this Chapter for the *Sargassum* model, I used a Monte Carlo approach to determine values that produce *Sargassum* values close to true values. As the satellite-derived biomass values are for the Equatorial Atlantic, a separate smaller particle tracking model needed to be run within this region. 100 particles were released every 5 days within the Equatorial Atlantic (40 - 30°W, 0 - 10°N) from 2011 to 2015. A post-process growth model was applied, as per the study experiment, however it was run 1000 times each with a different parameter set. Each parameter set included a randomly chosen value between the parameter ranges described within Jouanno et al. (2021).

The satellite-derived *Sargassum* was obtained using the AFAI, described within Section 2.4, which produced a coverage map of the Equatorial Atlantic.Then through *in situ* studies, the coverage values can be converted into wet-weight density maps of the observed regions. Therefore, it is key to note that these satellite observations can only detect *Sargassum* within cloud free images and on the surface of the ocean which may lead to underestimations, but also false postives can occur when calculating the AFAI, from issues such as sunglint, causing overestimations. However, due to the basin-wide scale of the *Sargassum* blooms, comparing the model data to the satellite observations is currently the best method of validation.

4.3 Results

This chapter aimed to explore the growth of *Sargassum* as it travelled from the Sargasso Sea to the Equatorial Atlantic where it formed the GASB. Change in particle carbon content was calculated for each particle at each 2-day timestep. Carbon content was then reverted to biomass, again using both the dry-to-wet and carbon-to-dry-weight ratios as previously.

The parameter values were determined by using a Monte Carlo approach to determine which combination of values, within the range from Jouanno et al. (2021), would provide the closest match to satellite observations of biomass across the Equatorial Atlantic. Monthly biomass totals within the Equatorial Atlantic, between 0-10°N and 90-0°W, from

2011 to 2016 were computed for each of the 1000 simulations (Figure 4.5). The monte carlo model outputs had a range of 800 million tons, 80 times larger than the range of the satellite dataset. Therefore, some of the parameter configurations produced datasets that vastly overestimated the biomass. However, when the mean of all 1000 model runs were overlayed on the satellite values, the general trends were consistent. The parameter set that produced the smallest root mean squared error, run 913, was used for the model and is detailed in Table 4.1.

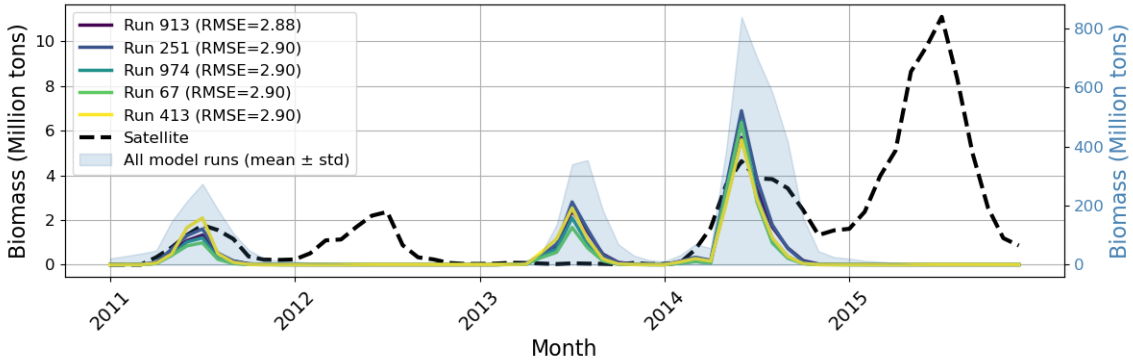

Figure 4.5: Monthly biomass values within the Equatorial Atlantic, between 0-10°N and 90-0°W, for the Monte Carlo approach model runs that had the lowest root mean squared error (left axis) when compared to the satellite data (dashed line). The mean ± standard deviation of all 1000 model runs is shaded in blue on the right axis. Satellite data was retrieved from Wang et al. (2019).

Particle biomass calculations are determined by changes in growth and mortality rates at each location which are determined by individual functions of temperature, nutrients, and irradiance. A more in depth look into these model variables can be seen in Figure 4.6, where two singular particle trajectories were selected from the particles that were able to travel from the Sargasso Sea into the Equatorial Atlantic. The biomass of both particles started to increase as the particle traveled east of the 20°W longitude line. For the left particle (4.6a), this is late 2009/into 2010. For the right particle (4.6i), this occurred earlier in 2008. When the biomass initially peaks for both particles, growth rates increase to over 0.1 d^{-1}, producing a biomass value of 50 tons. At these times, peaks were observed in nitrates and phosphates, at approximately 0.5 mmol/m^2 and 0.3 mmol/m^2, respectively. While the temperature was observed at relatively low values of approximately 20°C, note that the supposed optimum temperature for *Sargassum* growth is 27°C.

Two regions of enhanced growth were determined along a singular particle's transport route within Figure 4.6a. I investigated the spatial variations of the nitrates (Figure 4.7)

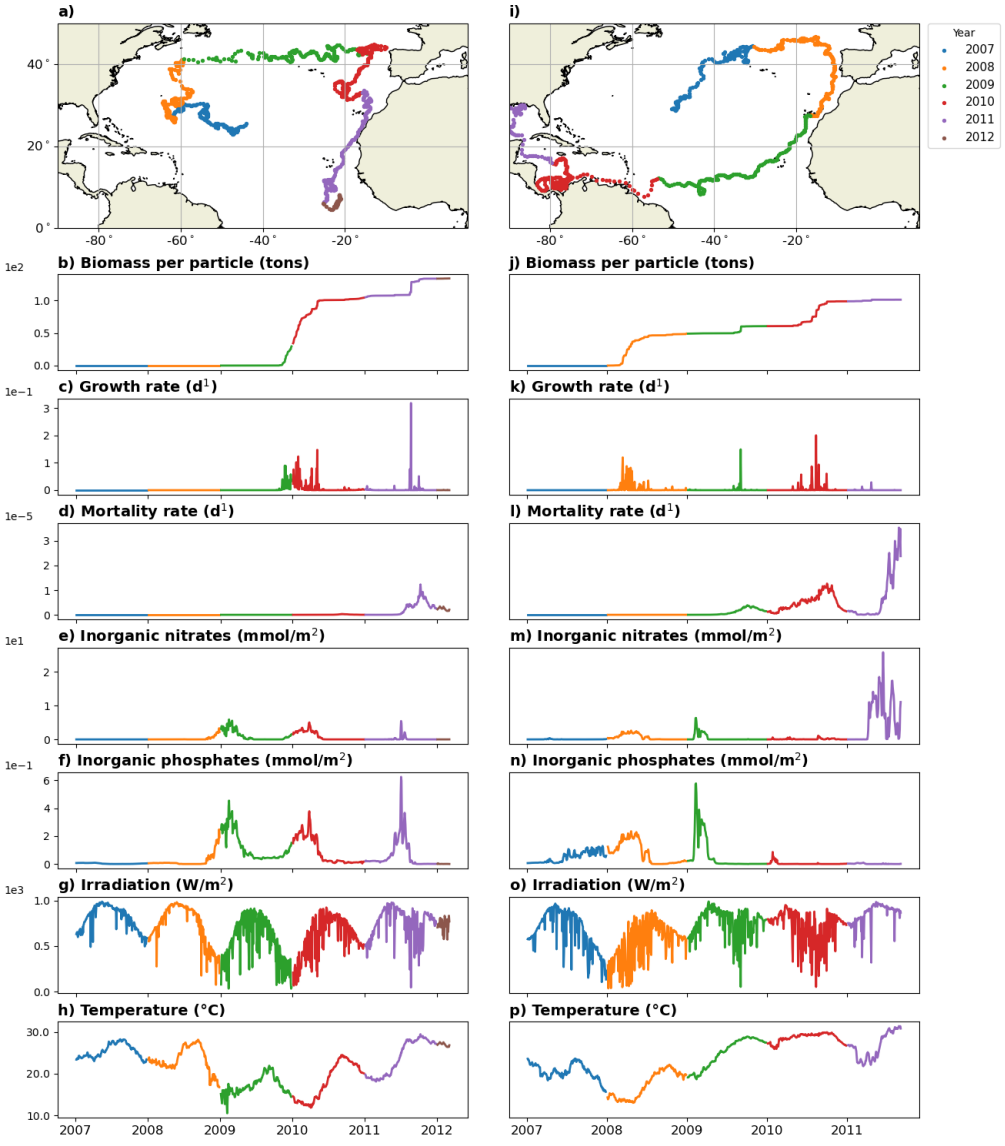

Figure 4.6: Two particles were selected to demonstrate their transport route through the North Atlantic ocean and their corresponding growth and decay terms (left particle: a - h; right particle: i - p). The particle's trajectory (a, i) its biomass (b,j), growth rate (c, k), mortality rate (d, l) and measured inorganic nitrates (e, m), inorganic phosphates (f, n), (g, o) irradiance, and temperature (h, p) are coloured by time to relate the spatial variations with the change in variable values.

and phosphates (Figure 4.8) within these regions; the Northeast Atlantic (between 30 to 10°W and 35 to 50°N) and off the coast of West Africa (between 30 to 10°W and 10 to 25°N).

In winter 2009/2010, the particle was seen to flow east and then swirl before flowing southwest. The particle flows close to an area high in nitrates and phosphates compared to surrounding water concentrations. This influx of nutrients are possibly an overspill from the nutrient rich subplolar gyre to the North (Figure 4.7b, c, d; Figure 4.8b, c, d). In the summer of 2011 (JJA), this particle reached the coast of West Africa. The particle travelled in a southwest direction, relatively close to the coast. The particle travelled through a patch rich in both nitrates and phosphates (Figure 4.7e, f, g; Figure 4.8e, f, g), a possible upwelling region.

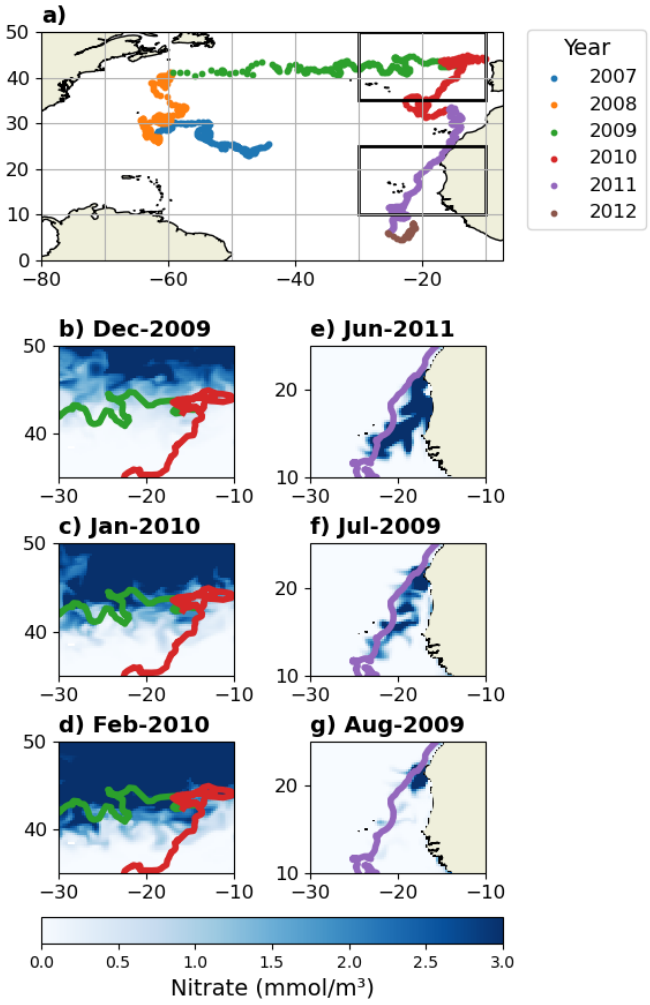

Figure 4.7: Nitrates within two key areas within the North Atlantic across the Northeast Atlantic (top box) and off the coast of West Africa (bottom box). The months of which the selected particle flows within the boxed regions (a) are plotted over the nitrate concentration maps to indicate the position and direction of particle in relation to nutrient values. Nitrates for the Northeast Atlantic, for the winter months of 2009/2010, are shown in the left column (b, c, d). Nitrates for the coast of West Africa, for the summer months of 2011, are shown in the right column (e, f, g).

For analysis, I isolated the 931 particles that travelled below 10°N to only examine the

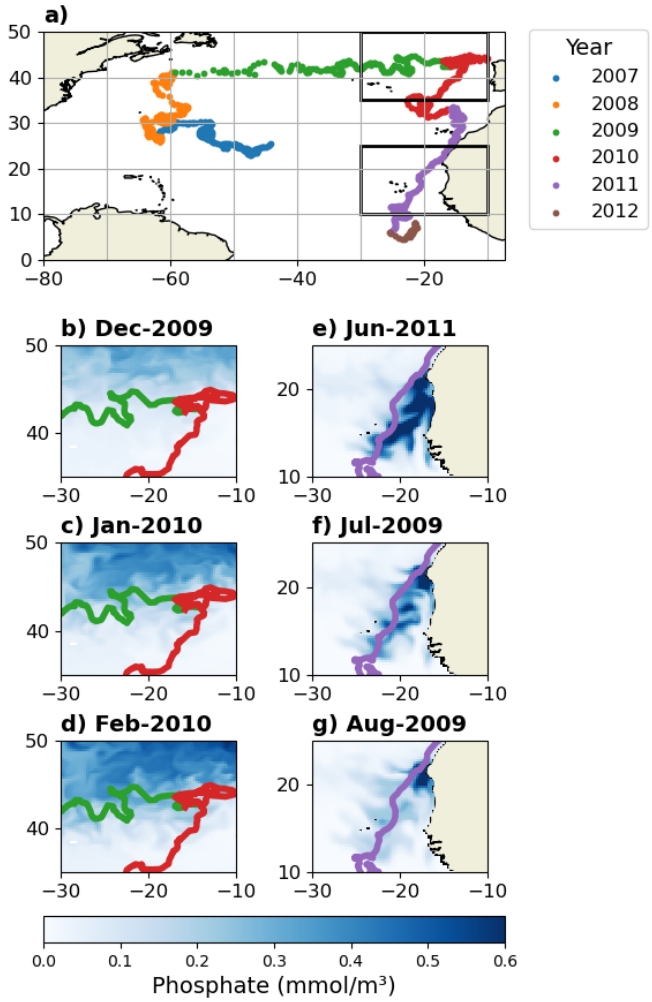

Figure 4.8: Phosphates within two key areas within the North Atlantic across the Northeast Atlantic (top box) and off the coast of West Africa (bottom box). The months of which the selected particle flows within the boxed regions (a) are plotted over the nitrate concentration maps to indicate the position and direction of particle in relation to nutrient values. Phosphates for the Northeast Atlantic, for the winter months of 2009/2010, are shown in the left column (b, c, d). Phosphates for the coast of West Africa, for the summer months of 2011, are shown in the right column (e, f, g).

particles that would form the GASB. While it was determined within

The monthly biomass within the Equatorial Atlantic indicated an initial small peak within 2009 followed by a drastic increase of over 15 million tons in 2010 (Figure 4.9); possibly sparking the formation of the GASB. From thereon, annual peaks form in the summer months. The number of particles within the Equatorial Atlantic, however, show a slightly different story (Figure 4.9). A prolonged peak in 2011 coincided with the sudden increase in biomass; a large influx of over 400 particles accounted for the bloom, however, the small peak in biomass in 2009 must have been caused by a change in conditions. Like 2010, the bloom in 2013 coincides with a particle influx, however, in 2014 biomass increases even

though the particle numbers are decreasing. Similarly in 2009, biomass forms a peak even though there was a small amount of particles within the Equatorial Atlantic that year.

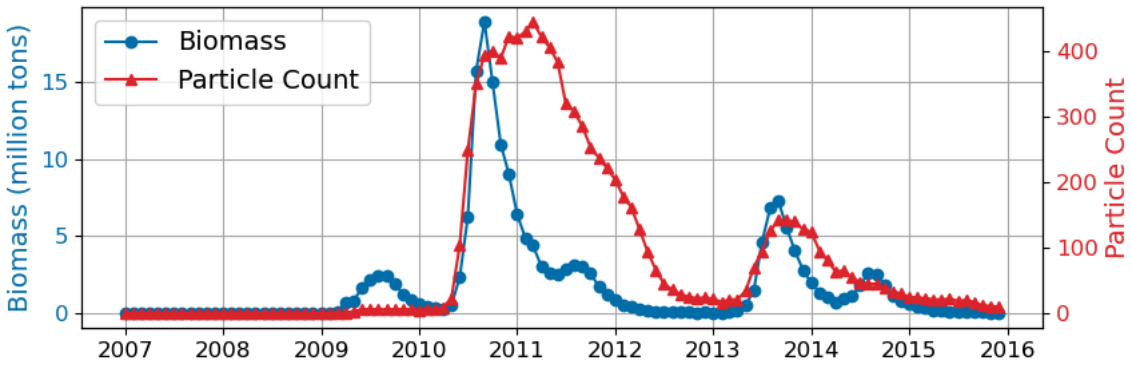

Figure 4.9: Monthly biomass values within the Equatorial Atlantic (blue), between 0-10°N and 90-0°W, and the number of particles within this region over time (red).

Observing the spatial changes in biomass in Figure 4.10 allowed an insight into the along-trajectory growth and decay per particle. Particle biomass is high within the release region, between 25-30°N 40-50°W, suggesting that the average carbon values assigned to the particles was not sustained by the conditions within the Sargasso Sea and it levels out to a baseline value of less than 0.9 tons per particle. Biomass values only then climb towards 1.10 tons as they flow east of the 20°W line of longitude, and again once within the Equatorial Atlantic.

Observing the spatial changes in biomass in Figure 4.10 allowed an insight into the differences between spatial distribution and biomass density. Biomass values are lower within the Sargasso Sea than along the described transport route, even with the continuous re-seeding within the centre of the Sargasso Sea. Biomass densities increase in the Northeast of the Atlantic (30-40°N and 30-10°W) and within the Canary Current parallel to the coast of West Africa. Biomass densities highlight the interannual variability of *Sargassum* blooms and underscore the patchy nature of its distribution.

The timing of the biomass peaks for the selected particle in Figure 4.6 suggest that this particle accounts for the model's initial 2009 bloom (Figure 4.9). Growth rates were driven by nutrient availability and mortality rates controlled by prolonged high irradiance and temperatures. Generally, when within the Sargasso Sea, there are low nutrient concentrations. This particle travelled to the Equatorial Atlantic in 2009 where the particle initially entered within what seems like the outflow of the GS, in a northeast direction,

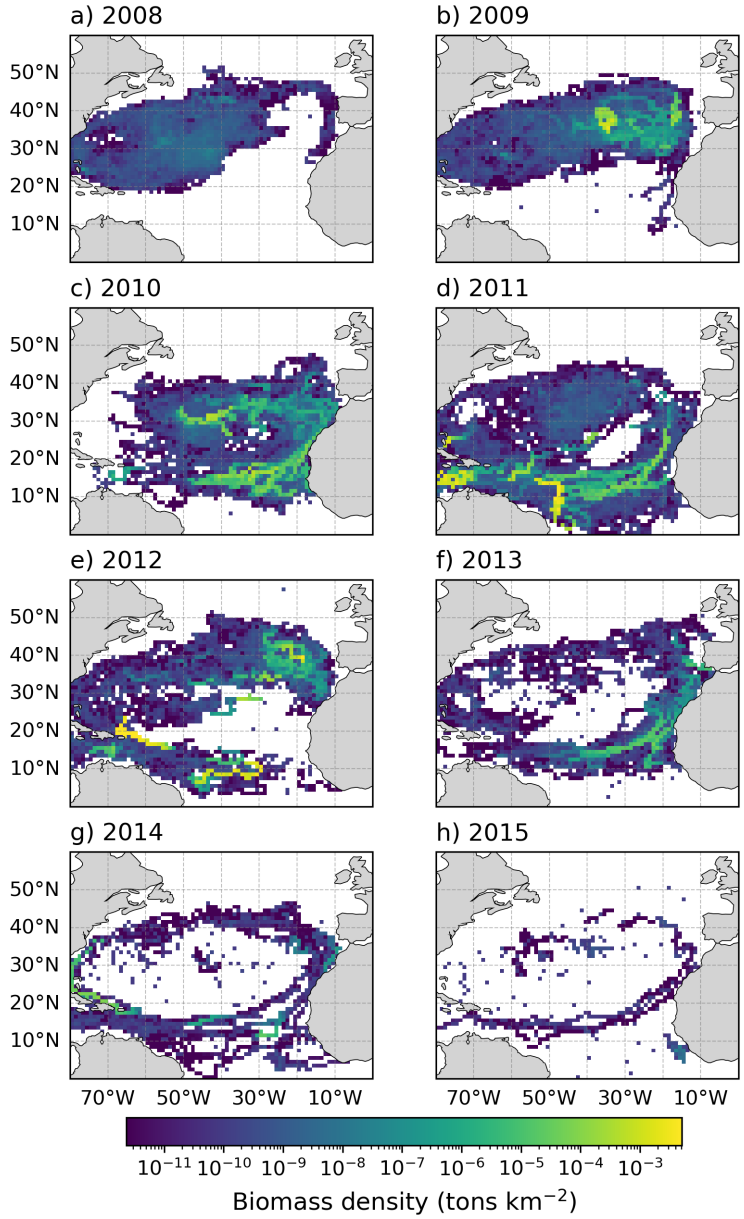

Figure 4.10: Annual biomass density plots of selected particles that reached below 15°N.

before entering a region north of the AzC (approx. 34°N; Figure 1.2). While the particle was swirling within the Sargasso Sea (in 2007 and 2008), the availability of nitrates and phosphates were low and seemingly accounting for the low growth rates during this period (Figure 4.6).

4.4 Conclusions

This chapter demonstrated that as *Sargassum* travelled from the Sargasso Sea to the Equatorial Atlantic during the 2009/2010 anomalous event, it was able to survive the

journey. The post-process analysis growth model of my particle tracking simulation was able to demonstrate that the particles which travelled to the Equatorial Atlantic were subject to higher growth rates after experiencing higher concentrations of nutrients and optimum temperature (Figure 4.7). This suggests that the few particles that escaped the Sargasso Sea experienced higher than normal growth rates than would be possible within the nutrient depleted gyre.

Chapter 5

Simple Box Model of the Equatorial Atlantic to Determine Drivers of Sargassum Growth

5.1 Introduction

So far, this study has determined that *Sargassum* travelled from the Sargasso Sea to the Equatorial Atlantic to form the GASB and grew during transport when exposed to an influx of nutrients overspilling from the North Atlantic Subpolar Gyre. In Chapter 3, I determined the transport of *Sargassum* into the Equatorial Atlantic was an anomalous event. The North Atlantic experienced extreme changes within the winter of 2009/2010, observed in major currents, gyre velocities and wind velocities. While the outflow of the Gulf Stream intensified, the overall strength of the gyre decreased, reducing the convergence zone. This allowed the *Sargassum* to escape the Sargasso Sea along the Azores Current and then travel south along the Canary Current. This extreme event coincides with the extreme negative phase of the NAO, indicating the NAO was the underlying cause of the formation of the GASB.

Annual blooms of the GASB have generally increased each year, with 2013 being an exception of little to no *Sargassum*. In 2011, the first GASB bloom measured approximately 9 million metric tonnes while in 2018 it reached over 20 million metric tonnes (Wang et al.

2019). Since the transport of *Sargassum* into the Equatorial Atlantic was an anomalous event, the population within the Equatorial Atlantic must be able to thrive alone to grow over time without a constant influx of *Sargassum*.

To recap, *Sargassum* is a large brown seaweed that spends its entire lifecycle floating at the surface of the ocean and is comprised of multiple species and sub-species with slightly varying morphological features. The three species that comprise most of the Atlantic populations are *S. fluitans III*, *S. natans I*, *S. natans VIII* (Schell et al. 2015; Fidai et al. 2020). These species of *Sargassum* behave similarly with the same lifecycle and with a similar size range (Lapointe et al. 2014). However, there is limited knowledge on how the physiology differs between the species, so *Sargassum* is known as a blanket term for all *Sargassum* present in the Atlantic. While originally found within the Sargasso Sea, in 2011 a new population was observed within the Equatorial Atlantic (Wang et al. 2019). Growth of *Sargassum* is controlled by nitrogen and phosphorus availability, as well as temperature and light (Lapointe 1986; Lapointe et al. 2014). Lapointe (1986) demonstrated that *Sargassum* growth was limited by phosphorus availability, but in revised studies both the nitrogen and phosphorus availability had a direct relationship with *Sargassum* abundance within the Sargasso Sea. *Sargassum* is known to have a seasonal cycle within the recently formed GASB region of the Equatorial Atlantic with peaks in biomass in summer and troughs in winter (Figure 5.1a). This cycle is vastly different to observations within the Sargasso Sea in 2017 where Jouanno et al. (2021) demonstrated multiple low peaks were observed across the winter months instead (Figure 5.1c).

The Sargasso Sea is known as a nutrient limited, oligotrophic gyre which may inhibit *Sargassum* growth. This is why it's thought that the population of *Sargassum* was constrained when in the Sargasso Sea but abundant in the Equatorial Atlantic, where there are multiple sources of nutrients from both upwelling regions and rivers (Gower and King 2011; Brooks et al. 2019; Wang et al. 2019). Satellite observations between 2002 and 2008 showed significant *Sargassum* within the Gulf of Mexico relative to the background values in the spring months, and then within the western Sargasso Sea in the summer months of those years (Gower and King 2011). Gower and King (2011) suggested that the presence of *Sargassum* in the Gulf of Mexico indicated that the gulf acted as a "nursery" for *Sargassum*, and the Sargasso Sea population was sustained by an annual influx from this nursery.

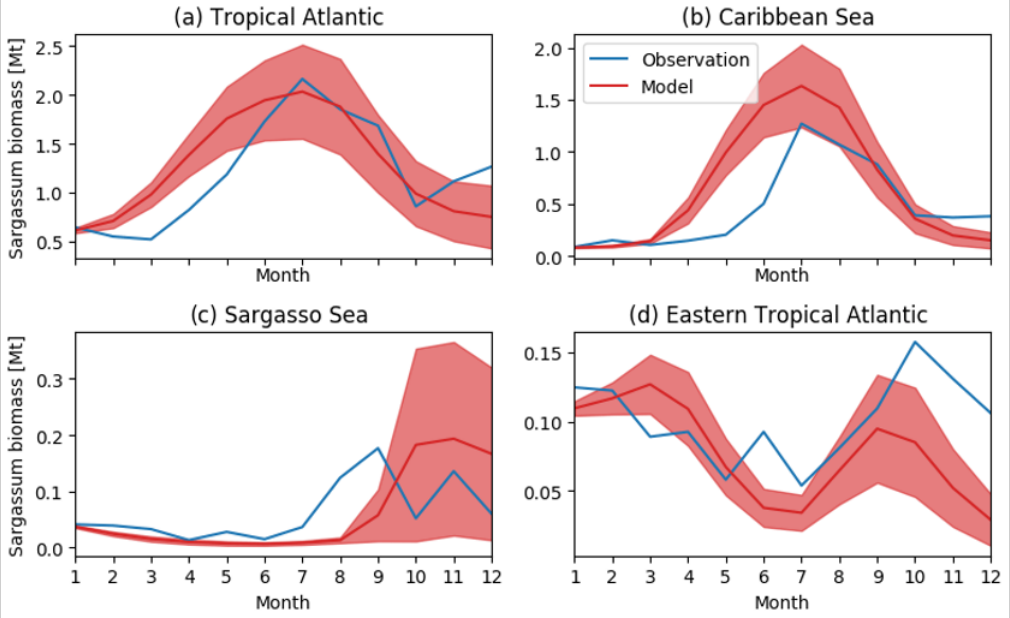

Figure 5.1: Timeseries of monthly mean *Sargassum* biomass in 2017 from satellite observations (blue) and from Jouanno et al. (2021)'s model outputs (mean in red and variance in shaded red) averaged over four different regions: (a) tropical Atlantic, also known as the Equatorial Atlantic, (0–30°N, 98–10°W), (b) Caribbean Sea (8–22°N, 85–55°W), (c) Sargasso Sea (23–30°N, 80–50°W), and (d) eastern tropical North Atlantic (0–15°N, 30°W–0°E). Figure retrieved from Jouanno et al. (2021).

The Gulf of Mexico provides *Sargassum* with nutrient rich waters from the outflow of the Mississippi River, possibly enhancing growth of young *Sargassum* strands. However, numerous studies have suggested that the Sargasso Sea population creates a habitat that in turn provides the *Sargassum* with nutrients. Migrating fish, sea turtles and sea birds take refuge within the *Sargassum* while travelling through the subtropical gyre. The seaweed provides food and shelter for passing fauna, while secretions of ammonium and phosphorus from these animals enrich the surface waters with additional nutrients (Lapointe et al. 2014).

Despite interannual variability, the density of GASB blooms has generally increased since their first occurrence in 2011. This raises two key questions: is this new population self-sustaining, and what conditions enable *Sargassum* to thrive in the Equatorial Atlantic? While previous studies have linked satellite-observed *Sargassum* biomass to measured ocean variables (e.g., sea surface temperature) to investigate drivers of interannual variability, *Sargassum* models have not yet been applied for this purpose. Existing models have primarily been used for forecasting bloom extent and predicting beaching events, rather than identifying the underlying drivers of biomass change. To address this gap, this

chapter develops a simple box model to examine how changes in temperature, nutrients, and irradiance within the Equatorial Atlantic influence GASB bloom variability.

5.2 Methods

A simple box model of the Equatorial Atlantic was used to simulate *Sargassum* growth within this region, assuming the surface waters are well mixed. Simple box models reduce the complexity of oceanic processes to produce clear and interpretable simulations within a defined region. Their low computational effort means they are ideal for exploring ocean processes without the overhead of high-resolution modelling. For *Sargassum*, box models enable the isolation of key drivers of growth and decay, such as temperature, nutrient availability and surface currents, providing a valuable framework. However, the ocean is a complex ecosystem and the box model can over simplify the circulation and ecological interactions. The simplified equations and lack of spatial resolution need to be considered when analysing the results.

Surface currents, Stokes drift, and windage were used to calculate the velocity flux across the boundaries of the box model. Velocities (V) for model grid cells either side of the boundary were averaged at either side of the box model boundaries (e.g. $V_{y_i} + V_{y_{i+0.25}}$) for the latitudinal boundaries at the western and eastern edges of the box. Flux values for the latitudinal and longitudinal boundaries are described as:

$$\psi_{lat} = \int_{x_{min}}^{x_{max}} \frac{1}{2}(V_{y_i} + V_{y_{i+0.25}})dx \tag{5.1}$$

$$\psi_{lon} = \int_{y_{min}}^{y_{max}} \frac{1}{2}(V_{x_i} + V_{x_{i+0.25}})dy \tag{5.2}$$

where the corner coordinates of the box model are represented by x_{min}, x_{max}, y_{min}, y_{max}.

For example, the flux (ψ) across the eastern boundary (at 15°W) was described as:

$$\psi_{-15} = \int_{x_0}^{x_{10}} \frac{1}{2}(V_{-15} + V_{-15.25})dx \tag{5.3}$$

to calculate flow across the 15°W line of longitude, between 0°to 10°N. However, after visualising velocities at boundaries over time, the boundary edges were split into sections

of inward and outward flows (Figure 5.2). For example, at the northern boundary of the box model, at 10°N, the flow was seen to flow north between 60-52°W and south between 52-15°W (Figure 5.2a).

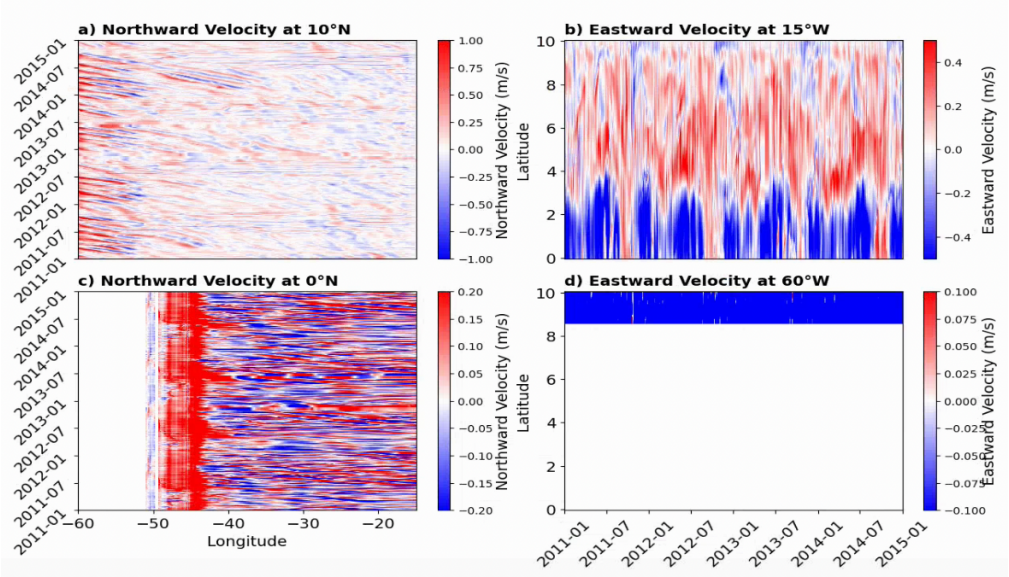

Figure 5.2: Hovmoller diagrams to demonstrate the direction of surface currents across the a) northern, b) eastern, c) southern, and d) western boundaries of the box model. Blank spaces within c) and d) are due to land.

At each two-day timestep, inward (outward) velocity fluxes were summed together to produce a flux in (flux out) term. To obtain *Sargassum*-in and *Sargassum*-out values, flux terms were multiplied by the *Sargassum* biomass concentrations. Particle tracking outputs obtained in Chapter 4, were used to obtain biomass values within the 1° surrounding grid cells of the box model boundaries, $C_{outside}$, at each timestep. Values were divided by the area to obtain concentrations. *Sargassum*-in was then described as:

$$F_{in} = \psi_{in} \times C_{outside} \tag{5.4}$$

While the *Sargassum*-out values were obtained by multiplying the concentration of *Sargassum* biomass within the box model, C_{inside}, by the outward flux term:

$$F_{out} = \psi_{out} \times C_{inside} \tag{5.5}$$

Similarly to the methods in Chapter 4, this model incorporated physical and biogeochemical data to model *Sargassum* biomass over time. The main input variables used

were surface ocean temperature, nitrate and phosphate concentrations and solar radiation. Datasets were geographically limited to the Equatorial Atlantic region, bounded by 0°–10°N latitude and 60°–15°W longitude, from 2008 to 2015 (Figure 5.3). Note that the box model assumes that everything contained within it is well mixed, essentially providing one value per variable per timestep.

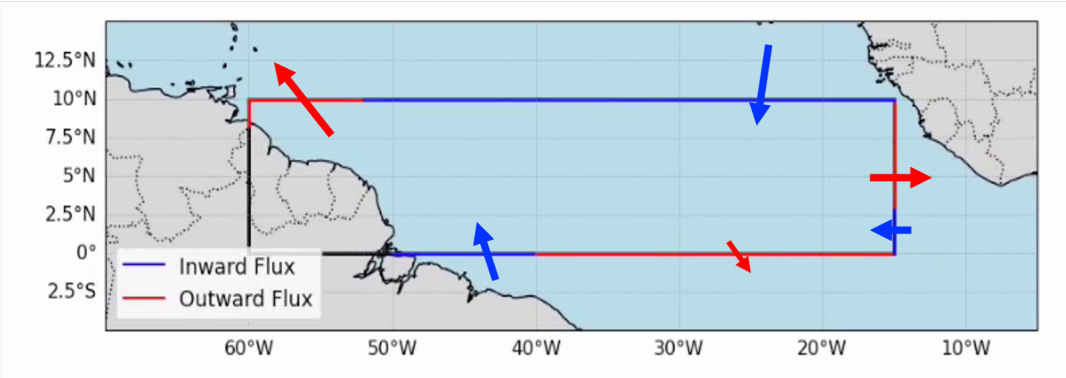

Figure 5.3: Diagram of box model region, between 60-15°W and 0-10°N, and the direction of the velocity flux across the boundaries. Blue indicates the velocities that flow into the box and red indicates the flux out of the box. Black lines denote land, where there is no data for the surface currents.

While the box model utilised Chapter 4's description of *Sargassum* physiological behaviours, there are some key changes due to modelling a bounded region rather than individual particles. While the growth and decay equations are the same (Equations 2.28 and 2.32, Section 2.5), there are additional source and loss terms described above as F_{in} and F_{out}. Therefore, change in biomass for this chapter was described as:

$$\frac{\partial C}{\partial t} = U_C - \theta_C + F_{in} - F_{out} \tag{5.6}$$

Both organic nitrate (N) and phosphate (P) uptake and loss rates are calculated during the box model, as in Chapter 4, therefore the additional source and loss terms are needed to balance the loss of biomass from the boundary fluxes. Methods described above to obtain biomass concentrations for outside and inside the box model were repeated with organic nitrate and phosphate values to obtain, N_{in}, N_{out}, P_{in}, and P_{out}. These terms were then added to the equations that described the change in N and P values:

$$\begin{aligned} \frac{\partial N}{\partial t} &= (U_N - \theta_N) + N_{\text{in}} - N_{\text{out}} \\ \frac{\partial P}{\partial t} &= (U_P - \theta_P) + P_{\text{in}} - P_{\text{out}} \end{aligned} \tag{5.7}$$

Constant parameter values used within this chapter are described within Table 4.1 (Section 4.2), as used for the *Sargassum* particle tracking model in Chapter 4. The only difference was the initial carbon value. Instead, the total biomass was averaged across the Equatorial Atlantic (between 0°to 10°N and 60°to 15°W) for January 2007 using satellite observations, provided by (Wang et al. 2019). *Sargassum* biomass was then converted to dry weight using the ratio of 15% and then into a carbon content value using the carbon-to-dry-weight ratio of 27% (Jouanno et al. 2021).

This model was run using a 2-day timestep from 2008 to the end of 2015, providing a single carbon value for each timestep to visualise biomass variablity for the entire Equatorial Atlantic region. This output timestep was chosen based on the particle tracking timestep used in Chapter 4. 2008 - 2010 was used as a spin-up to create the initial conditions of the first bloom in 2011. Therefore, only the model data from 2011 onwards was analysed in comparison to satellite data of the same time period and region.

5.3 Results

Initially, to explore the *Sargassum* population within the Equatorial Atlantic, a particle tracking simulation was run as in Chapters 3 and 4 but instead the particles were released between 40 to 30°W and 0 to 10°N from 2011 to 2015. The aim of this simulation was to attempt to recreate the GASB. Post-process growth calculations provide a density map of biomass that closely represents the extent of the GASB (Figure 5.4), as seen in the satellite observations shown in Section1.1 (Figure 1.3). For this simulation, a 100 by 100 grid of particles were released every January, within the Equatorial Atlantic, to represent the re-seeding from the winter GASB population. Biomass increases off the coast of South America and decreases into the Caribbean Sea. Particles are seen flowing into the Sargasso Sea, as seen in the results of Chapter 3, however the particles do not re-enter the Equatorial Atlantic.

Releasing particles in the GASB region produced density maps closer to the satellite observations than the particle tracking methods within Chapter 3 (Figure 1.3; Figure 5.4), however, can survive, or thrive, within the Equatorial Atlantic without a manual reseeding or external source? The four terms of the box model, and the resultant change in biomass, from Equation 5.6 was visualised within Figure 5.5. Note that the biomass and the four

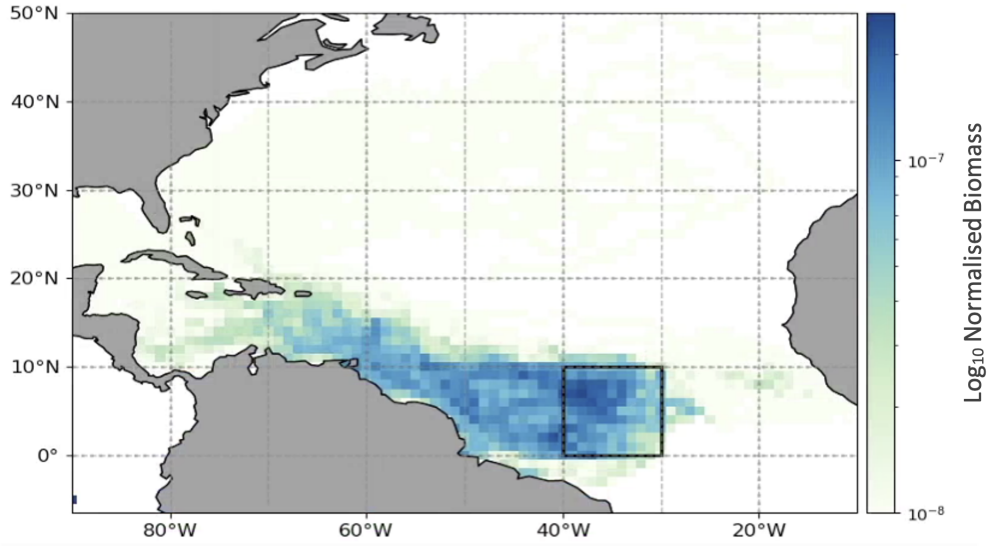

Figure 5.4: biomass, normalised using the natural logarithm of the values, from particle tracking outputs when particles are released within the Equatorial Atlantic (between 40-30°W and 0-10°N) from 2011 to 2015.

terms within Figure 5.5 are shown as kg C/day, the values of which the model is calculated in. *Sargassum* outflow, F_{out}, values were very small compared to inflow, the internal growth rates, and mortality rates. While *Sargassum* influx, F_{in}, produced high influx values in 2011, it levels off to close to zero after that. The addition of F_{in} and F_{out} helped produce a "life-like" model, however, internal growth and decay terms were relatively more important on the net change to the *Sargassum* biomass (Figure 5.5). Results determined that *Sargassum* influx was not detrimental to sustaining the *Sargassum* biomass within the Equatorial Atlantic.

Biomass within the Equatorial (Tropical) Atlantic typically shows a seasonal cycle with peaks over summer and the lowest values over the winter months (Figure 5.1); this cycle is visible within the satellite observations of this region (Figure 5.6, dashed line). Outputs of the simple box model show peaks in biomass of a similar value to the satellite observations, except for in 2014 and 2015.

However, the modelled biomass differs from the satellite observations by showing clear biannual peaks. The lifecycle patterns of *Sargassum* within the Eastern Tropical Atlantic typically produce biannual peaks, as seen within Figure 5.1d. As this box model assumes the Equatorial Atlantic is well mixed, the biannual peaks suggest that conditions within the east of the Equatorial Atlantic control *Sargassum* growth within this box model. Con-

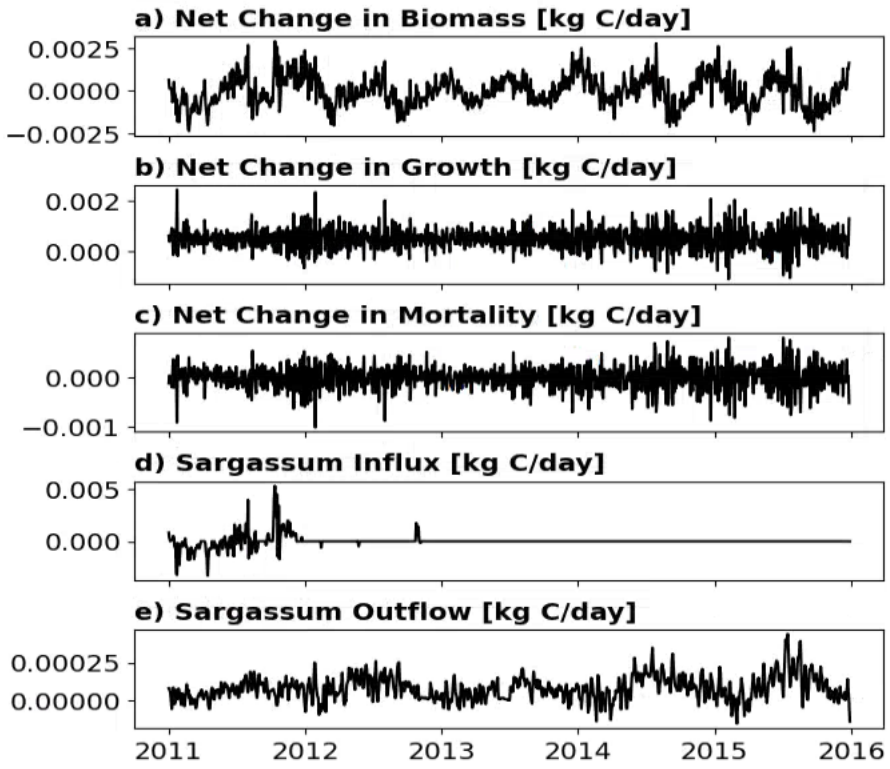

Figure 5.5: a) The change in biomass per day and the b) growth, c) mortality, d) influx (F_{in}) and e) outflow (F_{out}) terms used within the simple box model. The terms were plotted as their carbon content (kg C) that was used within the calculations.

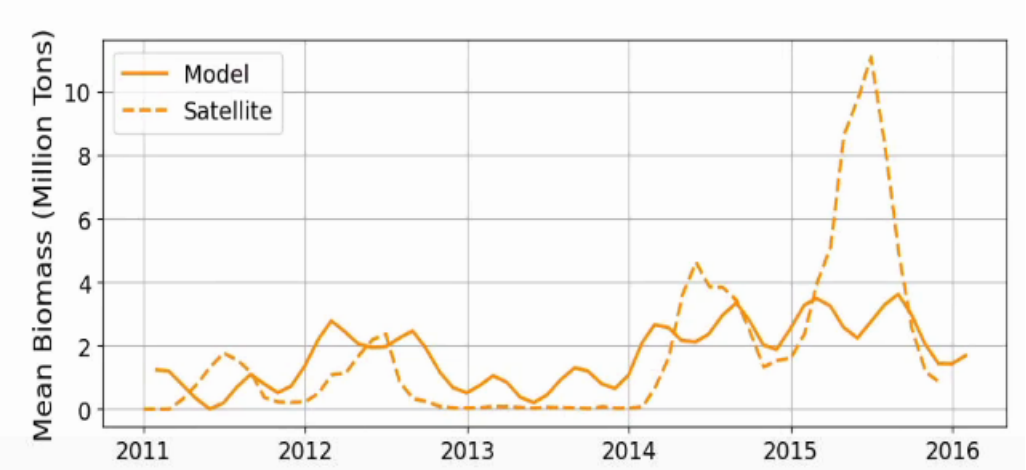

Figure 5.6: Timeline of biomass output of the box model (solid line) compared to the satellite observations (dashed line) within the Equatorial Atlantic. Satellite data was retrieved from Wang et al. (2019).

ditions within the eastern Equatorial Atlantic are visualised within Figure 5.7. Biannual trends are seen within the nitrates and temperature, however, they show an inverse with biannual troughs.

Four variables are used to calculate growth within this model: temperature, irradiance, ni-

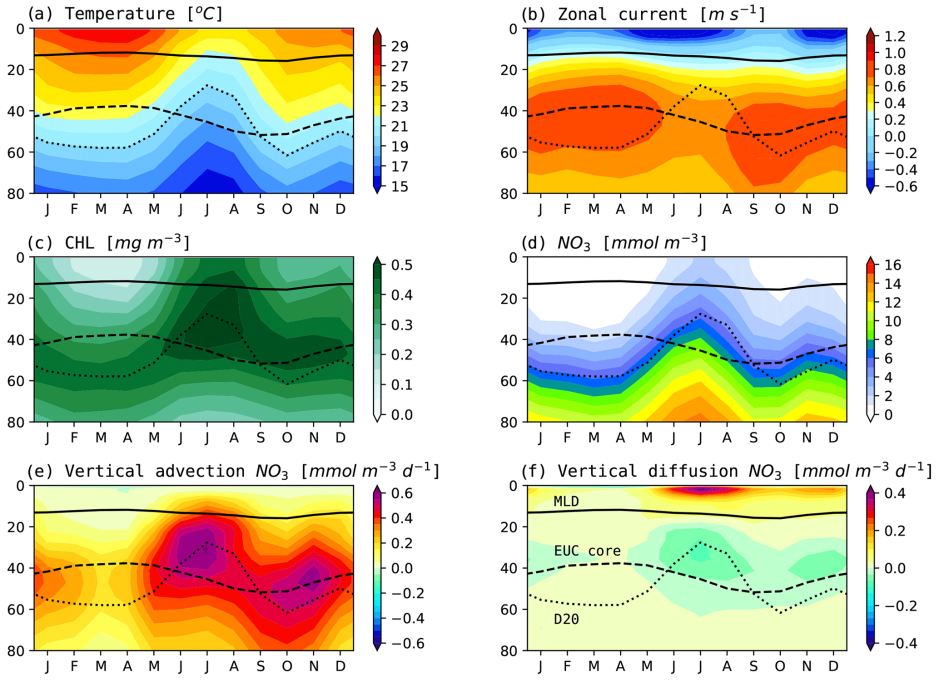

Figure 5.7: Seasonal cycle of vertical profiles of a) temperature, b) velocities, c) chlorophyll, d) nitrate, and vertical e) advection and f) diffusion. The profiles were averaged horizontally between 1.5°S - 0.5°N and 20 - 5°W. Figure was retrieved from Brandt et al. (2023). Note that this shows a depth profile, while the studies within this thesis focus on surface values.

trates, and phosphates. These variables are able to reproduce *Sargassum* blooms between 2011 and 2014 (Figure 5.6), therefore, I took a more in depth look into these variables across this time period. Nitrates and phosphates show a clear seasonal cycle, with peaks in summer and troughs in winter (Figure 5.8), but the phosphate values are significantly lower. Temperature and irradiance exhibit biannual peaks, similar to the biomass time series, but with a noticeable lag. These peaks occur shortly after those of biomass, suggesting that elevated temperatures may be associated with increased mortality, leading to a subsequent decline in biomass.

Simple linear regression was used to evaluate the relationship between biomass and four environmental variables: sea surface temperature, irradiance, nitrate concentration, and phosphate concentration (Figure 5.9). For each variable, univariate linear regression was performed using the ordinary least squares method, minimizing the residual sum of squares between the observed biomass and the values predicted by the linear model. The Pearson correlation coefficient (r) was calculated to quantify the strength and direction of the relationship. Regressions were applied to the box model data outputs, with a time-step

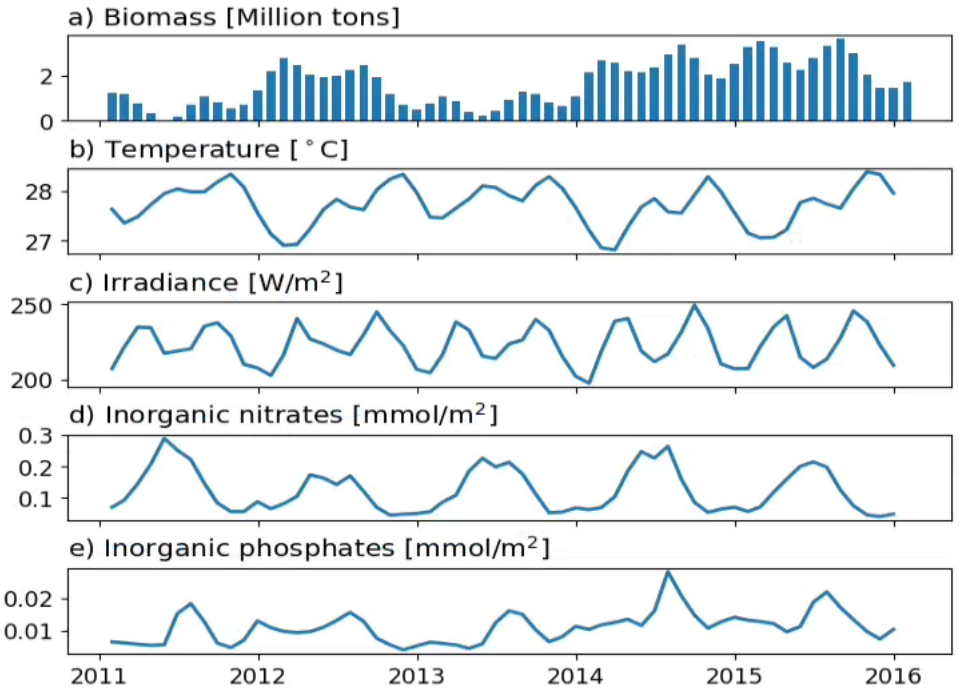

Figure 5.8: Monthly averages of biomass and driving variables for the Equatorial Atlantic from the box model, from 2011 to 2015. a) Changes in biomass are calculated within the model using individual functions of measured b) temperature, c) irradiance, d) nitrates, and e) phosphates.

of 2 days, between 2008 and 2015. Phosphates were the only variable showing a positive correlation with biomass values (Figure 5.9). Higher phosphate values are associated with higher biomass values, with a strong positive correlation ($r = 0.76$) that is statistically significant ($p < 0.05$). Meaning 57.8% of the variability in biomass is explained by the phosphate values. On the other hand, nitrate availability had very little impact on biomass variability. Temperature has the next greatest impact on variability showing a negative correlation ($r = -0.5$, $p < 0.05$). It is key to note that within the Equatorial Atlantic the temperature only varied by about 2°C. The higher temperatures (28°C and above) lead to increased mortality rates, suggesting why there was a high negative correlation with biomass.

The simple box model was able to successfully recreate annual trends in *Sargassum* biomass of an overall increase from 2011 to 2014 and even the anomalous year of 2013. However, in 2015, satellite observations show an increase of 6 million tons relative to these years, which is not reflected in the model output (Figure 5.6). Therefore, the results suggest that there may be conditions impacting *Sargassum* growth that were not included in this physiological model. As stated, the biannual peaks within the modelled biomass

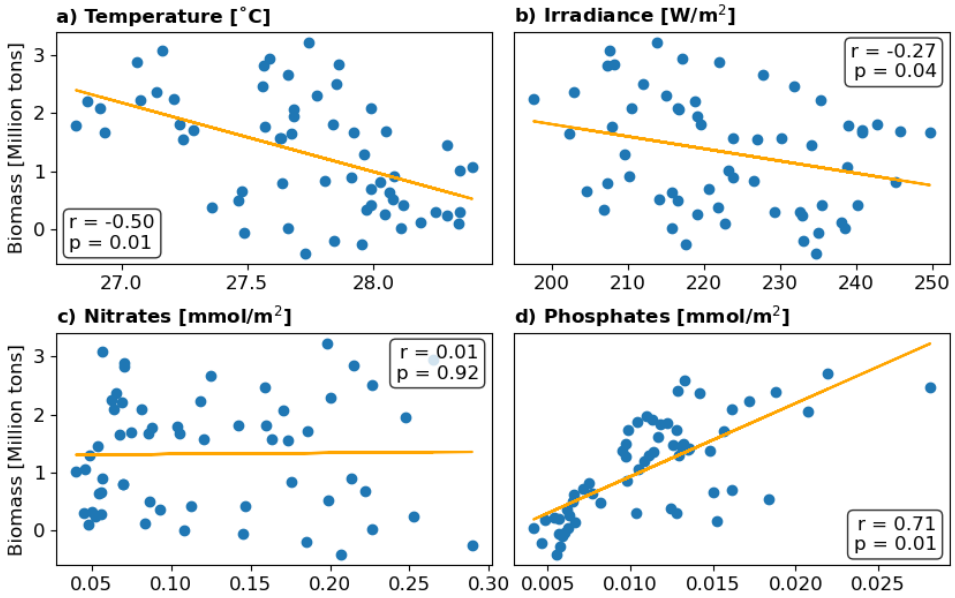

Figure 5.9: Linear regression analysis of *Sargassum* biomass (Million tons) against four factors that feature within the growth model: (a) temperature, (b) irradiance, (c) nitrates, and (d) phosphates.

(Figure 5.6) are typical of *Sargassum* observed within the East Equatorial Atlantic. The main input of nutrients in the West Equatorial Atlantic is the Amazon River. Both precipitation over the Amazon River basin and the resultant river discharge have been increasing since 1980 (Figure 5.10). Therefore, it can be deduced nutrients from the Amazon River discharge may be underestimated within the box model's forcing data.

Since over 50% of the variability within the modelled biomass was attributed to the phosphate availability, the phosphates used within the model were compared to data from the 2013 WOA dataset for the west Equatorial Atlantic region (60 - 40°W, 0 - 10°N) (Figure 5.11). Nutrient data from the WOA are derived from a wide range of *in situ* observations and are often used to initialize and validate numerical ocean models, such as the CMEMS model used within this study, as well as to validate satellite observations. Therefore, the data can be used as a good determination of "real-life" nutrient values. However, the WOA is only available for certain years and as such, could not be used to provide the nutrients for box model. Comparison of the two datasets show that phosphates are underestimated within the region of the Amazon River basin, especially within the summer months (Figure 5.11i).

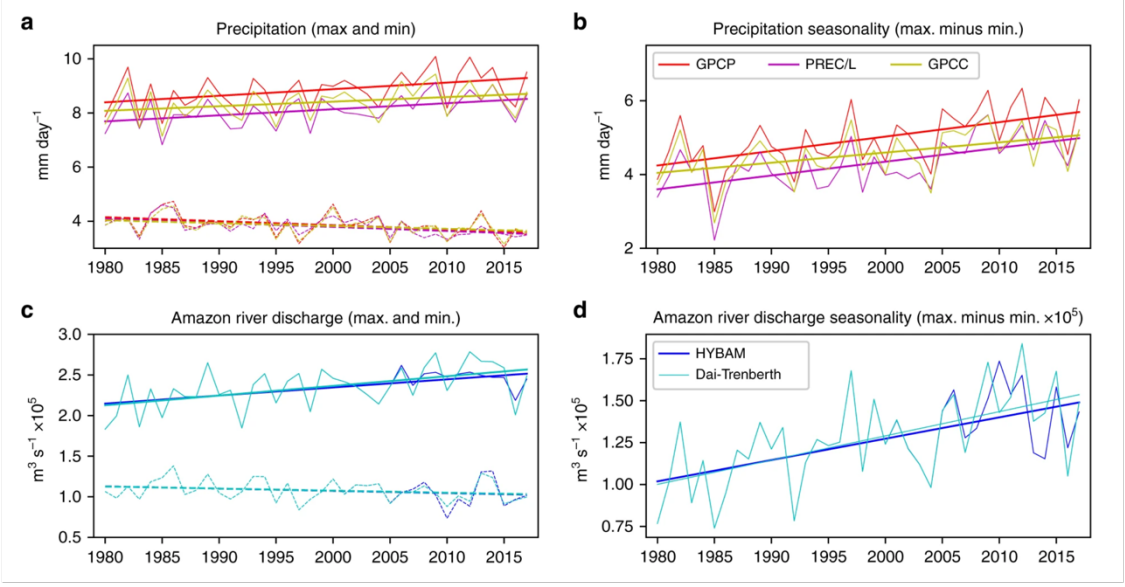

Figure 5.10: The precipitation (a) and seasonality of the precipitation (b) across the Amazon River basin from 1980 - 2018. The resultant Amazon River discharge (c) and seasonality (d) for the same period. Figure adapted from Liang et al. (2020).

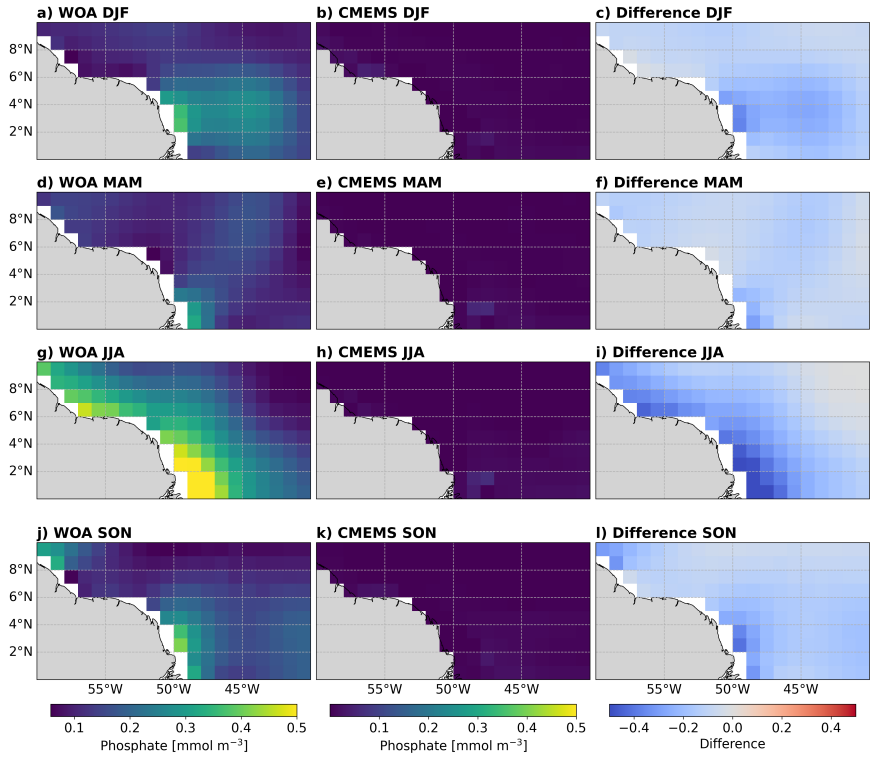

Figure 5.11: Seasonal average phosphate values for 2013 within the region of the Amazon River outflow (60 - 40°W, 0 - 10°N). Data is shown from the World Ocean Atlas dataset (left column) and the CMEMS BGC model (centre column) that was used within this study. The right column shows the difference between the two datasets (CMEMS - WOA). Red indicates where the CMEMS data may be overestimating phosphates, and blue underestimating.

If phosphates within the Western Equatorial Atlantic are likely to control GASB inter-annual variability, then there would be the expectation that phosphates would increase proportionally to the GASB. Obtaining a consistent time series of nutrient data from the Amazon River's outflow was challenging, instead SSS was used to see if there was a change in the Amazon River between 2011 and 2016. The ESA CCI+SSS dataset provided high-quality measurements of SSS derived from a combination of multiple radiometry satellite missions (Boutin et al. 2024). I calculated the rate of change of SSS per year for each 0.25° grid cell over 5 years (Figure 5.12). North of the equator, between 50°W and 47°W, surface waters freshen at a rate of approximately 2 PSU per year. This suggests that the Amazon River outflow increased within the time of the box model, therefore it can be assumed the nutrient influx within this region increased.

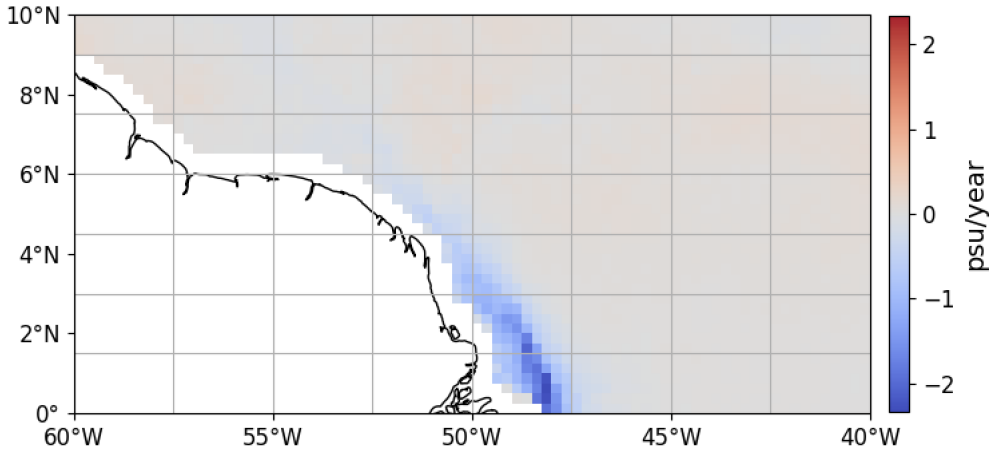

Figure 5.12: The rate of change of SSS per year for each grid cell over 5 years (from 2011 to 2016). Data was retrieved from the ESA CCI+SSS dataset (Boutin et al. 2024).

5.4 Conclusion

By producing a simple box model of the Equatorial Atlantic, this chapter was able to demonstrate that *Sargassum* not only was able to survive within this region but also grow with a similar seasonal cycle to that seen in satellite observations of the East Equatorial Atlantic (Figure 5.1; Figure 5.6). Out of the four parameters included within the calculation of *Sargassum* growth within the box model, phosphates were isolated as having a strong positive correlation with the changes in biomass (Figure 5.9). 58% of the changes in biomass can be attributed to the phosphate data. In the visualised timeseries of phosphate data, Figure 5.8d, phosphate values seem erratic compared to the other consistent

datasets of temperature, irradiance, and nitrates.

The model was unable to match the satellite observations within 2014 and 2015. After comparing the model's inorganic phosphates with a more accurate dataset, I concluded that the model had been underestimating coastal phosphate data near the outflow of the Amazon River. Better estimations of river runoff may improve the outputs of the box model to produce a timeseries that better matches satellite observations of the Equatorial Atlantic.

Chapter 6

Summary and Conclusions

This thesis aimed to develop and apply novel methods to simulate Sargassum transport and growth within the North Atlantic Ocean to understand why the GASB formed in 2011. Following on from the work by Johns et al. (2020), the aim was to demonstrate how Sargassum was able to escape the currents of the North Atlantic Subtropical Gyre and flow south into the Equatorial Atlantic. This aim was achieved using the Parcels (Delandmeter and Sebille 2019) particle tracking python package to produce individual particle trajectories (Chapter 3). Of which a post-process growth model could be applied to get along trajectory growth and decay of individual Sargassum particles (Chapter 4). Once it was demonstrated that Sargassum was able to enter the Equatorial Atlantic, a simple box model of the region was created to simulate the change in biomass over time to aid understanding what parameters within the model cause variations in growth (Chapter 5). Here, I will summarize the key findings from each chapter to outline how I met the original aims and research objectives before discussing areas of future work that arrived from the results presented within this thesis.

6.1 Summary and Synthesis of Findings

6.1.1 Use of Particle Tracking to Model *Sargassum* Transport and Growth

Particle tracking is a popular choice to model floating objects within the ocean, multiple studies had used variations of particle tracking to simulate Sargassum movement (Franks et al. 2016; Putman et al. 2018; Brooks et al. 2019; Marsh et al. 2021; Marsh et al. 2022).

While their use and setup varied, they all explored Sargassum transport within the GASB region of the Equatorial Atlantic for short periods of up to a year. However, other particle tracking applications, such as modelling plastics, have produced simulations of many years across the entirety of the world's oceans. A key strength to using particle tracking to model Sargassum is the low computational cost; long simulations (> 5 years) with large numbers of particles (>1 million) used relatively low memory and low CPU cost. When the correct storage method was used, particle tracking also produces outputs that require relatively low disk storage. This study was able to run multiple 7-year simulations with more than 6 million particles across the entire North Atlantic Ocean, and as a result understand long-term trends in basin wide Sargassum transport.

As well as creating a Sargassum particle tracking model, I was able to produce a post-process Sargassum growth model that applied physiological behaviours to the individual particles for along trajectory changes in biomass. This method has only been used for Sargassum twice, by Brooks et al. (2019) and Marsh et al. (2021), using a simplified equation to describe the changes in organic carbon. I incorporated the more complex equations described within Jouanno et al. (2021), with the basin-wide particle tracking simulations to explore the changes in biomass across the North Atlantic over time. In satellite observations, Sargassum biomass peaks over summer in 2011, 2012, 2014, and 2015, which is reflected within the biomass outputs of the growth model (Figure 4.5). Combining particle tracking with a four parameter biophysical model (Equation 2.28) demonstrated that coupled Eularian biogeochemical models, such as those in Jouanno et al. (2021), may not always be necessary depending on the application and that particle tracking can be effectively used beyond small-scale simulations.

As stated within Marsh et al. (2023), the physiological behaviours used within Chapters 4 and 5, however, were developed based on *in vitro* experiments on *Sargassum* from the Sargasso Sea. Therefore, it is key to note that differences in modelled biomass and observations may also be due to the model describing the wrong morphological type of *Sargassum* and validation from *in situ* measurements would improve the reliability of the results.

6.1.2 Role of Stokes Drift and Windage in the Formation of the GASB

Results from Chapter 3 demonstrated that Stokes drift was vital in transporting particles between the Sargasso Sea and Equatorial Atlantic. The inclusion of surface currents and Stokes drift to advection velocities increased the spread of particles across the North Atlantic, with a decreased concentration at the centre of the gyre (Figure 3.9). Stokes drift is known to increase particle dispersal when included into particle tracking model simulations (Bosi et al. 2021) explaining the increased spread seen in Chapter 3's results. When windage is added to the advection, however, transport out of the Sargasso Sea was reduced. The wind acted against the transport from waves, therefore the weaker winds allowed the increased dispersal of particles towards the outer boundary currents where they could escape the gyre, seen in the distribution of annual particle densities (Figure 3.9).

This study was able to demonstrate the ability of surface particles to physically escape the Sargasso Sea, as a one-off event, and determine a window in which it happened. Particle transport out of the Sargasso Sea peaked in 2010 (Figure 3.5). At this time, the North Atlantic was experiencing the most extreme negative phase of the NAO for 150 years (Jung et al. 2011). The negative phase of the NAO causes a southward shift of the westerlies and weakens the trade winds across the North Atlantic.

An observed increase in Stokes drift in the northwest of the subtropical gyre combined with the weakened winds is the cause of enhanced eastward transport of Sargassum back in 2010. Unlike windage, Stokes drift was not included in key Sargassum models due to the belief that it was not a major factor in transport within the open ocean (Zhang et al. 2024; Putman et al. 2018). Results from Chapter 3 agreed with the output of Jouanno et al. (2023) to demonstrate that Stokes drift has a significant impact on Sargassum's large-scale distribution (Figure 3.9). Why does it have such a large impact? Pärn et al. (2023) used Lagrangian particle tracking to reproduce surface drifter trajectories and demonstrated that the inclusion of Stokes drift produced better fit to the surface drifter trajectory. They concluded that adding Stokes drift accounts for the differences in wind and wave directions. Similarly, the inclusion of Stokes drift was also found to be important in improving the accuracy of oil spill models for simulations lasting 2 days or more (Yang et al. 2021). Therefore, results of this thesis have demonstrated the importance of including Stokes drift into Sargassum transport models.

6.1.3 Role of the Azores Current in the Formation of the GASB

Multiple studies noted a link in timing of the first GASB bloom and an extreme negative phase of the NAO, but had not explored how the NAO had caused the formation of the GASB (Wang et al. 2019; Johns et al. 2020). Johns et al. (2020) hypothesised that during this negative phase of the NAO, Sargassum was transported from the Sargasso Sea to the Equatorial Atlantic along the Canary Current (CC). Results of Chapter 3 were able to support this hypothesis by producing particle trajectories that flow within the path of the CC (Figure 3.6).

This study also went a step further and highlighted a key feature that allowed the particles to enter the CC, the AzC. Figure 3.6 illustrated that particles flowed along the line of latitude primarily associated with the AzC. Prolonged strengthening of the AzC in 2010, visualised in Figure 3.8, was likely able to transport the Sargassum out of the Sargasso Sea and into the CC. A long-term study by Frazão et al. (2022) demonstrated that changes in the AzC are linked to variability in the Gulf Stream and, more generally, decadal changes within the North Atlantic. Stokes drift and wind values across the GS region were higher in 2010 than average (Figure 3.11). This "higher than average" period extends into the AzC region, possibly explaining the enhanced velocities observed in 2010 (Figure 3.8). As demonstrated in Figure 3.12, the AzC is often observed with multiple eddies, and in fact is associated with a band of high Eddy Kinetic Energy (EKE) levels (Richardson 1983; Brügge 1995; Stammer 1997). Figure 6.2 plots the meridional distribution of EKE values at 30°W (averaged between 25°and 35°W) to show that the AzC EKE values, at roughly 34°N are much higher than the surrounding latitudes. Why would EKE have an impact on the outcomes of this study? Higher EKE values are associated with large eddies and fast flowing currents, however, Jia (2000) discovered that even high-resolution models of the North Atlantic, such as the CMEMS model used within this study, are not fully reproducing the instabilities and EKE values observed in in situ data of this current.

Therefore, the particle tracking methodology is limited to the numerical model used for advection of the particles when reproducing trajectories. A method to improve AzC variability within the model would be to use variable diffusivity coefficients. A function to calculate horizontal diffusivity was included in a very recent version of the Parcels particle tracking software. Instead of defining a diffusion coefficient, as in this study, the

user can get a diffusivity value, K, for each particle location and at each timestep based off the Smagorinsky method (Smagorinsky 1963). While the current numerical model velocities might not fully reproduce conditions within the AzC, adding in varied diffusivity values may further demonstrate the enhanced energy within the current compared to the surrounding waters and its impact on Sargassum transport. However, even with the limitations of this method, results still demonstrate a key link between the AzC, NAO, and the formation of the GASB that has not been defined in current literature.

6.1.4 Enhanced *Sargassum* Growth when Transported from the Sargasso Sea to the Equatorial Atlantic

Chapter 3 determined *Sargassum* was transported along the AzC and CC, and eventually into the Equatorial Atlantic. However, to form the GASB population Sargassum must survive the journey. It is unknown, within current literature, if the conditions within the AzC and CC can sustain a Sargassum population. The along trajectory *Sargassum* model, in Chapter 4, was able to visualise the spatial and temporal changes in particle biomass. To do this, a post-process growth model was applied to the particle tracking output from Chapter 3.

As the aim of this study was to determine if Sargassum was able to survive transportation to the Equatorial Atlantic, analysis focussed on particles that travelled along the CC. Of those particles, peaks in biomass values and growth rates occurred near West Africa regardless of their initial release date and coordinates (Figure 4.10). These particles flowed through regions of high nutrients and optimum temperatures, within this region of the CC, with biomass values increasing by over 80% (Figure 4.6). Upwelling has been observed within this region for decades (Mittelstaedt 1983). Large-scale coastal upwelling, at its peak, can occur between 10°N to 30°N due to the strong and persistent trade winds (Mittelstaedt 1983). This upwelling supplies nutrients to the surface waters directly within the modelled trajectory of Sargassum. Interestingly, the spatial extent and intensity of this upwelling region is affected by El Niño events which occurred during the winter of 2009/2010 (López-Parages et al. 2020). Knowing that the Sargassum was provided suitable conditions for growth along the calculated transport route, between the Sargasso Sea and the Equatorial Atlantic, strengthens the results of Chapter 3. Chapter 3 determined that the formation of the GASB was due to the transport of Sargassum from the Sargasso Sea

to the Equatorial Atlantic along the AzC and the CC, while Chapter 4 has now determined that this was a viable route that supported along-trajectory growth.

6.1.5 Use of a Simple Box Model to Simulate *Sargassum* Within the Equatorial Atlantic

One of the aims of this thesis was to explore what conditions are necessary for Sargassum to thrive within the Equatorial Atlantic once it was transported from the Sargasso Sea. To achieve this aim, a simple box model of the region (0 - 10°N, 60 - 15°W) was produced. This model estimated the Sargassum biomass in this region, using the growth and decay equations from Chapter 4, balanced by the calculated inflow and outflow. From 2011 onwards, peaks in the modelled biomass coincided with peaks in satellite observations of Sargassum blooms (Chapter 5; Figure 5.6). This both suggests the model was reproducing a life-like simulation of Sargassum within the Equatorial Atlantic and that parameters included within the model may contribute to the interannual variability of GASB bloom size. It is key to note that the box model covers a relatively large spatial area, of which it assumes it is well mixed. For any section of the ocean, this is usually not the case. However, for this use case, where the entirety of the GASB region was studied over a 9-year period, it was less of an issue.

Biomass, produced by the simple box model, peaked twice a year (Figure 5.6). This actually matches Jouanno et al. (2021)'s observed and modelled biomass within the Eastern Tropical Atlantic which they defined as between 0 - 15°N and 30 - 0°W. This suggests that conditions within the Eastern Tropical Atlantic are the driving forces for the box model. Brandt et al. (2023) studied seasonal cycles of temperature and nitrates within the Eastern Tropical Atlantic (1.5°S - 0.5°N, 20 - 5°W) (Figure 5.7). While this region only covers the lower .5°of the simple box model region, the seasonal changes show an obvious correlation with the box model biannual peaks (Figure 5.6) and the observations by Jouanno et al. (2021) within the East Equatorial Atlantic (Figure 5.1).

6.1.6 Role of Phosphates in the Variability of *Sargassum* Biomass in the Equatorial Atlantic

Within the Sargassum model, used in both Chapters 4 and 5, growth is determined by individual functions of temperature, irradiance, nitrates and phosphates (Equation 2.28).

Determining which conditions are necessary for growth, however, was more of a challenge. I explored the individual impact of each parameter on the monthly biomass values, from Chapter 5, using linear regression analysis. Interestingly, only the phosphates were shown to be linked to the changes in biomass. The relationship between biomass and phosphates were shown to have a strong positive correlation, with a correlation coefficient of 0.76, meaning higher phosphate values within the Equatorial Atlantic was attributed with higher biomass values.

Lapointe (1986) demonstrated that photosynthetic rates for *Sargassum* were doubled with phosphate enrichment within *in vivo* experiments. However, phosphate limitation has not been isolated, as a cause of variability, within recent studies on GASB variability. This study demonstrated that the box model was able to produce fairly accurate trends in *Sargassum* blooms, and that phosphate availability has accounted for 58% of the changes in biomass. The surface waters within the Equatorial Atlantic are generally depleted in phosphates (Martiny et al. 2019) and as seen in Figure 4.3. Figure 4.3 demonstrated that the main source of phosphates is coastal upwelling within the northeast of the region.

Results from Chapter 5 determined that the CMEMS BGC model underestimates phosphate values within the West Equatorial Atlantic (Figure 5.11) when compared to the WOA data. The Amazon River is known to inject considerable amounts of phosphates into this region both naturally, such as bacterial decomposition of organic material (Berner and Rao 1994), and anthropogenically. Land use surrounding the Amazon River has been increasingly used as farm land, with an increased use of fertilisers (Jankowski et al. 2018). Beusen et al. (2022) predict that by 2050, anthropogenic sources will contribute up to 80% of excess nutrients within rivers. The Amazon River discharge has been constantly increasing since 1980 (Liang et al. 2020), and with that increased discharge is an increase in phosphates that could be flowing into the Equatorial Atlantic that was underestimated in the box model (Figure 5.10). Interestingly, although the CMEMS BGC model does incorporate riverine inputs—using the NEMO-PISCES framework-comparisons with the WOA climatology in Figure 5.11 do not clearly reflect this influence. Coastal regions are more likely to be impacted by any of these discrepancies, as these riverine inputs are more pronounced.

6.2 Further Work

6.2.1 3D Particle Tracking with Sinking Parameter

I primarily focused on the horizontal transport of Sargassum for the particle tracking simulations and therefore only ran the model in 2D. However, as stated within Section 1.1, Sargassum reproduces using a fragmentation method where older strands lose buoyancy and detach from the main strand. Over time, the decayed strands sink. The methods used in this study did not account for sinking within the model's loss term. Jouanno et al. (2021) accounted for sinking within their BGC model, but it was not clear the impact sinking had on their results. Within Jouanno et al. (2021) model, sinking was described as a loss term. Therefore, the Sargassum model created within this thesis could possibly be underestimating mortality rates. Adding in sinking would not only improve estimates of Sargassum biomass but could even provide an estimate of the Sargassum carbon sequestration. As Sargassum grows, it converts atmospheric carbon to organic carbon and since it sinks once it dies, it takes that carbon with it to the depths of the ocean. Providing an estimate of this could help improve carbon models to provide further evidence as to why the ocean provides a clear role in the global carbon cycle.

The *Sargassum* model could also be improved by increasing its complexity. It has been hypothesised that *Sargassum* can store nutrients but also that the decaying *Sargassum* strands can provide nutrients (Lapointe et al. 2021). It was also shown within Hanisak and Samuel (1987) that *Sargassum* growth may be influenced by salinity. Salinity was another variable highlighted in the western Equatorial Atlantic that is highly variable and has changed over the course of the model simulations (Figure 5.12). Incorporating a salinity-dependent function into the carbon uptake term, as well as accounting for nutrient recycling within the nutrient uptake term, could enhance the model and provide new insights into *Sargassum* growth.

6.2.2 Further Fine-Tuning of the Box Model to Examine Causes of *Sargassum* Variation

In this thesis, the box model treated the Equatorial Atlantic as one box to cover the area the Sargassum belt population inhabits. This approach calculated change in the GASB biomass over time while assuming the box region was well mixed throughout, however,

the area is dynamic with localised regions of nutrient sources and sinks (Kawase and Sarmiento 1985). The GASB is also well known to show high interannual variability in its spatial distribution (Wang et al. 2019). To understand further the causes of variability, this model could be split into at least four boxes to produce separate biomass outputs.

As stated in Section 6.1.6, there is a possibility phosphates from the Amazon River outflow could be impacting GASB bloom interannual variability. A box model, split into four quadrants, would isolate the outflow area to explore the direct impact of the Amazon River on Sargassum biomass. It is key to note that for this further work to be completed, the nutrient input into the model needs to reflect the true nutrient values within the river discharge.

6.3 Concluding Remarks

This study was able to demonstrate the viable transport of *Sargassum* from the Sargasso Sea to the Equatorial Atlantic providing new insights into the formation of the GASB. Key contributions include:

- Highlighting the role of the Azores Current in the formation of the GASB
- Demonstrating the importance of including Stokes drift when modelling the physical transport of *Sargassum*
- Developing a novel *Sargassum* along-trajectory growth model
- Producing a simple box model of *Sargassum* within the Equatorial Atlantic
- Highlighting phosphate availability as a key driver of *Sargassum* interannual variability

This work has advanced our current knowledge of the GASB formation and key drivers influencing its growth and decay. A major challenge with *Sargassum* inundations is their unpredictable nature. By adding to existing knowledge of how the GASB forms and what controls its interannual variability, this research supports future prediction efforts and aligns with hypotheses proposed by Wang et al. (2019) and Johns et al. (2020). Additionally, the use of open-source and computationally efficient methods were confirmed to be capable of modelling basin-wide organic matter transport and growth. Therefore,

offering a viable framework for nations with limited resources to develop their own models. It also provides a platform that is applicable to any 2D floating particles, such as plastics or oil spills, while acknowledging the importance of including Stokes drift and dispersion.

References

Aijaz, Saima, Colberg, Frank, and Brassington, Gary B. (Apr. 2024). "Lagrangian and Eulerian modelling of river plumes in the Great Barrier Reef system, Australia". In: *Ocean Modelling* 188, p. 102310. ISSN: 1463-5003. DOI: 10.1016/J.OCEMOD.2023.102310.

Alliance, Sargasso Sea (2011). *Summary Science and Supporting Evidence Case*. Available at https://www.sargassoseacommission.org.

Ardhuin, Fabrice, Marié, Louis, Rascle, Nicolas, Forget, Philippe, and Roland, Aron (Nov. 2009). "Observation and estimation of Lagrangian, Stokes, and Eulerian currents induced by wind and waves at the sea surface". In: *Journal of Physical Oceanography* 39 (11), pp. 2820–2838. ISSN: 00223670. DOI: 10.1175/2009jpo4169.1.

Astudillo, Juan Carlos, Bravo, Macarena, Dumont, Clément P., and Thiel, Martin (2009). "Detached aquaculture buoys in the SE Pacific: Potential dispersal vehicles for associated organisms". In: *Aquatic Biology* 5 (3), pp. 219–231. ISSN: 18647782. DOI: 10.3354/ab00151.

Aumont, O., Ethé, C., Tagliabue, A., Bopp, L., and Gehlen, M. (Aug. 2015). "PISCES-v2: An ocean biogeochemical model for carbon and ecosystem studies". In: *Geoscientific Model Development* 8 (8), pp. 2465–2513. ISSN: 19919603. DOI: 10.5194/GMD-8-2465-2015.

Bendoricchio, G., Coffaro, G., and Marchi, C. De (Sept. 1994). "A trophic model for Ulva rigida in the Lagoon of Venice". In: *Ecological Modelling* 75-76 (C), pp. 485–496. ISSN: 0304-3800. DOI: 10.1016/0304-3800(94)90042-6.

Berline, Léo, Ody, Anouck, Jouanno, Julien, Chevalier, Cristèle, André, Jean Michel, Thibaut, Thierry, and Ménard, Frédéric (Sept. 2020). "Hindcasting the 2017 dispersal of Sargassum algae in the Tropical North Atlantic". In: *Marine Pollution Bulletin* 158, p. 111431. ISSN: 18793363. DOI: 10.1016/j.marpolbul.2020.111431.

Berloff, Pavel, Ryzhov, Evgeny, and Shevchenko, Igor (2021). "On dynamically unresolved oceanic mesoscale motions". In: *Journal of Fluid Mechanics* 920, A41. DOI: 10.1017/jfm.2021.477.

Berner, Robert A. and Rao, Ji Long (1994). "Phosphorus in sediments of the Amazon River and estuary: implications for the global flux of phosphorus to the sea". In: *Geochim. Cosmochim. Acta* 58 (10), pp. 2333–9. ISSN: 00167037. DOI: 10.1016/0016-7037(94)90014-0.

Beron-Vera, F. J., Olascoaga, M. J., and Lumpkin, R. (2016). "Inertia-induced accumulation of flotsam in the subtropical gyres". In: *Geophysical Research Letters* 43 (23), pp. 12,228–12,233. ISSN: 19448007. DOI: 10.1002/2016GL071443.

Beusen, A. H.W., Doelman, J. C., Beek, L. P.H. Van, Puijenbroek, P. J.T.M. Van, Mogollón, J. M., Grinsven, H. J.M. Van, Stehfest, E., Vuuren, D. P. Van, and Bouwman, A. F. (Jan. 2022). "Exploring river nitrogen and phosphorus loading and export to global coastal waters in the Shared Socio-economic pathways". In: *Global Environmental Change* 72, p. 102426. ISSN: 0959-3780. DOI: 10.1016/J.GLOENVCHA.2021.102426. URL: https://www.sciencedirect.com/science/article/pii/S0959378021002053?utm_source=chatgpt.com.

Biermann, Lauren, Clewley, Daniel, Martinez-Vicente, Victor, and Topouzelis, Konstantinos (Apr. 2020). "Finding Plastic Patches in Coastal Waters using Optical Satellite Data". In: *Scientific Reports 2020 10:1* 10 (1), pp. 1–10. ISSN: 2045-2322. DOI: 10.1038/s41598-020-62298-z. URL: https://www.nature.com/articles/s41598-020-62298-z.

Birchill, Antony J., Baker, Chelsey A., Wyatt, Neil J., Pabortsava, Katsiaryna, Venables, Hugh J., Moore, C. Mark, Turnbull, Isobel, Milne, Angela, Ussher, Simon J., Oliver, Sophy, and Martin, Adrian P. (Aug. 2024). "Pathways and timescales of Southern Ocean

hydrothermal iron and manganese transport". In: *Communications Earth Environment 2024 5:1* 5 (1), pp. 1–10. ISSN: 2662-4435. DOI: 10.1038/s43247-024-01564-8. URL: https://www.nature.com/articles/s43247-024-01564-8.

Bistafa, Sylvio R. (2018). "On the development of the Navier-Stokes equation by Navier". In: *Revista Brasileira de Ensino de Fisica* 40 (2). ISSN: 01024744. DOI: 10.1590/1806-9126-RBEF-2017-0239.

Blare, Trent, Abdool-Ghany, Afeefa A., and Solo-Gabriele, Helena M. (Feb. 2023). "Cost Estimates for Producing Sargassum spp. Compost: FE1128, 2/2023". In: *EDIS* 2023 (1). ISSN: 2576-0009. DOI: 10.32473/EDIS-FE1128-2023. URL: https://journals.flvc.org/edis/article/view/130891.

Bosi, Sofia, Broström, Göran, and Roquet, Fabien (Aug. 2021). "The Role of Stokes Drift in the Dispersal of North Atlantic Surface Marine Debris". In: *Frontiers in Marine Science* 8, p. 697430. ISSN: 22967745. DOI: 10.3389/FMARS.2021.697430/BIBTEX. URL: www.frontiersin.org.

Boutin, J., Vergely, J.-L., Reul, N., Catany, R., Jouanno, J., Martin, A., Rouffi, F., Bertino, L., Bonjean, F., Corato, G., Gévaudan, M., Guimbard, S., Khvorostyanov, D., Kolodziejczyk, N., Matthews, M., Olivier, L., Raj, R., Rémy, E., Reverdin, G., Supply, A., Thouvenin-Masson, C., Vialard, J., Sabia, R., and Mecklenburg, S. (2024). *ESA Sea Surface Salinity Climate Change Initiative (Sea_Surface_Salinity_cci): Weekly sea surface salinity product for the Southern Hemisphere on a 25 km EASE grid, v04.41, for 2010 to 2022*. NERC EDS Centre for Environmental Data Analysis. DOI: 10.5285/f2ca631f29a24c47a7e98654ddf2c7d9.

Brandt, Peter, Alory, Gaël, Awo, Founi Mesmin, Dengler, Marcus, Djakouré, Sandrine, Koungue, Rodrigue Anicet Imbol, Jouanno, Julien, Körner, Mareike, Roch, Marisa, and Rouault, Mathieu (May 2023). "Physical processes and biological productivity in the upwelling regions of the tropical Atlantic". In: *Ocean Science* 19 (3), pp. 581–601. ISSN: 18120792. DOI: 10.5194/OS-19-581-2023.

Breivik, Øyvind, Bidlot, Jean Raymond, and Janssen, Peter A.E.M. (Apr. 2016). "A Stokes drift approximation based on the Phillips spectrum". In: *Ocean Modelling* 100, pp. 49–56. ISSN: 1463-5003. DOI: 10.1016/J.OCEMOD.2016.01.005.

Brooks, Maureen T., Coles, Victoria J., and Coles, William C. (Mar. 2019). "Inertia Influences Pelagic Sargassum Advection and Distribution". In: *Geophysical Research Letters* 46 (5), pp. 2610–2618. ISSN: 19448007. DOI: 10.1029/2018GL081489.

Brügge, Bernd (Oct. 1995). "Near-surface mean circulation and kinetic energy in the central North Atlantic from drifter data". In: *Journal of Geophysical Research: Oceans* 100 (C10), pp. 20543–20554. ISSN: 2156-2202. DOI: 10.1029/95JC01501. URL: https://onlinelibrary.wiley.com/doi/full/10.1029/95JC01501https://onlinelibrary.wiley.com/doi/abs/10.1029/95JC01501https://agupubs.onlinelibrary.wiley.com/doi/10.1029/95JC01501.

Byers, James E. and Pringle, James M. (Sept. 2024). "Variation in Oceanographic Resistance of the World's Coastlines to Invasion by Species With Planktonic Dispersal". In: *Ecology letters* 27 (9), e14520. ISSN: 14610248. DOI: 10.1111/ELE.14520.

Carpenter, Edward J. and Cox, James L. (May 1974). "Production of pelagic Sargassum and a blue-green epiphyte in the western Sargasso Sea1". In: *Limnology and Oceanography* 19 (3), pp. 429–436. ISSN: 1939-5590. DOI: 10.4319/LO.1974.19.3.0429. URL: https://onlinelibrary.wiley.com/doi/full/10.4319/lo.1974.19.3.0429https://onlinelibrary.wiley.com/doi/abs/10.4319/lo.1974.19.3.0429https://aslopubs.onlinelibrary.wiley.com/doi/10.4319/lo.1974.19.3.0429.

Carr, Archie, Meylan, Anne, Mortimer, Jeanne, Bjorndal, Karen, and Carr, Thomas (1982). *I O F C 0* 9-SURVEYS OF SEA TURTLE POPULATIONS AND HABITATS IN THE WESTERN ATLANTIC "A'rES 0*.* Tech. rep.

Chelton, Dudley B, Deszoeke, Roland A, Schlax, Michael G, El, Karim, and Siwertz, Nicolas (1998). *Geographical Variability of the First Baroclinic Rossby Radius of Deformation*. Tech. rep. Oregon State University.

Chubarenko, I., Bagaev, A., Zobkov, M., and Esiukova, E. (July 2016). "On some physical and dynamical properties of microplastic particles in marine environment". In: *Marine Pollution Bulletin* 108 (1-2), pp. 105–112. ISSN: 0025-326X. DOI: 10.1016/J.MARPOLBUL.2016.04.048.

Crespo, Lander R., Keenlyside, Noel, and Koseki, Shunya (May 2019). "The role of sea surface temperature in the atmospheric seasonal cycle of the equatorial Atlantic". In: *Climate Dynamics* 52 (9-10), pp. 5927–5946. ISSN: 14320894. DOI: 10.1007/S00382-018-4489-4/FIGURES/13. URL: https://link.springer.com/article/10.1007/s00382-018-4489-4.

Cunningham, H. J., Higgins, C., and Bremer, T. S. van den (June 2022). "The Role of the Unsteady Surface Wave-Driven Ekman–Stokes Flow in the Accumulation of Floating Marine Litter". In: *Journal of Geophysical Research: Oceans* 127 (6), e2021JC018106. ISSN: 2169-9291. DOI: 10.1029/2021JC018106. URL: https://onlinelibrary.wiley.com/doi/full/10.1029/2021JC018106https://onlinelibrary.wiley.com/doi/abs/10.1029/2021JC018106https://agupubs.onlinelibrary.wiley.com/doi/10.1029/2021JC018106.

Dagestad, Knut Frode, Röhrs, Johannes, Breivik, Oyvind, and Ådlandsvik, Bjørn (Apr. 2018). "OpenDrift v1.0: A generic framework for trajectory modelling". In: *Geoscientific Model Development* 11 (4), pp. 1405–1420. ISSN: 19919603. DOI: 10.5194/GMD-11-1405-2018.

Davis, Doleasha, Simister, Rachael, Campbell, Sanjay, Marston, Melissa, Bose, Suranjana, McQueen-Mason, Simon J., Gomez, Leonardo D., Gallimore, Winklet A., and Tonon, Thierry (Mar. 2021). "Biomass composition of the golden tide pelagic seaweeds Sargassum fluitans and S. natans (morphotypes I and VIII) to inform valorisation pathways". In: *The Science of the total environment* 762. ISSN: 1879-1026. DOI: 10.1016/J.SCITOTENV.2020.143134. URL: https://pubmed.ncbi.nlm.nih.gov/33148447/.

Delandmeter, P. and Sebille, E. van (2019). "The Parcels v2.0 Lagrangian framework: new field interpolation schemes". In: *Geoscientific Model Development* 12.8, pp. 3571–3584.

DOI: 10.5194/gmd-12-3571-2019. URL: https://gmd.copernicus.org/articles/12/3571/2019/.

Deser, Clara, Hurrell, James W., and Phillips, Adam S. (Nov. 2017). "The role of the North Atlantic Oscillation in European climate projections". In: *Climate Dynamics* 49 (9-10), pp. 3141–3157. ISSN: 14320894. DOI: 10.1007/s00382-016-3502-z.

Djakouré, Sandrine, Penven, Pierrick, Bourlès, Bernard, Veitch, Jennifer, and Koné, Vamara (Oct. 2014). "Coastally trapped eddies in the north of the Gulf of Guinea". In: *Journal of Geophysical Research: Oceans* 119 (10), pp. 6805–6819. ISSN: 2169-9291. DOI: 10.1002/2014JC010243. URL: https://onlinelibrary.wiley.com/doi/full/10.1002/2014JC010243https://onlinelibrary.wiley.com/doi/abs/10.1002/2014JC010243https://agupubs.onlinelibrary.wiley.com/doi/10.1002/2014JC010243.

Drivdal, M., Broström, G., and Christensen, K. H. (2014). "Wave-induced mixing and transport of buoyant particles: application to the Statfjord A oil spill". In: *Ocean Science* 10.6, pp. 977–991. DOI: 10.5194/os-10-977-2014. URL: https://os.copernicus.org/articles/10/977/2014/.

Eriksen, Marcus, Lebreton, Laurent C.M., Carson, Henry S., Thiel, Martin, Moore, Charles J., Borerro, Jose C., Galgani, Francois, Ryan, Peter G., and Reisser, Julia (Dec. 2014). "Plastic Pollution in the World's Oceans: More than 5 Trillion Plastic Pieces Weighing over 250,000 Tons Afloat at Sea". In: *PLOS ONE* 9 (12), e111913. ISSN: 1932-6203. DOI: 10.1371/JOURNAL.PONE.0111913. URL: https://journals.plos.org/plosone/article?id=10.1371/journal.pone.0111913.

Ferronato, Carola, Berden, Giuliana, Rivarossa, Martín, and Guinder, Valeria A. (Oct. 2023). "Wind-driven currents and water masses shape spring phytoplankton distribution and composition in hydrologically complex, productive shelf waters". In: *Limnology and Oceanography* 68 (10), pp. 2195–2210. ISSN: 19395590. DOI: 10.1002/LNO.12413.

Fidai, Y. A., Dash, J., Tompkins, E. L., and Tonon, T. (Dec. 2020). "A systematic review of floating and beach landing records of Sargassum beyond the Sargasso Sea". In: *Environmental Research Communications* 2 (12), p. 122001. ISSN: 2515-7620. DOI:

10.1088/2515-7620/ABD109. URL: https://iopscience.iop.org/article/10.1088/2515-7620/abd109https://iopscience.iop.org/article/10.1088/2515-7620/abd109/meta.

Fox-Kemper, Baylor, Adcroft, Alistair, Böning, Claus W., Chassignet, Eric P., Curchitser, Enrique, Danabasoglu, Gokhan, Eden, Carsten, England, Matthew H., Gerdes, Rüdiger, Greatbatch, Richard J., Griffies, Stephen M., Hallberg, Robert W., Hanert, Emmanuel, Heimbach, Patrick, Hewitt, Helene T., Hill, Christopher N., Komuro, Yoshiki, Legg, Sonya, Sommer, Julien Le, Masina, Simona, Marsland, Simon J., Penny, Stephen G., Qiao, Fangli, Ringler, Todd D., Treguier, Anne Marie, Tsujino, Hiroyuki, Uotila, Petteri, and Yeager, Stephen G. (Feb. 2019). "Challenges and prospects in ocean circulation models". In: *Frontiers in Marine Science* 6 (FEB), p. 434281. ISSN: 22967745. DOI: 10.3389/FMARS.2019.00065/PDF. URL: www.frontiersin.org.

Franks, James S., Johnson, Donald R., and Ko, Dong S. (2016). "Pelagic Sargassum in the Tropical North Atlantic". In: *Gulf and Caribbean Research* 27 (1). ISSN: 1528-0470. DOI: 10.18785/gcr.2701.08.

Frazão, Helena C., Prien, Ralf D., Schulz-Bull, Detlef E., Seidov, Dan, and Waniek, Joanna J. (2022). "The Forgotten Azores Current: A Long-Term Perspective". In: *Frontiers in Marine Science* 9. ISSN: 2296-7745. DOI: 10.3389/fmars.2022.842251. URL: https://www.frontiersin.org/journals/marine-science/articles/10.3389/fmars.2022.842251.

Freitas, Pedro Paulo de, Cirano, Mauro, Teixeira, Carlos Eduardo Peres, Marta-Almeida, Martinho, Brito Borges, Francisco Flávio de, Guerrero-Martin, Camilo Andrés, and Gomes, Vando José Costa (Apr. 2024). "Pathways of surface oceanic water intrusion into the Amazon Continental Shelf". In: *Ocean Dynamics* 74 (4), pp. 321–334. ISSN: 16167228. DOI: 10.1007/S10236-024-01606-X/FIGURES/14. URL: https://link.springer.com/article/10.1007/s10236-024-01606-x.

Fried, Nora, Biló, Tiago C., Johns, William E., Katsman, Caroline A., Fogaren, Kristen E., Yoder, Meg, Palevsky, Hilary I., Straneo, Fiammetta, and de Jong, M. Femke (2024). "Recent Freshening of the Subpolar North Atlantic Increased the Transport of Lighter

Waters of the Irminger Current From 2014 to 2022". English. In: *Journal of Geophysical Research: Oceans* 129.11. ISSN: 2169-9275. DOI: 10.1029/2024JC021184.

García-Sánchez, Marta, Graham, Caroline, Vera, Elisa, Escalante-Mancera, Edgar, Filip, Lorenzo Álvarez, and Tussenbroek, Brigitta I. van (Oct. 2020). "Temporal changes in the composition and biomass of beached pelagic Sargassum species in the Mexican Caribbean". In: *Aquatic Botany* 167, p. 103275. ISSN: 0304-3770. DOI: 10.1016/J.AQUABOT.2020.103275.

Gleeson, Emily, Gallagher, Sarah, Clancy, Colm, and Dias, Frédéric (Feb. 2017). "NAO and extreme ocean states in the Northeast Atlantic Ocean". In: *Advances in Science and Research* 14, pp. 23–33. DOI: 10.5194/ASR-14-23-2017.

Goldstein, Miriam C., Titmus, Andrew J., and Ford, Michael (Nov. 2013). "Scales of Spatial Heterogeneity of Plastic Marine Debris in the Northeast Pacific Ocean". In: *PLOS ONE* 8 (11), e80020. ISSN: 1932-6203. DOI: 10.1371/JOURNAL.PONE.0080020. URL: https://journals.plos.org/plosone/article?id=10.1371/journal.pone.0080020.

Gower, J. F.R. and King, S. A. (2011). "Distribution of floating Sargassum in the Gulf of Mexico and the Atlantic Ocean mapped using MERIS". In: *International Journal of Remote Sensing* 32 (7), pp. 1917–1929. ISSN: 13665901. DOI: 10.1080/01431161003639660. URL: https://www.tandfonline.com/doi/abs/10.1080/01431161003639660.

Gower, J. and King, S. (Aug. 2020). "The distribution of pelagic Sargassum observed with OLCI". In: *International Journal of Remote Sensing* 41 (15), pp. 5669–5679. ISSN: 13665901. DOI: 10.1080/01431161.2019.1658240.

Gower, Jim, Young, Erika, and King, Stephanie (2013). "Satellite images suggest a new Sargassum source region in 2011". In: *Remote Sensing Letters* 4 (8), pp. 764–773. ISSN: 2150704X. DOI: 10.1080/2150704X.2013.796433.

Gruber, Nicolas, Lachkar, Zouhair, Frenzel, Hartmut, Marchesiello, Patrick, Münnich, Matthias, McWilliams, James C., Nagai, Takeyoshi, and Plattner, Gian Kasper (Oct. 2011). "Eddy-induced reduction of biological production in eastern boundary upwelling

systems". In: *Nature Geoscience 2011 4:11* 4 (11), pp. 787–792. ISSN: 1752-0908. DOI: 10.1038/ngeo1273. URL: https://www.nature.com/articles/ngeo1273.

Gupta, Mukund, Williams, Richard G, Lauderdale, Jonathan M, Jahn, Oliver, Hill, Christopher, Dutkiewicz, Stephanie, and Follows, Michael J (2022). "A nutrient relay sustains subtropical ocean productivity". In: DOI: 10.1073/pnas. URL: https://doi.org/10.1073/pnas.2206504119.

Hanisak, M. Denni (Apr. 1993). "Nitrogen release from decomposing seaweeds: species and temperature effects". In: *Journal of Applied Phycology* 5 (2), pp. 175–181. ISSN: 09218971. DOI: 10.1007/BF00004014/METRICS. URL: https://link.springer.com/article/10.1007/BF00004014.

Hanisak, M. Dennis and Samuel, Mary A. (1987). "Growth rates in culture of several species of Sargassum from Florida, USA". In: *Twelfth International Seaweed Symposium*, pp. 399–404. DOI: 10.1007/978-94-009-4057-4_59. URL: https://link.springer.com/chapter/10.1007/978-94-009-4057-4_59.

Hardman-Mountford, N. J. and McGlade, J. M. (Aug. 2003). "Seasonal and interannual variability of oceanographic processes in the Gulf of Guinea: An investigation using AVHRR sea surface temperature data". In: *International Journal of Remote Sensing* 24 (16), pp. 3247–3268. ISSN: 01431161. DOI: 10.1080/0143116021000021297.

Hersbach, Hans, Bell, Bill, Berrisford, Paul, Hirahara, Shoji, Horányi, András, Muñoz-Sabater, Joaquín, Nicolas, Julien, Peubey, Carole, Radu, Raluca, Schepers, Dinand, Simmons, Adrian, Soci, Cornel, Abdalla, Saleh, Abellan, Xavier, Balsamo, Gianpaolo, Bechtold, Peter, Biavati, Gionata, Bidlot, Jean, Bonavita, Massimo, Chiara, Giovanna De, Dahlgren, Per, Dee, Dick, Diamantakis, Michail, Dragani, Rossana, Flemming, Johannes, Forbes, Richard, Fuentes, Manuel, Geer, Alan, Haimberger, Leo, Healy, Sean, Hogan, Robin J., Hólm, Elías, Janisková, Marta, Keeley, Sarah, Laloyaux, Patrick, Lopez, Philippe, Lupu, Cristina, Radnoti, Gabor, Rosnay, Patricia de, Rozum, Iryna, Vamborg, Freja, Villaume, Sebastien, and Thépaut, Jean Noël (July 2020). "The ERA5 global reanalysis". In: *Quarterly Journal of the Royal Meteorological Society* 146 (730), pp. 1999–2049. ISSN: 1477870X. DOI: 10.1002/QJ.3803.

Hogg, Nelson G. and Johns, William E. (1995). "Western boundary currents". In: *Reviews of Geophysics* 33 (2 S), pp. 1311–1334. ISSN: 19449208. DOI: 10.1029/95RG00491.

Hopkinson, Charles S. and Vallino, Joseph J. (Jan. 2005). "Efficient export of carbon to the deep ocean through dissolved organic matter". In: *Nature* 433 (7022), pp. 142–145. ISSN: 1476-4687. DOI: 10.1038/NATURE03191. URL: https://pubmed.ncbi.nlm.nih.gov/15650735/.

Hu, Chuanmin, Feng, Lian, Hardy, Robert F., and Hochberg, Eric J. (Sept. 2015). "Spectral and spatial requirements of remote measurements of pelagic Sargassum macroalgae". In: *Remote Sensing of Environment* 167, pp. 229–246. ISSN: 00344257. DOI: 10.1016/j.rse.2015.05.022.

Huffard, C. L., Thun, S. von, Sherman, A. D., Sealey, K., and Smith, K. L. (Nov. 2014). "Pelagic Sargassum community change over a 40-year period: temporal and spatial variability". In: *Marine Biology* 161 (12), pp. 2735–2751. ISSN: 14321793. DOI: 10.1007/S00227-014-2539-Y/TABLES/3. URL: https://link.springer.com/article/10.1007/s00227-014-2539-y.

Hurrell, James W. (Aug. 1995). "Decadal Trends in the North Atlantic Oscillation: Regional Temperatures and Precipitation". In: *Science* 269 (5224), pp. 676–679. ISSN: 00368075. DOI: 10.1126/SCIENCE.269.5224.676. URL: https://www.science.org/doi/10.1126/science.269.5224.676.

Häder, Donat P., Gröniger, Almut, Hallier, Caroline, Lebert, Michael, Figueroa, Felix L., and Jiménez, Carlos (1999). "Photoinhibition by visible and ultraviolet radiation in the red macroalga Porphyra umbilicalis grown in the laboratory". In: *Plant Ecology* 145 (2), pp. 351–358. ISSN: 13850237. DOI: 10.1023/A:1009833520770/METRICS. URL: https://link.springer.com/article/10.1023/A:1009833520770.

Ingham, Merton C (1971). "COASTAL UPWELLING IN THE NORTHWESTERN GULF OF GUINEAl". In: *BULLETIN OF MARINE SCIENCE* 20.

Jankowski, Kathi Jo, Neill, Christopher, Davidson, Eric A., Macedo, Marcia N., Costa, Ciniro, Galford, Gillian L., Santos, Leonardo Maracahipes, Lefebvre, Paul, Nunes, Darlis-

son, Cerri, Carlos E.P., McHorney, Richard, O'Connell, Christine, and Coe, Michael T. (Dec. 2018). "Deep soils modify environmental consequences of increased nitrogen fertilizer use in intensifying Amazon agriculture". In: *Scientific Reports* 8 (1), p. 13478. ISSN: 20452322. DOI: 10.1038/S41598-018-31175-1. URL: https://pmc.ncbi.nlm.nih.gov/articles/PMC6128839/.

Jean-Michel, Lellouche, Eric, Greiner, Romain, Bourdallé Badie, Gilles, Garric, Angélique, Melet, Marie, Drévillon, Clément, Bricaud, Mathieu, Hamon, Olivier, Le Galloudec, Charly, Regnier, Tony, Candela, Charles-Emmanuel, Testut, Florent, Gasparin, Giovanni, Ruggiero, Mounir, Benkiran, Yann, Drillet, and Pierre-Yves, Le Traon (July 2021). "The Copernicus Global 1/12° Oceanic and Sea Ice GLORYS12 Reanalysis". In: *Frontiers in Earth Science* 9, p. 698876. ISSN: 22966463. DOI: 10.3389/FEART.2021.698876/PDF. URL: www.frontiersin.org.

Jia, Yanli (2000). "Formation of an Azores Current due to Mediterranean overflow in a modeling study of the North Atlantic". In: *Journal of Physical Oceanography* 30.9, pp. 2342–2358.

Johns, Elizabeth M., Lumpkin, Rick, Putman, Nathan F., Smith, Ryan H., Muller-Karger, Frank E., Rueda-Roa, Digna T., Hu, Chuanmin, Wang, Mengqiu, Brooks, Maureen T., Gramer, Lewis J., and Werner, Francisco E. (Mar. 2020). "The establishment of a pelagic Sargassum population in the tropical Atlantic: Biological consequences of a basin-scale long distance dispersal event". In: *Progress in Oceanography* 182, p. 102269. ISSN: 0079-6611. DOI: 10.1016/J.POCEAN.2020.102269.

Jones-Kellett, Alexandra E. and Follows, Michael J. (Mar. 2024). "A Lagrangian coherent eddy atlas for biogeochemical applications in the North Pacific Subtropical Gyre". In: *Earth System Science Data* 16 (3), pp. 1475–1501. ISSN: 18663516. DOI: 10.5194/ESSD-16-1475-2024.

Jouanno, J., Benshila, R., Berline, L., Soulié, A., Radenac, M.-H., Morvan, G., Diaz, F., Sheinbaum, J., Chevalier, C., Thibaut, T., Changeux, T., Menard, F., Berthet, S., Aumont, O., Ethé, C., Nabat, P., and Mallet, M. (2021). "A NEMO-based model of *Sargassum* distribution in the tropical Atlantic: description of the model and sensitivity

analysis (NEMO-Sarg1.0)". In: *Geoscientific Model Development* 14.6, pp. 4069–4086. DOI: 10.5194/gmd-14-4069-2021. URL: https://gmd.copernicus.org/articles/14/4069/2021/.

Jouanno, Julien, Morvan, Guillaume, Berline, Léo, Benshila, Rachid, Aumont, Olivier, Sheinbaum, Julio, and Ménard, Frederic (Nov. 2023). "Skillful Seasonal Forecast of Sargassum Proliferation in the Tropical Atlantic". In: *Geophysical Research Letters* 50 (21). ISSN: 19448007. DOI: 10.1029/2023GL105545.

Jung, Martin, Reichstein, Markus, Margolis, Hank A., Cescatti, Alessandro, Richardson, Andrew D., Arain, M. Altaf, Arneth, Almut, Bernhofer, Christian, Bonal, Damien, Chen, Jiquan, Gianelle, Damiano, Gobron, Nadine, Kiely, Gerald, Kutsch, Werner, Lasslop, Gitta, Law, Beverly E., Lindroth, Anders, Merbold, Lutz, Montagnani, Leonardo, Moors, Eddy J., Papale, Dario, Sottocornola, Matteo, Vaccari, Francesco, and Williams, Christopher (Sept. 2011). "Global patterns of land-atmosphere fluxes of carbon dioxide, latent heat, and sensible heat derived from eddy covariance, satellite, and meteorological observations". In: *Journal of Geophysical Research: Biogeosciences* 116 (G3), pp. 0–07. ISSN: 2156-2202. DOI: 10.1029/2010JG001566. URL: https://onlinelibrary.wiley.com/doi/full/10.1029/2010JG001566https://onlinelibrary.wiley.com/doi/abs/10.1029/2010JG001566https://agupubs.onlinelibrary.wiley.com/doi/10.1029/2010JG001566.

Jutras, Mathilde, Dufour, Carolina O., Mucci, Alfonso, and Talbot, Lauryn C. (May 2023). "Large-scale control of the retroflection of the Labrador Current". In: *Nature Communications 2023 14:1* 14 (1), pp. 1–9. ISSN: 2041-1723. DOI: 10.1038/s41467-023-38321-y. URL: https://www.nature.com/articles/s41467-023-38321-y.

Kawase, M. and Sarmiento, J. L. (Sept. 1985). "Nutrients in the Atlantic thermocline". In: *Journal of Geophysical Research: Oceans* 90 (C5), pp. 8961–8979. ISSN: 2156-2202. DOI: 10.1029/JC090IC05P08961. URL: https://onlinelibrary.wiley.com/doi/full/10.1029/JC090iC05p08961https://onlinelibrary.wiley.com/doi/abs/10.1029/JC090iC05p08961https://agupubs.onlinelibrary.wiley.com/doi/10.1029/JC090iC05p08961.

Lapointe, B. E., Brewton, R. A., Herren, L. W., Wang, M., Hu, C., McGillicuddy, D. J., Lindell, S., Hernandez, F. J., and Morton, P. L. (Dec. 2021). "Nutrient content and stoichiometry of pelagic Sargassum reflects increasing nitrogen availability in the Atlantic Basin". In: *Nature Communications* 12 (1). ISSN: 20411723. DOI: 10.1038/s41467-021-23135-7.

Lapointe, Brian E. (Mar. 1986). "Phosphorus-limited photosynthesis and growth of Sargassum natans and Sargassum fluitans (Phaeophyceae) in the western North Atlantic". In: *Deep Sea Research Part A. Oceanographic Research Papers* 33 (3), pp. 391–399. ISSN: 0198-0149. DOI: 10.1016/0198-0149(86)90099-3.

Lapointe, Brian E., West, Lorin E., Sutton, Tracey T., and Hu, Chuanmin (2014). "Ryther revisited: Nutrient excretions by fishes enhance productivity of pelagic Sargassum in the western North Atlantic Ocean". In: *Journal of Experimental Marine Biology and Ecology* 458 (September), pp. 46–56. ISSN: 00220981. DOI: 10.1016/j.jembe.2014.05.002.

Lara-Hernández, J. A., Enriquez, C., Zavala-Hidalgo, J., Cuevas, E., Tussenbroek, B. van, and Uribe-Martínez, A. (Jan. 2024). "Sargassum transport towards Mexican Caribbean shores: Numerical modeling for research and forecasting". In: *Journal of Marine Systems* 241, p. 103923. ISSN: 0924-7963. DOI: 10.1016/J.JMARSYS.2023.103923.

Law-Chune, Stéphane, Aouf, Lotfi, Dalphinet, Alice, Levier, Bruno, Drillet, Yann, and Drevillon, Marie (Mar. 2021). "WAVERYS: a CMEMS global wave reanalysis during the altimetry period". In: *Ocean Dynamics* 71 (3), pp. 357–378. ISSN: 16167228. DOI: 10.1007/S10236-020-01433-W/FIGURES/17. URL: https://link.springer.com/article/10.1007/s10236-020-01433-w.

Law, Kara Lavender, Morét-Ferguson, Skye, Maximenko, Nikolai A., Proskurowski, Giora, Peacock, Emily E., Hafner, Jan, and Reddy, Christopher M. (Sept. 2010). "Plastic accumulation in the North Atlantic subtropical gyre". In: *Science* 329 (5996), pp. 1185–1188. ISSN: 00368075. DOI: 10.1126/SCIENCE.1192321/SUPPL_FILE/LAW_SOM_REVISION_1.PDF. URL: https://www.science.org/doi/10.1126/science.1192321.

Lett, Christophe, Verley, Philippe, Mullon, Christian, Parada, Carolina, Brochier, Timothée, Penven, Pierrick, and Blanke, Bruno (Sept. 2008). "A Lagrangian tool for mod-

elling ichthyoplankton dynamics". In: *Environmental Modelling Software* 23 (9), pp. 1210–1214. ISSN: 1364-8152. DOI: 10.1016/J.ENVSOFT.2008.02.005.

León-Pérez, Mariana C., Reisinger, Anthony S., and Gibeaut, James C. (Mar. 2023). "Spatial-temporal dynamics of decaying stages of pelagic Sargassum spp. along shorelines in Puerto Rico using Google Earth Engine". In: *Marine Pollution Bulletin* 188, p. 114715. ISSN: 0025-326X. DOI: 10.1016/J.MARPOLBUL.2023.114715.

Liang, Yu Chiao, Lo, Min Hui, Lan, Chia Wei, Seo, Hyodae, Ummenhofer, Caroline C., Yeager, Stephen, Wu, Ren Jie, and Steffen, John D. (Sept. 2020). "Amplified seasonal cycle in hydroclimate over the Amazon river basin and its plume region". In: *Nature Communications 2020 11:1* 11 (1), pp. 1–11. ISSN: 2041-1723. DOI: 10.1038/s41467-020-18187-0. URL: https://www.nature.com/articles/s41467-020-18187-0.

Liu, Feng, Liu, Xingfeng, Wang, Yu, Jin, Zhe, Moejes, Fiona Wanjiku, and Sun, Song (July 2018). "Insights on the Sargassum horneri golden tides in the Yellow Sea inferred from morphological and molecular data". In: *Limnology and Oceanography* 63 (4), pp. 1762–1773. ISSN: 1939-5590. DOI: 10.1002/LNO.10806. URL: https://onlinelibrary.wiley.com/doi/full/10.1002/lno.10806https://onlinelibrary.wiley.com/doi/abs/10.1002/lno.10806https://aslopubs.onlinelibrary.wiley.com/doi/10.1002/lno.10806.

Luning, Klaus (1994). "When do algae grow the third founders lecture". In: *European Journal of Phycology* 29 (2), pp. 61–67. ISSN: 14694433. DOI: 10.1080/09670269400650501/ASSET//CMS/ASSET/4FAC53DA-FCEE-442C-99E1-2CBDA2C82620/09670269400650501.FP.PNG. URL: https://www.tandfonline.com/doi/abs/10.1080/09670269400650501.

López-Parages, Jorge, Auger, Pierre Amaël, Rodríguez-Fonseca, Belén, Keenlyside, Noel, Gaetan, Carlo, Rubino, Angelo, Arisido, Maeregu Woldeyes, and Brochier, Timothée (July 2020). "El Niño as a predictor of round sardinella distribution along the northwest African coast". In: *Progress in Oceanography* 186, p. 102341. ISSN: 0079-6611. DOI: 10.1016/J.POCEAN.2020.102341.

Malul, Dror, Berman, Hadar, Solodoch, Aviv, Tal, Omri, Barak, Noga, Mizrahi, Gur, Berenshtein, Igal, Toledo, Yaron, Lotan, Tamar, Sher, Daniel, Shavit, Uri, and Lehahn,

Yoav (Sept. 2024). "Directional swimming patterns in jellyfish aggregations". In: *Current Biology* 34 (17), 4033–4038.e5. ISSN: 18790445. DOI: 10.1016/J.CUB.2024.07.038/ATTACHMENT/66A5EDB2-B3EC-4820-B40F-9B0FCEC21286/MMC4.PDF. URL: https://www.cell.com/action/showFullText?pii=S0960982224009412https://www.cell.com/action/showAbstract?pii=S0960982224009412https://www.cell.com/current-biology/abstract/S0960-9822(24)00941-2.

Marez, Charly de, Ruiz-Angulo, Angel, and Corre, Mathieu Le (2024). "Structure of the Bottom Boundary Current South of Iceland and Spreading of Deep Waters by Submesoscale Processes". In: *Geophysical Research Letters* 51 (5).

Marsh, Robert, Addo, Kwasi Appeaning, Jayson-Quashigah, Philip Neri, Oxenford, Hazel A., Maxam, Ava, Anderson, Romario, Skliris, Nikolaos, Dash, Jadu, and Tompkins, Emma L. (Oct. 2021). "Seasonal Predictions of Holopelagic Sargassum Across the Tropical Atlantic Accounting for Uncertainty in Drivers and Processes: The SARTRAC Ensemble Forecast System". In: *Frontiers in Marine Science* 8, p. 722524. ISSN: 22967745. DOI: 10.3389/FMARS.2021.722524/BIBTEX.

Marsh, Robert, Oxenford, Hazel A., Cox, Shelly-Ann L., Johnson, Donald R., and Bellamy, Joshua (2022). "Forecasting seasonal sargassum events across the tropical Atlantic: Overview and challenges". In: *Frontiers in Marine Science* Volume 9 - 2022. ISSN: 2296-7745. DOI: 10.3389/fmars.2022.914501. URL: https://www.frontiersin.org/journals/marine-science/articles/10.3389/fmars.2022.914501.

Marsh, Robert, Skliris, Nikolaos, Tompkins, Emma L., Dash, Jadunandan, Almela, Victoria Dominguez, Tonon, Thierry, Oxenford, Hazel A., and Webber, Mona (July 2023). "Climate-sargassum interactions across scales in the tropical Atlantic". In: *PLOS Climate* 2 (7), e0000253. ISSN: 2767-3200. DOI: 10.1371/JOURNAL.PCLM.0000253. URL: https://journals.plos.org/climate/article?id=10.1371/journal.pclm.0000253.

Martinez, Elodie, Maamaatuaiahutapu, Keitapu, and Taillandier, Vincent (Sept. 2009). "Floating marine debris surface drift: Convergence and accumulation toward the South

Pacific subtropical gyre". In: *Marine Pollution Bulletin* 58 (9), pp. 1347–1355. ISSN: 0025-326X. DOI: 10.1016/J.MARPOLBUL.2009.04.022.

Martins, I. and Marques, J. C. (Aug. 2002). "A Model for the Growth of Opportunistic Macroalgae (Enteromorpha sp.) in Tidal Estuaries". In: *Estuarine, Coastal and Shelf Science* 55 (2), pp. 247–257. ISSN: 0272-7714. DOI: 10.1006/ECSS.2001.0900.

Martiny, Adam C., Lomas, Michael W., Fu, Weiwei, Boyd, Philip W., L. Chen, Yuh ling, Cutter, Gregory A., Ellwood, Michael J., Furuya, Ken, Hashihama, Fuminori, Kanda, Jota, Karl, David M., Kodama, Taketoshi, Li, Qian P., Ma, Jian, Moutin, Thierry, Woodward, E. Malcolm S., and Moore, J. Keith (Aug. 2019). "Biogeochemical controls of surface ocean phosphate". In: *Science Advances* 5 (8). ISSN: 23752548. DOI: 10.1126/SCIADV.AAX0341/SUPPL_FILE/AAX0341_SM.PDF. URL: https://www.science.org/doi/10.1126/sciadv.aax0341.

Maréchal, Jean Philippe, Hellio, Claire, and Hu, Chuanmin (Jan. 2017). "A Simple, Fast, and Reliable Method to Predict Sargassum Washing Ashore in the Lesser Antilles". In: *Remote Sensing Applications: Society and Environment* 5, pp. 54–63. ISSN: 23529385. DOI: 10.1016/J.RSASE.2017.01.001. URL: https://pure.lib.usf.edu/en/publications/a-simple-fast-and-reliable-method-to-predict-sargassum-washing-as-2.

Maurer, Andrew S., Neef, Emma De, and Stapleton, Seth (Sept. 2015). "Sargassum accumulation may spell trouble for nesting sea turtles". In: *Frontiers in Ecology and the Environment* 13 (7), pp. 394–395. ISSN: 1540-9309. DOI: 10.1890/1540-9295-13.7.394. URL: https://onlinelibrary.wiley.com/doi/full/10.1890/1540-9295-13.7.394https://onlinelibrary.wiley.com/doi/abs/10.1890/1540-9295-13.7.394https://esajournals.onlinelibrary.wiley.com/doi/10.1890/1540-9295-13.7.394.

McGillicuddy, Dennis Joseph, Morton, Peter Lynn, Brewton, Rachel Aileen, Hu, Chuanmin, Kelly, Thomas Bryce, Solow, Andrew Robert, and Lapointe, Brian Edward (Oct. 2023). "Nutrient and arsenic biogeochemistry of Sargassum in the western Atlantic". In: *Nature Communications 2023 14:1* 14 (1), pp. 1–8. ISSN: 2041-1723. DOI: 10.1038/

s41467-023-41904-4. URL: https://www.nature.com/articles/s41467-023-41904-4.

McWilliams, James C. (May 2016). "Submesoscale currents in the ocean". In: *Proceedings. Mathematical, Physical, and Engineering Sciences / The Royal Society* 472 (2189), p. 20160117. ISSN: 14712946. DOI: 10.1098/RSPA.2016.0117. URL: https://pmc.ncbi.nlm.nih.gov/articles/PMC4893189/.

Mendez-Tejeda, Rafael and Jiménez, Gladys A. Rosado (Oct. 2019). "Influence of climatic factors on Sargassum arrivals to the coasts of the Dominican Republic". In: *Journal of Oceanography and Marine Science* 10 (2), pp. 22–32. ISSN: 2141-2294. DOI: 10.5897/JOMS2019.0156. URL: https://bvearmb.do/handle/123456789/1558.

Michotey, Valérie, Blanfuné, Aurélie, Chevalier, Cristèle, Garel, Marc, Diaz, Frédéric, Berline, Léo, Grand, Louis Le, Armougom, Fabrice, Guasco, Sophie, Ruitton, Sandrine, Changeux, Thomas, Belloni, Bruno, Blanchot, Jean, Ménard, Frédéric, and Thibaut, Thierry (Dec. 2020). "In situ observations and modelling revealed environmental factors favouring occurrence of Vibrio in microbiome of the pelagic Sargassum responsible for strandings". In: *The Science of the total environment* 748. ISSN: 1879-1026. DOI: 10.1016/J.SCITOTENV.2020.141216. URL: https://pubmed.ncbi.nlm.nih.gov/32798861/.

Milledge, John J. and Harvey, Patricia J. (2016). "Golden Tides: Problem or Golden Opportunity? The Valorisation of Sargassum from Beach Inundations". In: *Journal of Marine Science and Engineering* 4.3. ISSN: 2077-1312. DOI: 10.3390/jmse4030060. URL: https://www.mdpi.com/2077-1312/4/3/60.

Mittelstaedt, Ekkehard (Jan. 1983). "The upwelling area off Northwest Africa—A description of phenomena related to coastal upwelling". In: *Progress in Oceanography* 12 (3), pp. 307–331. ISSN: 0079-6611. DOI: 10.1016/0079-6611(83)90012-5.

Muller-Karger, F.E., Richardson, P.L., and Mcgillicuddy, D. (1995). "On the offshore dispersal of the Amazon's Plume in the North Atlantic: Comments on the paper by A. Longhurst, "Seasonal cooling and blooming in tropical oceans"". In: *Deep Sea Research Part I: Oceanographic Research Papers* 42.11, pp. 2127–2137. ISSN: 0967-0637.

DOI: https://doi.org/10.1016/0967-0637(95)00085-2. URL: https://www.sciencedirect.com/science/article/pii/0967063795000852.

Muller-Karger, Frank E., McClain, Charles R., and Richardson, Philip L. (1988). "The dispersal of the Amazon's water". In: *Nature 1988 333:6168* 333 (6168), pp. 56–59. ISSN: 1476-4687. DOI: 10.1038/333056a0. URL: https://www.nature.com/articles/333056a0.

Nakajima, Ryota, Nagano, Akira, Osafune, Satoshi, Tsuchiya, Masashi, and Fujikura, Katsunori (Sept. 2024). "Aggregation and transport of microplastics by a cold-core ring in the southern recirculation of the Kuroshio Extension: the role of mesoscale eddies on plastic debris distribution". In: *Ocean Dynamics* 74 (9), pp. 773–782. ISSN: 16167228. DOI: 10.1007/S10236-024-01635-6/FIGURES/5. URL: https://link.springer.com/article/10.1007/s10236-024-01635-6.

Niermann, U. (Dec. 1986). "Distribution of Sargassum natans and some of its epibionts in the Sargasso Sea". In: *Helgoländer Meeresuntersuchungen* 40 (4), pp. 343–353. ISSN: 01743597. DOI: 10.1007/BF01983817/METRICS. URL: https://hmr.biomedcentral.com/articles/10.1007/BF01983817.

Nobre, Paulo, Lemos, Angelo T., Giarolla, Emanuel, Camayo, Rosio, Namikawa, Laercio, Kampel, Milton, Rudorff, Natália, Bezerra, Diego X., Lorenzzetti, João, Gomes, Jorge, SILVA, Manoel B. DA, Lage, Carla P.M., Paes, Rafael L., Beisl, Carlos, Lobão, Márcio M., Bignelli, Pedro A., MOURA, Najla DE, Galvão, Wougran S., and Polito, Paulo S. (Sept. 2022). "The 2019 northeast Brazil oil spill: scenarios". In: *Anais da Academia Brasileira de Ciências* 94, e20210391. ISSN: 0001-3765. DOI: 10.1590/0001-3765202220210391. URL: https://www.scielo.br/j/aabc/a/KJtdXzjnSt7DKQfNBQJMnqg/?lang=en.

Ody, Anouck, Thibaut, Thierry, Berline, Léo, Changeux, Thomas, André, Jean Michel, Chevalier, Cristèle, Blanfuné, Aurélie, Blanchot, Jean, Ruitton, Sandrine, StigerPouvreau, Valérie, Connan, Solène, Grelet, Jacques, Aurelle, Didier, Guéné, Mathilde, Bataille, Hubert, Bachelier, Céline, Guillemain, Dorian, Schmidt, Natascha, Fauvelle, Vincent, Guasco, Sophie, and Ménard, Frédéric (Sept. 2019). "From in Situ to satellite observa-

tions of pelagic Sargassum distribution and aggregation in the Tropical North Atlantic Ocean". In: *PLoS ONE* 14 (9). ISSN: 19326203. DOI: 10.1371/journal.pone.0222584.

Olascoaga, M. J., Beron-Vera, F. J., Beyea, R. T., Bonner, G., Castellucci, M., Goni, G. J., Guigand, C., and Putman, N. F. (Nov. 2023). "Physics-informed laboratory estimation of Sargassum windage". In: *Physics of Fluids* 35 (11). ISSN: 10897666. DOI: 10.1063/5.0175179/18206379/111702_1_5.0175179.AM.PDF. URL: /aip/pof/article/35/11/111702/2920880/Physics-informed-laboratory-estimation-of.

Olguin-Maciel, Edgar, Leal-Bautista, Rosa Maria, Alzate-Gaviria, Liliana, Domínguez-Maldonado, Jorge, and Tapia-Tussell, Raul (Dec. 2022). "Environmental impact of Sargassum spp. landings: an evaluation of leachate released from natural decomposition at Mexican Caribbean coast". In: *Environmental science and pollution research international* 29 (60), pp. 91071–91080. ISSN: 1614-7499. DOI: 10.1007/S11356-022-22123-8. URL: https://pubmed.ncbi.nlm.nih.gov/35882736/.

Onink, Victor, Wichmann, David, Delandmeter, Philippe, and Sebille, Erik van (Mar. 2019). "The Role of Ekman Currents, Geostrophy, and Stokes Drift in the Accumulation of Floating Microplastic". In: *Journal of Geophysical Research: Oceans* 124 (3), pp. 1474–1490. ISSN: 21699291. DOI: 10.1029/2018JC014547.

Parr, Albert (Jan. 1939). "Volume 6. Article 7. Quantitative observations on the pelagic Sargassum vegetation of the western North Atlantic. With preliminary discussion of morphology and relationships." In: *Bulletin of the Bingham Oceanographic Collection*. URL: https://elischolar.library.yale.edu/bulletin_yale_bingham_oceanographic_collection/40.

Pearson, Jenna, Fox-Kemper, Baylor, Pearson, Brodie, Chang, Henry, Haus, Brian K., Horstmann, Jochen, Huntley, Helga S., Kirwan, A. D., Lund, Björn, and Poje, Andrew (June 2020). "Biases in Structure Functions from Observations of Submesoscale Flows". In: *Journal of Geophysical Research: Oceans* 125 (6), e2019JC015769. ISSN: 2169-9291. DOI: 10.1029/2019JC015769. URL: https://onlinelibrary.wiley.com/doi/full/10.1029/2019JC015769https://onlinelibrary.wiley.com/doi/abs/

10.1029/2019JC015769https://agupubs.onlinelibrary.wiley.com/doi/10.1029/2019JC015769.

Prospero, Joseph M., Barkley, Anne E., Gaston, Cassandra J., Gatineau, Alexandre, Sansano, Arthur Campos y, and Panechou, Kathy (Sept. 2020). "Characterizing and Quantifying African Dust Transport and Deposition to South America: Implications for the Phosphorus Budget in the Amazon Basin". In: *Global Biogeochemical Cycles* 34 (9), e2020GB006536. ISSN: 1944-9224. DOI: 10.1029/2020GB006536. URL: https://onlinelibrary.wiley.com/doi/full/10.1029/2020GB006536https://onlinelibrary.wiley.com/doi/abs/10.1029/2020GB006536https://agupubs.onlinelibrary.wiley.com/doi/10.1029/2020GB006536.

Putman, Nathan F., Goni, Gustavo J., Gramer, Lewis J., Hu, Chuanmin, Johns, Elizabeth M., Trinanes, Joaquin, and Wang, Mengqiu (July 2018). "Simulating transport pathways of pelagic Sargassum from the Equatorial Atlantic into the Caribbean Sea". In: *Progress in Oceanography* 165, pp. 205–214. ISSN: 0079-6611. DOI: 10.1016/J.POCEAN.2018.06.009.

Putman, Nathan F. and Hu, Chuanmin (Sept. 2022). *Sinking Sargassum*. DOI: 10.1029/2022GL100189.

Putman, Nathan F., Lumpkin, Rick, Olascoaga, Maria J., Trinanes, Joaquin, and Goni, Gustavo J. (2020). "Improving transport predictions of pelagic Sargassum". In: *Journal of Experimental Marine Biology and Ecology* 529 (May), p. 151398. ISSN: 00220981. DOI: 10.1016/j.jembe.2020.151398. URL: https://doi.org/10.1016/j.jembe.2020.151398.

Pärn, Ove, Moy, Diego Macias, and Stips, Adolf (May 2023). "Determining the distribution and accumulation patterns of floating litter in the Baltic Sea using modelling tools". In: *Marine Pollution Bulletin* 190, p. 114864. ISSN: 0025-326X. DOI: 10.1016/J.MARPOLBUL.2023.114864.

Ren, Yixin, West-Foylea, Hoku, Surcela, Alexra, Millera, Christopher, and Robinsona, Douglas N. (Dec. 2014). "Genetic suppression of a phosphomimic myosin II identifies system-level factors that promote myosin II cleavage furrow accumulation". In: *Molecu-*

lar biology of the cell 25 (25), pp. 4150–4165. ISSN: 1939-4586. DOI: 10.1091/MBC.E14-08-1322. URL: https://pubmed.ncbi.nlm.nih.gov/25318674/.

Resiere, Dabor, Mehdaoui, Hossein, Florentin, Jonathan, Gueye, Papa, Lebrun, Thierry, Blateau, Alain, Viguier, Jerome, Valentino, Ruddy, Brouste, Yannick, Kallel, Hatem, Megarbane, Bruno, Cabie, André, Banydeen, Rishika, and Neviere, Remi (2021). "Sargassum seaweed health menace in the Caribbean: clinical characteristics of a population exposed to hydrogen sulfide during the 2018 massive stranding". In: *Clinical toxicology (Philadelphia, Pa.)* 59 (3), pp. 1–9. ISSN: 1556-9519. DOI: 10.1080/15563650.2020.1789162. URL: https://pubmed.ncbi.nlm.nih.gov/32633580/.

Ribbe, Joachim and Brieva, Daniel (Dec. 2016). "A western boundary current eddy characterisation study". In: *Estuarine, Coastal and Shelf Science* 183, pp. 203–212. ISSN: 02727714. DOI: 10.1016/j.ecss.2016.10.036.

Richardson, Philip L. (1983). "EDDY KINETIC ENERGY IN THE NORTH ATLANTIC FROM SURFACE DRIFTERS." In: *Journal of Geophysical Research* 88 (C7), pp. 4355–4367. ISSN: 01480227. DOI: 10.1029/JC088iC07p04355.

Rodríguez-Martínez, Rosa E., Roy, Priyadarsi D., Torrescano-Valle, Nuria, Cabanillas-Terán, Nancy, Carrillo-Domínguez, Silvia, Collado-Vides, Ligia, García-Sánchez, Marta, and Tussenbroek, Brigitta I. van (2020). "Element concentrations in pelagic Sargassum along the Mexican Caribbean coast in 2018-2019". In: *PeerJ* 8 (2). ISSN: 2167-8359. DOI: 10.7717/PEERJ.8667. URL: https://pubmed.ncbi.nlm.nih.gov/32149030/.

Rogers, Jeffrey C (1997). "North Atlantic Storm Track Variability and Its Association to the North Atlantic Oscillation and Climate Variability of Northern Europe". In: *Journal of Climate* 10.

Ryther, John H. (Jan. 1956). "The Sargasso Sea". In: *Scientific American* 194 (1), pp. 98–104. ISSN: 0036-8733. DOI: 10.1038/SCIENTIFICAMERICAN0156-98. URL: https://www.scientificamerican.com/article/the-sargasso-sea/.

Röhrs, Johannes, Christensen, Kai Häkon, Hole, Lars Robert, Broström, Göran, Drivdal, Magnus, and Sundby, Svein (Dec. 2012). "Observation-based evaluation of surface wave

effects on currents and trajectory forecasts". In: *Ocean Dynamics* 62 (10-12), pp. 1519–1533. ISSN: 16167341. DOI: 10.1007/S10236-012-0576-Y/FIGURES/7. URL: https://link.springer.com/article/10.1007/s10236-012-0576-y.

Sainte-Rose, Bruno, Lebreton, Laurent, Rego, Joao, Kleissen, Frank, and Reisser, Julia (June 2016). "Multi-Scale Numerical Analysis of the Field Efficiency of an Ocean Plastic Cleanup Array". In: DOI: 10.1115/OMAE2016-54926.

Saporta-Katz, Ori, Mantel, Nadav, Liran, Rotem, Rom-Kedar, Vered, and Gildor, Hezi (June 2024). "Northbound Transport of the Mediterranean Outflow and the Role of Time-Dependent Chaotic Advection". In: *Geophysical Research Letters* 51 (12), e2023GL105662. ISSN: 1944-8007. DOI: 10.1029/2023GL105662. URL: https://onlinelibrary.wiley.com/doi/full/10.1029/2023GL105662https://onlinelibrary.wiley.com/doi/abs/10.1029/2023GL105662https://agupubs.onlinelibrary.wiley.com/doi/10.1029/2023GL105662.

Schell, Jeffrey M., Goodwin, Deborah S., and Siuda, Amy N.S. (Sept. 2015). "Recent sargassum inundation events in the caribbean: Shipboard observations reveal dominance of a previously rare form". In: *Oceanography* 28 (3), pp. 8–10. ISSN: 10428275. DOI: 10.5670/OCEANOG.2015.70.

Schlag, Zachary R, North, Elizabeth W, North, Elizabeth, and Schlag, Zachary (2012). *Lagrangian TRANSport model (LTRANS) v.2 User's Guide User's Guide This User's Guide is based on the v.1 User's Guide (Schlag et al. 2008) and was updated by.* Tech. rep. University of Maryland.

Schneider, C.W. and Searles, R.B. (1991). "Seaweeds of Southeastern United States: Cape Hatteras to Cape Canaveral." In: *Duke University Press.*

Sebille, Erik Van, Aliani, Stefano, Law, Kara Lavender, Maximenko, Nikolai, Alsina, José M., Bagaev, Andrei, Bergmann, Melanie, Chapron, Bertrand, Chubarenko, Irina, Cózar, Andrés, Delandmeter, Philippe, Egger, Matthias, Fox-Kemper, Baylor, Garaba, Shungudzemwoyo P., Goddijn-Murphy, Lonneke, Hardesty, Britta Denise, Hoffman, Matthew J., Isobe, Atsuhiko, Jongedijk, Cleo E., Kaandorp, Mikael L.A., Khatmullina, Liliya, Koelmans, Albert A., Kukulka, Tobias, Laufkötter, Charlotte, Lebreton, Laurent, Lo-

belle, Delphine, Maes, Christophe, Martinez-Vicente, Victor, Maqueda, Miguel Angel Morales, Poulain-Zarcos, Marie, Rodríguez, Ernesto, Ryan, Peter G., Shanks, Alan L., Shim, Won Joon, Suaria, Giuseppe, Thiel, Martin, Bremer, Ton S. Van Den, and Wichmann, David (Feb. 2020). "The physical oceanography of the transport of floating marine debris". In: *Environmental Research Letters* 15 (2), p. 023003. ISSN: 1748-9326. DOI: 10.1088/1748-9326/AB6D7D. URL: https://iopscience.iop.org/article/10.1088/1748-9326/ab6d7dhttps://iopscience.iop.org/article/10.1088/1748-9326/ab6d7d/meta.

Sebille, Erik van, Griffies, Stephen M., Abernathey, Ryan, Adams, Thomas P., Berloff, Pavel, Biastoch, Arne, Blanke, Bruno, Chassignet, Eric P., Cheng, Yu, Cotter, Colin J., Deleersnijder, Eric, Döös, Kristofer, Drake, Henri F., Drijfhout, Sybren, Gary, Stefan F., Heemink, Arnold W., Kjellsson, Joakim, Koszalka, Inga Monika, Lange, Michael, Lique, Camille, MacGilchrist, Graeme A., Marsh, Robert, Adame, C. Gabriela Mayorga, McAdam, Ronan, Nencioli, Francesco, Paris, Claire B., Piggott, Matthew D., Polton, Jeff A., Rühs, Siren, Shah, Syed H.A.M., Thomas, Matthew D., Wang, Jinbo, Wolfram, Phillip J., Zanna, Laure, and Zika, Jan D. (Jan. 2018). "Lagrangian ocean analysis: Fundamentals and practices". In: *Ocean Modelling* 121, pp. 49–75. ISSN: 1463-5003. DOI: 10.1016/J.OCEMOD.2017.11.008.

Silva-Fernandes, S. M. and Peliz, A. J. (Nov. 2020). "The Turbulent Structure of the Azores Current System: A Statistical Analysis". In: *Journal of Geophysical Research: Oceans* 125 (11), e2020JC016327. ISSN: 2169-9291. DOI: 10.1029/2020JC016327. URL: https://onlinelibrary.wiley.com/doi/full/10.1029/2020JC016327https://onlinelibrary.wiley.com/doi/abs/10.1029/2020JC016327https://agupubs.onlinelibrary.wiley.com/doi/10.1029/2020JC016327.

Smagorinsky, J. (Mar. 1963). "GENERAL CIRCULATION EXPERIMENTS WITH THE PRIMITIVE EQUATIONS: I. THE BASIC EXPERIMENT". In: *Monthly Weather Review* 91 (3), pp. 99–164. ISSN: 1520-0493. DOI: 10.1175/1520-0493(1963)091. URL: https://journals.ametsoc.org/view/journals/mwre/91/3/1520-0493_1963_091_0099_gcewtp_2_3_co_2.xml.

Stammer, Detlef (Aug. 1997). "Global Characteristics of Ocean Variability Estimated from Regional TOPEX/POSEIDON Altimeter Measurements". In: *Journal of Physical Oceanography* 27 (8), pp. 1743–1769. ISSN: 0022-3670. DOI: 10.1175/1520-0485(1997)027. URL: https://journals.ametsoc.org/view/journals/phoc/27/8/1520-0485_1997_027_1743_gcoove_2.0.co_2.xml.

Stokes, G (1847). "On the Theory of Oscillatory Waves". In: *Transactions of the Cambridge Philosophical Society* 8, pp. 441–455.

Thompson, T. M., Young, B. R., and Baroutian, S. (Feb. 2020). *Pelagic Sargassum for energy and fertiliser production in the Caribbean: A case study on Barbados*. DOI: 10.1016/j.rser.2019.109564.

Tolman, Hendrik L (2009). *User manual and system documentation of WAVEWATCH III TM version 3.14 †*. Tech. rep. Environmental Modeling Center.

Trinanes, Joaquin A., Olascoaga, M. Josefina, Goni, Gustavo J., Maximenko, Nikolai A., Griffin, David A., and Hafner, Jan (July 2016). "Analysis of flight MH370 potential debris trajectories using ocean observations and numerical model results". In: *Journal of Operational Oceanography* 9 (2), pp. 126–138. ISSN: 2. DOI: 10.1080/1755876X.2016.1248149. URL: https://repository.library.noaa.gov/view/noaa/17681.

Vizy, Edward K. and Cook, Kerry H. (Nov. 2010). "Influence of the Amazon/Orinoco Plume on the summertime Atlantic climate". In: *Journal of Geophysical Research: Atmospheres* 115 (D21). ISSN: 2156-2202. DOI: 10.1029/2010JD014049. URL: https://onlinelibrary.wiley.com/doi/full/10.1029/2010JD014049https://onlinelibrary.wiley.com/doi/abs/10.1029/2010JD014049https://agupubs.onlinelibrary.wiley.com/doi/10.1029/2010JD014049.

Vogt-Vincent, Noam S., Burt, April J., Ven, Rosa M. van der, and Johnson, Helen L. (Aug. 2024). "Coral reef potential connectivity in the southwest Indian Ocean". In: *Coral Reefs* 43 (4), pp. 1037–1051. ISSN: 14320975. DOI: 10.1007/S00338-024-02521-9/FIGURES/5. URL: https://link.springer.com/article/10.1007/s00338-024-02521-9.

Volkov, Denis L. and Fu, Lee Lueng (Nov. 2011). "Interannual variability of the Azores Current strength and eddy energy in relation to atmospheric forcing". In: *Journal of Geophysical Research: Oceans* 116 (C11), p. 11011. ISSN: 2156-2202. DOI: 10.1029/2011JC007271. URL: https://onlinelibrary.wiley.com/doi/full/10.1029/2011JC007271https://onlinelibrary.wiley.com/doi/abs/10.1029/2011JC007271https://agupubs.onlinelibrary.wiley.com/doi/10.1029/2011JC007271.

Vázquez, R., Parras-Berrocal, I. M., Koseki, S., Cabos, W., Sein, D. V., and Izquierdo, A. (Nov. 2023). "Seasonality of coastal upwelling trends in the Mauritania-Senegalese region under RCP8.5 climate change scenario". In: *Science of The Total Environment* 898, p. 166391. ISSN: 0048-9697. DOI: 10.1016/J.SCITOTENV.2023.166391.

Wang, Mengqiu and Hu, Chuanmin (Apr. 2017). "Predicting Sargassum blooms in the Caribbean Sea from MODIS observations". In: *Geophysical Research Letters* 44 (7), pp. 3265–3273. ISSN: 1944-8007. DOI: 10.1002/2017GL072932. URL: https://onlinelibrary.wiley.com/doi/full/10.1002/2017GL072932https://onlinelibrary.wiley.com/doi/abs/10.1002/2017GL072932https://agupubs.onlinelibrary.wiley.com/doi/10.1002/2017GL072932.

Wang, Mengqiu, Hu, Chuanmin, Barnes, Brian B., Mitchum, Gary, Lapointe, Brian, and Montoya, Joseph P. (2019). "The great Atlantic Sargassum belt". In: *Science* 364 (6448), pp. 83–87. ISSN: 10959203. DOI: 10.1126/science.aaw7912.

Wang, Mengqiu, Hu, Chuanmin, Cannizzaro, Jennifer, English, David, Han, Xingxing, Naar, David, Lapointe, Brian, Brewton, Rachel, and Hernandez, Frank (Nov. 2018). "Remote Sensing of Sargassum Biomass, Nutrients, and Pigments". In: *Geophysical Research Letters* 45 (22), pp. 12,359–12,367. ISSN: 1944-8007. DOI: 10.1029/2018GL078858. URL: https://onlinelibrary.wiley.com/doi/full/10.1029/2018GL078858https://onlinelibrary.wiley.com/doi/abs/10.1029/2018GL078858https://agupubs.onlinelibrary.wiley.com/doi/10.1029/2018GL078858.

Wang, Shuangqiang, Kenchington, Ellen, Murillo, F. Javier, Lirette, Camille, Wang, Zeliang, Koen-Alonso, Mariano, Kenny, Andrew, Sacau, Mar, and Pepin, Pierre (May 2024). "Quantifying the effects of fragmentation of connectivity networks of deep-sea vulnerable

marine ecosystems". In: *Diversity and Distributions* 30 (5), e13824. ISSN: 1472-4642. DOI: 10.1111/DDI.13824. URL: https://onlinelibrary.wiley.com/doi/full/10.1111/ddi.13824https://onlinelibrary.wiley.com/doi/abs/10.1111/ddi.13824https://onlinelibrary.wiley.com/doi/10.1111/ddi.13824.

Witherington, Blair, Hirama, Shigetomo, and Hardy, Robert (Aug. 2012). "Young sea turtles of the pelagic Sargassum-dominated drift community: Habitat use, population density, and threats". In: *Marine Ecology Progress Series* 463, pp. 1–22. ISSN: 01718630. DOI: 10.3354/MEPS09970. URL: https://www.researchgate.net/publication/270087545_Young_sea_turtles_of_the_pelagic_Sargassum-dominated_drift_community_Habitat_use_population_density_and_threats.

Wysocki, Laura A., Bianchi, Thomas S., Powell, Rodney T., and Reuss, Nina (Aug. 2006). "Spatial variability in the coupling of organic carbon, nutrients, and phytoplankton pigments in surface waters and sediments of the Mississippi River plume". In: *Estuarine, Coastal and Shelf Science* 69 (1-2), pp. 47–63. ISSN: 0272-7714. DOI: 10.1016/J.ECSS.2006.03.022.

Xiang, Yang, Quay, Paul D., Sonnerup, Rolf E., and Fassbender, Andrea J. (July 2023). "Subtropical Gyre Nutrient Cycling in the Upper Ocean: Insights From a Nutrient-Ratio Budget Method". In: *Geophysical Research Letters* 50 (13), e2023GL103213. ISSN: 1944-8007. DOI: 10.1029/2023GL103213. URL: https://onlinelibrary.wiley.com/doi/full/10.1029/2023GL103213https://onlinelibrary.wiley.com/doi/abs/10.1029/2023GL103213https://agupubs.onlinelibrary.wiley.com/doi/10.1029/2023GL103213.

Yang, Yiqiu, Li, Yan, Li, Juan, Liu, Jingui, Gao, Zhiyi, Guo, Kaixuan, and Yu, Han (Oct. 2021). "The influence of Stokes drift on oil spills: Sanchi oil spill case". In: *Acta Oceanologica Sinica* 40 (10), pp. 30–37. ISSN: 18691099. DOI: 10.1007/S13131-021-1889-9/METRICS. URL: https://link.springer.com/article/10.1007/s13131-021-1889-9.

Zhai, Xiaoming and Greatbatch, Richard J. (Dec. 2006). "Inferring the eddy-induced diffusivity for heat in the surface mixed layer using satellite data". In: *Geophysical Research Letters* 33 (24). ISSN: 00948276. DOI: 10.1029/2006GL027875.

Zhang, Yingjun, Hu, Chuanmin, McGillicuddy, Dennis J., Barnes, Brian B., Liu, Yonggang, Kourafalou, Vassiliki H., Zhang, Shuai, and Hernandez, Frank J. (Feb. 2024). "Pelagic Sargassum in the Gulf of Mexico driven by ocean currents and eddies". In: *Harmful Algae* 132, p. 102566. ISSN: 1568-9883. DOI: 10.1016/J.HAL.2023.102566.

Zhong, Yisen, Bracco, Annalisa, and Villareal, Tracy A. (Apr. 2012). "Pattern formation at the ocean surface: Sargassum distribution and the role of the eddy field". In: *Limnology and Oceanography: Fluids and Environments* 2 (1), pp. 12–27. ISSN: 2157-3689. DOI: 10.1215/21573689-1573372. URL: https://onlinelibrary.wiley.com/doi/full/10.1215/21573689-1573372https://onlinelibrary.wiley.com/doi/abs/10.1215/21573689-1573372https://aslopubs.onlinelibrary.wiley.com/doi/10.1215/21573689-1573372.